Fall 10-1-2021

Development of the Nuclear-Electronic Orbital Method for Applications to Molecular Electrocatalyst Systems

Patrick Schneider
Yale University Graduate School of Arts and Sciences, schneider1765@gmail.com

Abstract

Development of the Nuclear-Electronic Orbital Method for Applications to Molecular

Electrocatalyst Systems

Patrick Eugene Schneider

2021

Studies of molecular electrocatalysts often involve input from quantum chemical computations in the pursuit of catalyst design targeting several desirable features. To this end, conventional density functional theory (DFT) calculations have proven to be a good match with a reasonable balance between computational accuracy and cost. However, a multicomponent method that treats select nuclei on the same quantum mechanical level as electrons would be useful for a more proper treatment of nuclear quantum effects. Such a multicomponent DFT method has been developed in recent years within the nuclear-electronic orbital (NEO) framework. However, for the multicomponent method to be practically applied to large, chemically interesting systems, several functionalities were necessary. The NEO diagonal Born-Oppenheimer correction was calculated and shown to be small enough to validate the underlying Born-Oppenheimer-like separation between light and heavy nuclei. Analytical NEO Hessian expressions were derived and implemented, and they were utilized to identify transition states and generate multicomponent minimum energy paths. Lastly, the calculation of infrared spectra in the NEO framework was formulated and shown to produce accurate values compared to experiment. These developments have each been significant steps in preparing NEO-DFT for utilization in modeling molecular electrocatalysts.

Development of the Nuclear-Electronic Orbital Method for Application to Molecular

Electrocatalyst Systems

A Dissertation

Presented to the Faculty of the Graduate School

of

Yale University

In Candidacy for the Degree of

Doctor of Philosophy

by

Patrick Eugene Schneider

Dissertation Director: Sharon Hammes-Schiffer

December 2021

Table of Contents

List of Figures

List of Tables

Acknowledgments

While putting together this dissertation was certainly one of the most difficult tasks I have ever undertaken, I am now surprised to find it equally hard to properly convey here my gratitude for co-workers, friends, and family that have made this work possible. Chief among them are my scientific supervisors – in particular my research advisor throughout graduate school, Dr. Sharon Hammes-Schiffer. Without Sharon's excellent guidance and resourcefulness, I would be long past abandoning these research goals. Sincere thanks are also owed to a trio of researchers who oversaw my work during my undergraduate career: Dr. Wayne Bosma, Dr. Jill Moser, and Dr. Bob Behle. Through my experiences with each of them, I gleaned important skills that only helped to prepare me for obstacles I would encounter in my graduate pursuits.

I am indebted to my co-workers in the Hammes-Schiffer group. I wish to thank who I consider to be my research group mentors, Dr. Zach Goldsmith and Dr. Kurt Brorsen. I am glad that I have been able to catch up to them and can now provide guidance to more junior students. Next, I frequently found myself turning to Zhen (Coraline) Tao and Dr. David Stevens for advice on our collective graduate school experience, and I have greatly enjoyed their company in and out of the office over these past years. While I thank each member who overlapped with me in this group, I particularly want to thank NEO subgroup members for their commitment to see each other thrive in their work. I would be lucky to find myself working with people like Coraline, Kurt, Dr. Tanner Culpitt, Dr. Yang Yang, Dr. Fabijan Pavošević, Ben Rousseau, Dr. Qi Yu, Dr. Saswata Roy, Mathew Chow, and Dr. Chris Malbon in the future.

I would also like to acknowledge my experimental collaborators at the Center for Molecular Electrocatalysis. After all, without collaborators like Dr. Shannon Stahl, Dr. Larry Wang, Dr. Aaron Appel, and Dr. Spencer Heins, I would have no basis for large portions of the

research I have published. I thank them and other members of the CME for lively discussions and the learning opportunities for me as a theorist that came with those discussions.

I will always hold a special place in my memory for my first two years at the University of Illinois at Urbana-Champaign. I shared much time with my closest friends from my incoming class, whether it was celebrating the end of our first year in a house seemingly optimally designed to host our graduate student parties or routinely grabbing lunch together in the hallways between our busy schedules. It was difficult being uprooted from this network by making the move to Yale, but that only gave me a deeper appreciation for the opportunity to catch up over dinner at Golden Harbor when I could visit. Larry Salvati, Dr. Kori Sye, Aastha Sharma, and Allan Sykes – I wish you the best and hope to find myself across a dinner table from you in the future. Thank you for being my friends.

Likewise, spending my hard-earned free time with my other friends helped me to recharge and prepare for whatever roadblock would come next. I miss each of my close friends from Bradley University – Felicia Staiger, Betsy Podkowa, and Dr. Tom Carty – more and more each day, but I know we will continue to find the time to catch up with each other's lives. I consider my longest and deepest friendships to date to be those within the group of Ky Hamon, James Wylie, Andrew and Emily Bosma, and Griffin and Queta Polonus. May the memories of our adventures be long-lasting, even if we can only all be together at our annual bashes going forward. Thank you all for the escapism provided by your company.

The long process of my education would be a drastically different story without the support of my parents, Gene and Kathy, and family friends like Dr. Gary List. I know they will always have my best interests in mind and care for me in the increasingly infrequent chances I find to visit home. I am also unfathomably fortunate and grateful for the love and support I have received from my partner, Min Jung Han, over the nearly four years we have been together.

Through the movie nights, grocery runs, and her pep talks, I have stayed grounded and

relaxed. I love you very much, MJ, and look forward to the next step we take together.

Chapter One

Introduction

Designing more efficient molecular electrocatalysts is currently an important research area for evolving energy needs. These efforts are intended to produce catalysts with higher turnover frequencies (TOFs), with lower required overpotentials, and composed of earth abundant materials. Collaboration between experimental and theoretical groups has provided a useful dialogue on the design of these systems. In those collaborations, density functional theory (DFT) has proven to be the most popular computational tool for studying molecular electrocatalysts.[1] This popularity is due to the method's tractable scaling for larger systems, as well as the relative accuracy of computed geometries and energies. Interesting quantities of molecular electrocatalyst systems that can be practically calculated with DFT include pK_a and $E_{1/2}$ values of species in a catalytic cycle.[2] These values can be computed with near-quantitative accuracy when referenced to an experimentally known value and can be directly related to the desired attributes noted above.

As popular as DFT calculations are, computed pK_a values are usually less quantitatively reliable than computed reduction potentials. This trend can be partially attributed to conventional methods utilizing the Born-Oppenheimer approximation and treating the nuclei as classical point charges, thus missing important characteristics of key protons that may exhibit proton delocalization and anharmonicity. These nuclear quantum effects may also be significant for electron transfer and proton transfer steps in a catalytic cycle, as exemplified in certain $Ni(P_2N_2)_2$ systems.[3] Concerted proton-coupled electron transfer (PCET) is also important in some molecular electrocatalysts, and the theoretical treatment of concerted PCET would benefit from a three-dimensional quantum mechanical treatment of the transferring proton(s), as contemporary applications of PCET theory often require the costly calculation of proton potentials on a grid to ultimately yield excited proton vibrational states.[4-5]

The nuclear-electronic orbital (NEO) method is a multicomponent quantum chemistry

2

method that provides an option for treating specific nuclei quantum mechanically, on the same level as the electrons. In other words, the NEO framework does not invoke the Born-Oppenheimer approximation between select nuclei, usually key protons, and the electrons.[6] However, a Born-Oppenheimer-like separation is still maintained between the remaining "classical" nuclei and the quantum particles (electrons and select nuclei), with the latter responding instantaneously to any change in the configuration of classical nuclei. In order to validate the separation between quantum and classical nuclei inherent to NEO methods, a multicomponent counterpart of the diagonal Born-Oppenheimer correction (DBOC)[7] must be calculated and studied. The DBOC is also called the "adiabatic correction" as it is a correction to the conventional electronic energy that accounts for the kinetic energy operator of the fixed point-charge nuclei, resulting in an adiabatic surface.[8] If this adiabatic surface differs appreciably from the original electronic surface, then the DBOC is significant and the Born-Oppenheimer approximation is ill fit to meaningfully describe the physics of the system.

The NEO formalism can be adapted into multicomponent analogs of conventional electronic structure methods, such as Hartree-Fock (HF) theory, to include nuclear quantum effects in such calculations. Similarly, a variety of wavefunction-based NEO methods have been developed in recent years with the multicomponent coupled cluster[9-10] and orbital-optimized MP2[11] methods being highlights. While these NEO wavefunction methods are robust and can yield more accurate computed quantities, a method with lower computational cost is necessary for practical applications involving the relatively large molecular electrocatalyst systems. To meet this need, a multicomponent variant of DFT, denoted NEO-DFT, has been developed.[12-13] The NEO-DFT method has been implemented within a Kohn-Sham style formalism,[13] which can be viewed as a density functional analog of HF theory. This NEO-DFT implementation benefits from the attractive computational scaling and relative accuracy that

has made conventional DFT the method of choice for studying larger systems.

As NEO-DFT is a density functional method, it requires the use of several density functionals. Among these are the familiar electronic exchange-correlation (exc) functional, as well as the multicomponent-specific protonic exchange-correlation functional and an electron-proton correlation (epc) functional. In practice, common conventionally developed exc functionals, such as B3LYP or PBE0, can be employed in a NEO-DFT calculation, allowing a particular exc functional to be chosen based on each system's needs. As the protons are relatively localized in space, development of a sophisticated proton exchange-correlation functional can be avoided by simply using exact exchange for the protons and neglecting a treatment for proton-proton correlation. Ultimately, the epc functional is arguably the most important quantity to capture even a qualitatively correct physical picture within the NEO-DFT implementation, as an attractive potential exists between the two charged particles. A great amount of work has been conducted in deriving proper epc functionals.

A handful of epc functionals have been derived, parametrized, and implemented for NEO-DFT. The development of these functionals followed a Colle-Salvetti formulation that resulted in the creation and subsequent parametrization of both local density approximation-type[14] and generalized gradient approximation-type[15] epc functionals. These functionals allow calculations of qualitatively correct proton densities compared to a grid reference and quantitative accuracy in calculations of proton affinities with NEO-DFT.[16] The accuracy in proton affinity values rivals conventional DFT while including nuclear quantum effects into the self-consistent field procedure to enable certain types of calculations not possible with conventional DFT.[14, 16] Previous work has found these developed epc functionals to be transferrable in the sense that the accuracy of the functional is not dependent on the choice of the exc functional.[17] For the treatment of excited states, multicomponent time-dependent HF

4

and time-dependent DFT analogs, NEO-TDHF and NEO-TDDFT, respectively, have been developed and provide not only accurate electronic excitation energies of the system, but also the vibrational excitation energies of the chosen quantum nuclei.[18-20]

As described to this point, the NEO-DFT method seems the perfect multicomponent candidate for utilization in the calculation of molecular electrocatalyst properties. However, major utilities for the characterization of the NEO reaction surface and vibrational analysis have yet to be developed and would be required for any serious study of molecular electrocatalysts. From a computational standpoint, the potential energy surface (PES) is a function of the nuclear coordinates of the system. The PES can, in a sense, be mapped through calculating energies at different geometries. Energy gradients on this surface are useful in determining local and global minima of the PES, which correspond to optimized geometries of the chemical species. For a better characterization of the PES, further derivatives are desired. The second derivatives of this energy surface with respect to atomic displacements can be used to generate a force constant matrix called the energy coordinate Hessian, hereon referred to as simply the Hessian. This Hessian provides information on the curvature of the PES and can be used to characterize stationary points as transition states or local minima.

As the Hessian can characterize transition states, it is thus integral in determining minimum energy paths between reactants and products on the PES that, by definition, pass through a transition state. At stationary points, the Hessian can be employed in a harmonic approximation to yield vibrational modes and corresponding frequencies. In turn, these vibrational frequencies would be required in the calculation of thermodynamic quantities integral to the description of catalytic pathways, such as free energy differences. The Hessian is a derivative quantity and can be computed numerically in a straightforward manner, although

at greater computational expense. Ideally, an analytical procedure is desired for the calculation of these second derivatives, as this will make computations involving the NEO Hessian tractable in terms of cost.

The NEO Hessian will provide characterization of points on the NEO PES, as well as vibrational modes for the classical nuclei. However, these vibrational modes will not be comparable to experimentally obtained infrared (IR) spectroscopy data, as the NEO modes entail instantaneous response of the quantum nuclei to the motion of the classical nuclei. In other words, while the NEO Hessian produces vibrational modes that accurately describe the NEO PES, there is improper coupling between the quantum and classical nuclei for comparison to IR spectroscopy. Furthermore, the NEO PES has lesser dimensionality than the conventional counterpart, so certain vibrational modes dominated by the motion of the quantum nuclei would not be obtained through vibrational analysis using only the NEO Hessian. Rather, it has been found that information is required from both the NEO Hessian and NEO-TDHF/TDDFT to yield a complete set of molecular vibrational frequencies that can be compared to IR spectra.

In the next chapter of this dissertation, the NEO DBOC is developed and calculated for a range of typical small molecular systems. The effect of this DBOC on the NEO PES is measured and is shown to be negligible for the systems studied, validating the quantum/classical separation made in the NEO method between different types of nuclei.

In chapter 3, the derivation for the analytical calculation of NEO Hessian elements is presented and implemented. Analytically calculated NEO Hessians are then used in transition state searches for an S_N2 reaction and a hydride transfer reaction. The Hessian is once again employed to determine minimum energy paths for each of these reactions, and differences between the calculated NEO and conventional paths are discussed.

Chapters 4 and 5 cover the development of the NEO-DFT(V) method, which couples the classical nuclear vibrational modes from the NEO Hessian with the quantum nuclear vibrational excitations from NEO-TDDFT to produce a complete set of molecular vibrational modes and frequencies. The theory for this coupling is shown, and calculations are conducted to demonstrate the performance of the method compared to conventional harmonic and anharmonic vibrational analysis relative to experimental data. Cases involving single and multiple quantum nuclei are studied in each chapter, respectively. In addition to providing calculated IR spectra based on the NEO method, the NEO-DFT(V) results show promising agreement with experiment, mostly due to anharmonicity of the quantum nuclei through the inclusion of the NEO-TDDFT vibrational excitation energies in the overall vibrational analysis.

The final chapter then briefly summarizes the preceding work and provides a broad outlook on the state of NEO methods considering these developments. In addition to the work presented in this dissertation, several other projects concerning both NEO method development and computational studies of molecular electrocatalysts in conjunction with experimental collaborators have been completed in recent years and are complementary to the main body of this dissertation. While not featured as individual chapters, it is worthwhile to highlight these works, which have been published and are available at the following references: [17, 21-25].

References

(1)   Maseras, F.; Lledos, A., Computational Modeling of Homogeneous Catalysis. Kluwer Academic Publishers: 2002.

(2)   Solis, B. H.; Hammes-Schiffer, S., Proton-Coupled Electron Transfer in Molecular Electrocatalysis: Theoretical Methods and Design Principles. *Inorg. Chem.* **2014,** *53*, 6427-6443.

(3)   Horvath, S.; Fernandez, L. E.; Soudackov, A. V.; Hammes-Schiffer, S., Insights into proton-coupled electron transfer mechanisms of electrocatalytic H_2 oxidation and production. *Proc. Natl. Acad. Sci. U.S.A.* **2012,** *109*, 15663-15668.

(4)   Soudackov, A.; Hammes-Schiffer, S., Derivation of rate expressions for nonadiabatic proton-coupled electron transfer reactions in solution. *J. Chem. Phys.* **2000,** *113*, 2385-2396.

(5)   Hammes-Schiffer, S.; Stuchebrukhov, A. A., Theory of Coupled Electron and Proton Transfer Reactions. *Chem. Rev.* **2010,** *110*, 6939-6960.

(6)   Webb, S. P.; Iordanov, T.; Hammes-Schiffer, S., Multiconfigurational nuclear-electronic orbital approach: Incorporation of nuclear quantum effects in electronic structure calculations. *J. Chem. Phys.* **2002,** *117*, 4106-4118.

(7)   Handy, N. C.; Yamaguchi, Y.; III, H. F. S., The diagonal correction to the Born–Oppenheimer approximation: Its effect on the singlet–triplet splitting of CH2 and other molecular effects. *J. Chem. Phys.* **1986,** *84*, 4481-4484.

(8)   Ioannou, A. G.; Amos, R. D.; Handy, N. C., The diagonal born-oppenheimer correction for He2+ and F+H2. *Chem. Phys. Lett.* **1996,** *251*, 52-58.

(9)   Pavošević, F.; Culpitt, T.; Hammes-Schiffer, S., Multicomponent Coupled Cluster Singles and Doubles Theory within the Nuclear-Electronic Orbital Framework. *J. Chem. Theory Comput.* **2019,** *15*, 338-347.

(10)   Pavošević, F.; Hammes-Schiffer, S., Multicomponent coupled cluster singles and doubles and Brueckner doubles methods: Proton densities and energies. *J. Chem. Phys.* **2019,** *151*, 074104.

(11)   Pavošević, F.; Rousseau, B. J. G.; Hammes-Schiffer, S., Multicomponent Orbital-Optimized Perturbation Theory Methods: Approaching Coupled Cluster Accuracy at Lower Cost. *J. Phys. Chem. Lett.* **2020,** *11*, 1578-1583.

(12)   Pak, M. V.; Chakraborty, A.; Hammes-Schiffer, S., Density Functional Theory Treatment of Electron Correlation in the Nuclear−Electronic Orbital Approach. *J. Phys. Chem. A* **2007,** *111*, 4522-4526.

(13)   Chakraborty, A.; Pak, M. V.; Hammes-Schiffer, S., Development of Electron-Proton Density Functionals for Multicomponent Density Functional Theory. *Phys. Rev. Lett.* **2008,** *101*, 153001.

(14)   Yang, Y.; Brorsen, K. R.; Culpitt, T.; Pak, M. V.; Hammes-Schiffer, S., Development of a practical multicomponent density functional for electron-proton correlation to produce accurate proton densities. *J. Chem. Phys.* **2017,** *147*, 114113.

(15)   Tao, Z.; Yang, Y.; Hammes-Schiffer, S., Multicomponent density functional theory: Including the density gradient in the electron-proton correlation functional for hydrogen and deuterium. *J. Chem. Phys.* **2019,** *151*, 124102.

(16)   Brorsen, K. R.; Yang, Y.; Hammes-Schiffer, S., Multicomponent Density Functional Theory: Impact of Nuclear Quantum Effects on Proton Affinities and Geometries. *J. Phys. Chem. Lett.* **2017,** *8*, 3488-3493.

(17)   Brorsen, K. R.; Schneider, P. E.; Hammes-Schiffer, S., Alternative forms and transferability of electron-proton correlation functionals in nuclear-electronic orbital density functional theory. *J. Chem. Phys.* **2018,** *149*, 044110.

(18)   Yang, Y.; Culpitt, T.; Hammes-Schiffer, S., Multicomponent Time-Dependent Density Functional Theory: Proton and Electron Excitation Energies. *J. Phys. Chem. Lett.* **2018,** *9*, 1765-1770.

(19)   Yang, Y.; Culpitt, T.; Tao, Z.; Hammes-Schiffer, S., Stability conditions and local minima in multicomponent Hartree-Fock and density functional theory. *J. Chem. Phys.* **2018,** *149*, 084105.

(20)   Culpitt, T.; Yang, Y.; Pavošević, F.; Tao, Z.; Hammes-Schiffer, S., Enhancing the applicability of multicomponent time-dependent density functional theory. *J. Chem. Phys.* **2019,** *150*, 201101.

(21)   Wang, Y.-H.; Goldsmith, Z. K.; Schneider, P. E.; Anson, C. W.; Gerken, J. B.; Ghosh, S.; Hammes-Schiffer, S.; Stahl, S. S., Kinetic and Mechanistic Characterization of Low-Overpotential, H2O2-Selective Reduction of O2 Catalyzed by N2O2-Ligated Cobalt Complexes. *J. Am. Chem. Soc.* **2018,** *140*, 10890-10899.

(22)   Wang, Y.-H.; Schneider, P. E.; Goldsmith, Z. K.; Mondal, B.; Hammes-Schiffer, S.; Stahl, S. S., Brønsted Acid Scaling Relationships Enable Control Over Product Selectivity from O2 Reduction with a Mononuclear Cobalt Porphyrin Catalyst. *ACS Cent. Sci.* **2019,** *5*, 1024-1034.

(23)   Zhao, L.; Wildman, A.; Tao, Z.; Schneider, P.; Hammes-Schiffer, S.; Li, X., Nuclear–electronic orbital Ehrenfest dynamics. *J. Chem. Phys.* **2020,** *153*, 224111.

(24)   Heins, S. P.; Schneider, P. E.; Speelman, A. L.; Hammes-Schiffer, S.; Appel, A. M., Electrocatalytic Oxidation of Alcohol with Cobalt Triphosphine Complexes. *ACS Catal.* **2021,** *11*, 6384-6389.

(25)   Tao, Z.; Roy, S.; Schneider, P. E.; Pavošević, F.; Hammes-Schiffer, S., Analytical Gradients for Nuclear–Electronic Orbital Time-Dependent Density Functional Theory: Excited-State Geometry Optimizations and Adiabatic Excitation Energies. *J. Chem. Theory Comput.* **2021**.

Chapter Two

Diagonal Born-Oppenheimer Corrections within the Nuclear-Electronic Orbital

Framework

Portions of this chapter are adapted and excerpted from the following reference with the

permission of the publisher:

Patrick E. Schneider, Fabijan Pavošević, and Sharon Hammes-Schiffer

Author contributions

P.E.S., F.P., and S.H.S. designed calculations. P.E.S. and F.P. derived the theory.

P.E.S. implemented the code for the computations and performed the calculations.

P.E.S. created the figures and tables. All authors wrote the manuscript.

Abstract

The nuclear-electronic orbital (NEO) method treats specified nuclei, typically protons, quantum mechanically on the same level as the electrons. This approach invokes the Born-Oppenheimer separation between the quantum and classical nuclei, as well as the conventional separation between the electrons and classical nuclei. To test the validity of this additional adiabatic approximation, herein the diagonal Born-Oppenheimer correction (DBOC) within the NEO framework is derived, analyzed, and calculated numerically for a set of eight molecules. Inclusion of the NEO DBOC is found to change the equilibrium bond lengths by only 10^{-4} Å and the heavy atom vibrational stretching frequencies by $\sim 1 - 2$ cm^{-1} per quantum proton bonded to an atom participating in the vibrational mode. These results imply that the DBOC does not significantly impact molecular properties computed with the NEO approach. Understanding the physical characteristics and quantitative contributions of the DBOC has broad implications for applications of multicomponent density functional theory and wavefunction methods.

11

Introduction

Nuclear quantum effects are manifested by phenomena such as zero-point energy, vibrational excitations, and hydrogen tunneling. Moreover, non-Born-Oppenheimer effects are significant in a wide range of chemical and biological processes, including those involving proton-coupled electron transfer.[1] Multicomponent methods, where more than one type of particle is treated quantum mechanically, have been developed to include nuclear quantum effects as well as some non-Born-Oppenheimer effects in quantum chemistry calculations.[2-5] A computationally tractable multicomponent method is the nuclear-electronic orbital (NEO) method.[5] The NEO method differs from conventional electronic structure methods in that specified nuclei, typically key protons, are treated quantum mechanically on the same level as the electrons, avoiding the Born-Oppenheimer separation between the specified nuclei and the electrons. Popular conventional electronic methods such as Hartree-Fock theory, density functional theory (DFT), or coupled cluster theory with single and double excitations (CCSD) have been adapted to the NEO framework in the form of NEO-HF, NEO-DFT, and NEO-CCSD, respectively.[5-9]

In the NEO approach, the system is divided into electrons, quantum nuclei, and other nuclei, which are typically denoted classical nuclei for simplicity, although they may be treated quantum mechanically in a different manner. The electrons and quantum nuclei are treated on the same level using molecular orbital techniques, and at least two classical nuclei are required to avoid difficulties with translations and rotations. The NEO potential energy surface depends on only the coordinates of the classical nuclei, and each point on this potential energy surface is determined by solving the

time-independent Schrödinger equation for the electrons and quantum nuclei with fixed

classical nuclei. Thus, at the core of the NEO method is the Born-Oppenheimer

separation between the classical nuclei and the subsystem consisting of the electrons

and quantum nuclei. In other words, the electrons and quantum nuclei are assumed to

respond instantaneously to the motion of the classical nuclei. Analogous to conventional

electronic structure calculations,[10-13] the diagonal Born-Oppenheimer corrections

(DBOCs) can be computed within the NEO framework and added to the NEO potential

energy surface to account for the most significant non-Born-Oppenheimer effects. The

magnitudes of these terms are related to the ratio of the masses of the two types of

particles, leading to the expectation that the DBOCs are significantly larger for protons

relative to other nuclei than for electrons relative to protons. The objective of this

chapter is to derive the equations for the NEO DBOCs and to compute them for a set of

eight molecules with varying numbers of quantum protons, analyzing their magnitudes

and impact on the NEO potential energy surfaces.

Theory

The adiabatic approximation for the total wavefunction within the NEO-HF and

NEO-DFT frameworks is

$$
\begin{aligned}
\Psi &= \psi_c(\mathbf{R})\psi_{NEO}(\mathbf{r}_e, \mathbf{r}_p; \mathbf{R}) \\
&= \psi_c(\mathbf{R})\psi_e(\mathbf{r}_e; \mathbf{R})\psi_p(\mathbf{r}_p; \mathbf{R})
\end{aligned}
\tag{2.1}
$$

where $\mathbf{r}_e$, $\mathbf{r}_p$, and $\mathbf{R}$ denote the collective coordinates of the electrons, quantum protons,

and classical nuclei, respectively, and $\psi_e(\mathbf{r}_e; \mathbf{R})$, $\psi_p(\mathbf{r}_p; \mathbf{R})$, and $\psi_c(\mathbf{R})$ denote the

wavefunctions associated with the electrons, quantum protons, and "classical" nuclei,

respectively. Here $\psi_{\mathrm{NEO}}(\mathbf{r}_{\mathrm{e}}, \mathbf{r}_{\mathrm{p}}; \mathbf{R})$ is the NEO wavefunction satisfying

$$H_{\mathrm{NEO}}\psi_{\mathrm{NEO}}(\mathbf{r}_{\mathrm{e}}, \mathbf{r}_{\mathrm{p}}; \mathbf{R}) = E_{\mathrm{NEO}}(\mathbf{R})\psi_{\mathrm{NEO}}(\mathbf{r}_{\mathrm{e}}, \mathbf{r}_{\mathrm{p}}; \mathbf{R}) \tag{2.2}$$

where the NEO Hamiltonian includes the kinetic energies of the electrons and quantum protons but not the kinetic energy of the classical nuclei. The second equality in Eq. (2.1) is valid only for NEO wavefunctions of the form $\psi_{\mathrm{NEO}}(\mathbf{r}_{\mathrm{e}}, \mathbf{r}_{\mathrm{p}}; \mathbf{R}) = \psi_{\mathrm{e}}(\mathbf{r}_{\mathrm{e}}; \mathbf{R})\psi_{\mathrm{p}}(\mathbf{r}_{\mathrm{p}}; \mathbf{R})$, as for NEO-HF and NEO-DFT. Furthermore, although the quantum nuclei are assumed to be protons, the expressions derived herein are valid for other types of quantum nuclei as well.

The variational optimization of $\psi_{\mathrm{c}}(\mathbf{R})$ leads to the following equation for the "classical" nuclei

$$\left[-\frac{1}{2}\sum_{I}\frac{1}{M_{I}}\nabla_{I}^{2} - \left\langle \psi_{\mathrm{e}}\psi_{\mathrm{p}} \left| \frac{1}{2}\sum_{I}\frac{1}{M_{I}}\nabla_{I}^{2}(\psi_{\mathrm{e}}\psi_{\mathrm{p}}) \right\rangle + E_{\mathrm{NEO}}(\mathbf{R}) \right]\psi_{\mathrm{c}} = E\psi_{\mathrm{c}} \tag{2.3}$$

where the summations are over all "classical" nuclei, which have masses M_I. The Born-Oppenheimer NEO potential energy surface is $E_{\mathrm{NEO}}(\mathbf{R})$, and the NEO DBOC is the second term on the left side of Eq. (2.3). The NEO DBOC can be expressed as

$$\begin{aligned} E_{\mathrm{DBOC}} &= -\sum_{I}\frac{1}{2M_{I}}\left\langle \psi_{\mathrm{e}}\psi_{\mathrm{p}} \,|\, \nabla_{I}^{2}(\psi_{\mathrm{e}}\psi_{\mathrm{p}}) \right\rangle \\ &= -\sum_{I}\frac{1}{2M_{I}}\left[\left\langle \psi_{\mathrm{e}} \,|\, \nabla_{I}^{2}\psi_{\mathrm{e}} \right\rangle + \left\langle \psi_{\mathrm{p}} \,|\, \nabla_{I}^{2}\psi_{\mathrm{p}} \right\rangle \right] \\ &= \sum_{I}\frac{1}{2M_{I}}\left[\left\langle \nabla_{I}\psi_{\mathrm{e}} \,|\, \nabla_{I}\psi_{\mathrm{e}} \right\rangle + \left\langle \nabla_{I}\psi_{\mathrm{p}} \,|\, \nabla_{I}\psi_{\mathrm{p}} \right\rangle \right] \end{aligned} \tag{2.4}$$

The electronic term has the identical form as the DBOC in conventional electronic

14

structure theory.[10-13] Note that the DBOC would have a more complicated form if the NEO wavefunction were not simply the product of electronic and protonic wavefunctions. Extensions of this NEO DBOC derivation to correlated wavefunction NEO methods, such as NEO-CCSD[9] and configuration interaction methods, may be implemented following the analogous derivations for conventional electronic structure theory.[13-17] Note also that the DBOC is rigorously derived for wave function theories but in practice can be computed for the Kohn-Sham determinant within the framework of DFT, as discussed further below.

The programmable equations for the numerical calculation of the electronic and protonic DBOCs, respectively, are as follows:

$$E_{\text{DBOC}}^{\text{e}} = \sum_I \frac{1}{2M_I} \langle \nabla_I \psi_{\text{e}} | \nabla_I \psi_{\text{e}} \rangle = \sum_I \frac{1 - S_{\pm I}^{\text{e}}}{4\delta^2 M_I} \qquad (2.5)$$

$$E_{\text{DBOC}}^{\text{p}} = \sum_I \frac{1}{2M_I} \langle \nabla_I \psi_{\text{p}} | \nabla_I \psi_{\text{p}} \rangle = \sum_I \frac{1 - S_{\pm I}^{\text{p}}}{4\delta^2 M_I} \qquad (2.6)$$

$$S_{\pm I}^{j} = \langle \psi_j(\mathbf{R} + \delta_I) | \psi_j(\mathbf{R} - \delta_I) \rangle, \quad j = \text{e, p} \qquad (2.7)$$

where δ is the step size in the numerical differentiation, and $S_{\pm I}^{\text{e}}$ and $S_{\pm I}^{\text{p}}$ are electronic and protonic wavefunction overlaps of perturbed geometries, respectively.[13] Typically the quantum subsystem includes both α- and β-spin electrons but only high-spin quantum protons (i.e., the protons are localized with only a single proton occupying each molecular orbital).

To provide a qualitative comparison of the electronic and protonic DBOCs, we examine two simple model systems. The electronic DBOC for the hydrogen atom in

units of Hartree is $E_{\text{DBOC}}^{\text{e}} = \dfrac{m_{\text{e}}}{2m_{\text{p}}}$, which is 0.27 mH or 60 cm⁻¹.[18] The analog for the

protonic DBOC is a diatomic molecule, in which the heavy atom has mass M_C and the

hydrogen atom has mass m_{p}, with a single vibrational mode of frequency v that can be

described by a one-dimensional harmonic oscillator model. The protonic DBOC for this

model system is $E_{\text{DBOC}}^{\text{p}} = \dfrac{m_{\text{p}}}{2M_C} \dfrac{hv}{2}$, where the second factor is the zero-point energy

associated with the vibrational mode (see Appendix A for details). To provide a

qualitative estimate, if v = 2000 cm⁻¹ and M_C = 10m_{p}, then $E_{\text{DBOC}}^{\text{p}}$ = 50 cm⁻¹, which is of

similar magnitude as $E_{\text{DBOC}}^{\text{e}}$ for the hydrogen atom. Moreover, $E_{\text{DBOC}}^{\text{e}}$ and $E_{\text{DBOC}}^{\text{p}}$ for these

model systems are each expressed as the product of a ratio of masses and an intrinsic

energy (i.e., the Hartree for the hydrogen atom and the zero-point energy associated

with the vibrational mode for the diatomic molecule). We emphasize that these model

systems do not account for the complexities of molecules, which involve many heavy

nuclei of varying masses and nuclear charges, multiple types of electrons (i.e., core and

valence), and proton vibrational modes of different types and frequencies.

Nevertheless, these model systems illustrate the common form of the electronic and

protonic DBOCs, as well as the dependence of the protonic DBOC on the frequencies

associated with the quantum protons.

Results and Discussion

We computed the DBOCs for a diverse set of molecules with varying numbers of

quantum protons. For each molecule, all electrons and all protons were treated

quantum mechanically, as depicted for two molecules in Figure 2.1. The geometry of

each system was optimized at the NEO-DFT level using the B3LYP electronic exchange-correlation functional[19-21] and the epc17-2 electron-proton correlation functional[8] unless otherwise specified. Note that the choice of electronic exchange-correlation functional is not expected to impact the conclusions based on the analysis herein.[22] The cc-pVTZ electronic basis set[23] was used in conjunction with an even-tempered $8s8p8d8f$ nuclear basis set with $\alpha = 2\sqrt{2}$ and $\beta = \sqrt{2}$.[24] The electronic and nuclear basis function centers for each quantum hydrogen were chosen to be the same and were optimized variationally as part of the single-point NEO energy calculations. All of the conventional electronic DFT calculations were performed at the B3LYP/cc-pVTZ level. An in-house developmental version of the GAMESS quantum chemistry package[25] was used for the NEO calculations. The convergence criteria for both the electronic and nuclear densities in the self-consistent-field (SCF) procedure were 10^{-8}, which is tighter than the default values because the numerical DBOC is highly sensitive to slight changes in the wavefunction between perturbed geometries. Equations (2.5)–(2.7) were used to compute the total NEO DBOC, as well as the electronic and protonic components, by perturbing each classical coordinate by $\delta = 10^{-3}$ Bohr, which was found to be sufficient for the desired level of accuracy (Tables A2 and A3 of Appendix A). For comparison, the DBOC computed with conventional electronic DFT was also calculated.

Table 2.1 presents the total NEO DBOC, the corresponding electronic and protonic components, and the conventional electronic DBOC, denoted $E_{\text{DBOC}}^{\text{e,conv}}$, for eight molecules. The numerical precision of the calculated values of the DBOC is ~0.1 cm^{-1} (Table S1). For each of these molecules, the electronic component of the NEO DBOC is 30–45 cm^{-1} lower per quantum proton than the DBOC computed with conventional

electronic DFT. This trend is a direct consequence of the quantization of the protons in the NEO-DFT framework, leading to a reduced number of "classical" nuclear coordinates and a smaller number of terms in the NEO-DBOC compared to the conventional electronic DBOC. As further validation of our calculations, the conventional DFT DBOC values for HCN and HCC$^-$ are in agreement with literature values of 838 and 769 cm^{-1}, respectively, using Hartree-Fock theory with the aug-cc-pVTZ basis set.[26]

The protonic components of the NEO DBOC exhibit more widely varying behavior in Table 1. The three terminal single-proton systems all yield comparable values for the protonic contribution to the NEO DBOC. The magnitude of $E_{\text{DBOC}}^{\text{p}}$ is somewhat smaller than the magnitude of $E_{\text{DBOC}}^{\text{e}}$, an apparent contradiction given the significantly larger mass of a proton compared to an electron, which would be expected to lead to larger non-Born-Oppenheimer effects. However, accounting for the significantly larger number of electrons than quantum protons, a single proton is found to contribute more to the DBOC than does a single electron for most systems studied. Moreover, as discussed above in the context of simple model systems, the DBOC is expected to depend qualitatively on an intrinsic energy, which is related to the proton vibrational frequencies for $E_{\text{DBOC}}^{\text{p}}$, as well as the masses.

Although $E_{\text{DBOC}}^{\text{e,conv}}$ per electron in analogous conventional electronic structure calculations has been suggested to be approximately constant,[27] $E_{\text{DBOC}}^{\text{p}}$ per quantum proton is not generally constant. In particular, the value of $E_{\text{DBOC}}^{\text{p}}$ for the internal single-proton system of FHF$^-$ is nearly an order of magnitude smaller than the values for the terminal single-proton systems, most likely due to the significantly lower vibrational

frequency associated with the internal hydrogen. On the other hand, comparison of $E_{\text{DBOC}}^{\text{p}}$ for HCC⁻ and HCCH demonstrates an additive effect for the terminal protons in these systems. Specifically, $E_{\text{DBOC}}^{\text{p}}$ almost exactly doubles for HCCH compared to HCC⁻, indicating a constant $E_{\text{DBOC}}^{\text{p}}$ per quantum proton in this case, which is consistent with the nearly identical vibrational frequencies associated with these two hydrogens. In contrast, further increasing the number of protons to generate H_2CCH_2 and H_3CCH_3 does not add a constant amount per proton, but rather adds a smaller amount per proton as the total number of protons increases, reflecting the lower vibrational frequencies associated with the hydrogens in these molecules.

The effect of electron-proton correlation on the NEO DBOC and its components was also investigated. As shown in Table 2.2, the electronic contribution to the NEO DBOC, $E_{\text{DBOC}}^{\text{e}}$, is not significantly influenced by electron-proton correlation. In contrast, the protonic contribution, $E_{\text{DBOC}}^{\text{p}}$, is strongly influenced by electron-proton correlation. Specifically, the $E_{\text{DBOC}}^{\text{p}}$ values obtained with NEO-HF and NEO-DFT/no-epc, which do not include any electron-proton correlation, are over twice the values obtained with NEO-DFT/epc17-1 and NEO-DFT/epc17-2, which include electron-proton correlation. This difference can be attributed to the highly localized proton densities produced by the methods neglecting electron-proton correlation,[7] manifesting in smaller overlaps between the perturbed geometries in Eq (2.6) and thus leading to larger values of $E_{\text{DBOC}}^{\text{p}}$. Electron correlation does not impact either the electronic[13] or the protonic contributions to the DBOC, as indicated by the nearly identical results obtained from NEO-HF and NEO-DFT/no-epc. Although the DBOC is rigorously derived for wave function theories,

19

the similar values of the DBOC obtained with Hartree-Fock and DFT (Table 2.1

compared to Ref. [26] and Table 2.2) provides some justification for computing the DBOC

within the DFT framework as an estimate of non-Born-Oppenheimer effects.

Despite the relatively large magnitudes of the NEO DBOC values, the impact of

the DBOC on the NEO potential energy surface is more important for determining its

practical significance. In the context of conventional electronic Hartree-Fock

calculations, Handy and Lee examined the impact of the electronic DBOC on the

potential energy surface for a set of diatomic molecules.[18] Although the conventional

electronic DBOC can be on the order of ~1000 cm^{-1} for these diatomics, the equilibrium

bond length was found to change by less than 10^{-3} Bohr for H_2 and less than 10^{-4} Bohr

for the other diatomics, and the frequencies were found to change by only ~3 cm^{-1} for

H_2 and by less than 0.1 cm^{-1} for the diatomics that do not contain hydrogen.

With this previous work as inspiration, we examined the equilibrium bond lengths

and vibrational frequencies corresponding to $E_{\mathrm{NEO}}(\mathbf{R}) + E_{\mathrm{DBOC}}^{\mathrm{tot}}(\mathbf{R})$ for eight molecules.

Each molecule contains only two classical nuclei because all protons are treated

quantum mechanically on the same level as the electrons. The frequency for the heavy

atom stretching motion for each molecule was calculated via a finite difference second

derivative, effectively making the DBOC contribution to the stretching frequency a

numerical fourth derivative. As a result, the numerical precision is estimated to be lower

for the vibrational frequency than for the magnitude of the DBOC. In particular, the

numerical precision for the vibrational frequencies is estimated to be ~1 cm^{-1} or slightly

greater in some cases (Tables A2 and A3 of Appendix A). When the DBOC is included

in the potential energy surface, the equilibrium bond length for the heavy nuclei changes

on the order of 10^{-4} Å for a stabilization in energy of less than 1 μHartree. This extremely small change in bond length was not considered when calculating the effect of the DBOC on the vibrational frequencies presented herein. However, the frequencies computed at the DBOC optimized geometries for several of the triatomic molecules are available in Appendix A (Table A4).

Table 2.3 presents the vibrational stretching frequencies for the heavy atom mode in each molecule computed with and without the NEO DBOC. These data illustrate that inclusion of the electronic component of the DBOC, $E_{\mathrm{DBOC}}^{\mathrm{e}}$, increases the vibrational frequency by no more than 1 cm^{-1}. The protonic component, $E_{\mathrm{DBOC}}^{\mathrm{p}}$, has a similarly small effect of ~1 cm^{-1} for the molecules with one or two quantum protons, but this effect increases for molecules with more quantum protons. The quantum protons are expected to influence only the stretching modes associated with atoms to which they are bonded. Even in the extreme case of ethane, with six quantum protons adjacent to the heavy atom vibrational mode, $E_{\mathrm{DBOC}}^{\mathrm{p}}$ only changes the vibrational frequency by 11 cm^{-1}. Although this effect is expected to be even smaller for typical modes, the DBOC could be included in the NEO potential energy surface routinely by computing it analytically. The analytical computation of the NEO Hessian and the DBOC is a direction of current research.

Furthermore, when the DBOC effects are considered to be significant, they can be included in the calculation of the molecular vibrational frequencies using the NEO methodology developed recently to couple the classical and quantum mechanical vibrational modes.[28] This approach entails diagonalization of an extended NEO Hessian that depends on the expectation values of the quantum protons as well as the

coordinates of the classical nuclei. The practical incorporation of the DBOCs within this strategy requires the assumption that the partial second derivatives of the DBOCs with respect to the expectation values of the quantum protons are negligible.

Conclusions

In this chapter, the diagonal Born-Oppenheimer correction within the NEO multicomponent framework was derived, and its magnitude and significance were analyzed for a set of molecules. In terms of the magnitude of the DBOC, the contribution from the quantum protons was found to be of similar order of magnitude as the contribution from the electrons for the molecules studied. The contribution per proton is greater than the contribution per electron, but the molecules contain significantly more electrons than quantum protons. Inclusion of the DBOC was found to change the equilibrium bond lengths on the order of 10^{-4} Å and to change the vibrational frequencies by ~1–2 cm^{-1} per quantum proton bonded to one of the atoms participating in the vibrational mode. These results suggest that the non-Born-Oppenheimer effects arising from the adiabatic separation between the quantum protons and the other nuclei in the NEO framework do not significantly impact molecular properties and may simply shift the energy of the entire potential energy surface by a constant amount. In this case, the DBOC would not need to be considered when generating reaction paths and dynamics on the NEO potential energy surface. If the DBOC becomes important at certain nonequilibrium geometries, it can be incorporated using the formalism described in this work.

Figures and Tables
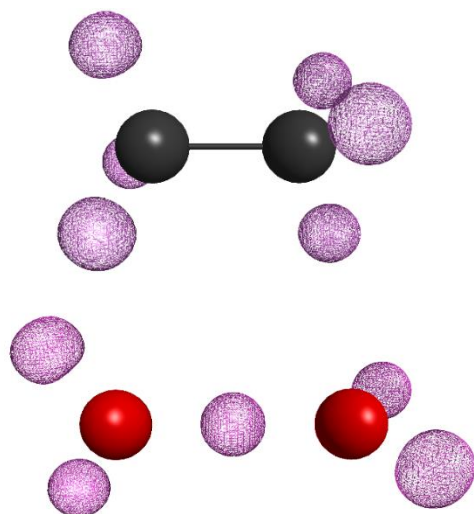
Figure 2.1: Proton orbitals (pink mesh) obtained from NEO-DFT/B3LYP/epc17-2 calculations of ethane (top) and $H_5O_2^+$ (bottom).

Table 2.1: Total NEO DBOC, the Electronic and Protonic Components, and the Conventional Electronic DBOC.[a]

	HCN	HNC	HCC$^-$	HCCH	H$_2$CCH$_2$	H$_3$CCH$_3$	FHF$^-$	H$_5$O$_2^+$
$E_{\text{DBOC}}^{\text{tot}}$	1335	1210	1250	1790	2187	2502	1173	1745
$E_{\text{DBOC}}^{\text{e}}$	805	802	728	742	751	760	1130	1043
$E_{\text{DBOC}}^{\text{p}}$	530	407	522	1048	1435	1742	43	702
$E_{\text{DBOC}}^{\text{e,conv}}$	839	833	770	808	928	1035	1159	1193

[a]All NEO calculations were performed at the DFT/B3LYP/epc17-2 level of theory with the basis sets given in the text. The conventional electronic calculations were performed at the DFT/B3LYP/cc-pVTZ level of theory. All energies are given in units of cm^{-1}.

Table 2.2: Effect of Electron-Proton Correlation on NEO DBOC and its Components for HCN.[a]

	NEO-HF	NEO-DFT		
		no-epc	epc17-1	epc17-2
$E_{\text{DBOC}}^{\text{tot}}$	1928	1928	1237	1335
$E_{\text{DBOC}}^{\text{e}}$	807	806	804	805
$E_{\text{DBOC}}^{\text{p}}$	1121	1122	433	530

[a]All NEO-DFT calculations were performed with the B3LYP electronic functional and with no electron-proton correlation, denoted no-epc, or the epc17-1 or epc17-2 electron-proton correlation functional. The geometry was optimized at each level of theory. All energies are given in units of cm^{-1}.

Table 2.3: Vibrational Stretching Frequencies for the Heavy Atom Mode in the NEO Framework with and without the NEO DBOC and its Components.[a]

	HCN	HNC	HCC⁻	HCCH	H_2CCH_2	H_3CCH_3	FHF⁻	$H_5O_2^+$
No DBOC	2293	2160	1963	2207	1642	1061	607	642
With E_{DBOC}^{e}	2293	2160	1963	2208	1642	1062	607	643
With E_{DBOC}^{p}	2293	2161	1962	2209	1648	1072	606	648
With E_{DBOC}^{tot}	2293	2161	1962	2209	1648	1073	606	648

[a]For all of these molecules, the NEO potential energy surface is one-dimensional with a single vibrational mode because all protons are treated quantum mechanically and each molecule has only two heavy atoms. All calculations were performed at the NEO-DFT/B3LYP/epc17-2 level of theory with the basis sets given in the text. All energies are given in units of cm⁻¹. The numerical precision of the vibrational frequency calculations including the DBOC was determined to be typically 1 cm⁻¹ or slightly greater in some cases (see Appendix A for details).

Supplemental Information

The Supporting Information is available free of charge on the ACS Publications website at DOI: 10.1021/acs.jpclett.9b01803. Analysis of a simple model for protonic DBOC and tests of numerical precision are found in Appendix A.

Acknowledgments

References

(1)   Hammes-Schiffer, S.; Stuchebrukhov, A. A., Theory of Coupled Electron and Proton Transfer Reactions. *Chem. Rev.* **2010,** *110*, 6939-6960.

(2)   Thomas, I. L., Protonic Structure of Molecules. I. Ammonia Molecules. *Phys. Rev.* **1969,** *185*, 90-94.

(3)   Capitani, J. F.; Nalewajski, R. F.; Parr, R. G., Non-Born–Oppenheimer density functional theory of molecular systems. *J. Chem. Phys.* **1982,** *76*, 568-573.

(4)   Kreibich, T.; Gross, E. K. U., Multicomponent Density-Functional Theory for Electrons and Nuclei. *Phys. Rev. Lett.* **2001,** *86*, 2984-2987.

(5)   Webb, S. P.; Iordanov, T.; Hammes-Schiffer, S., Multiconfigurational nuclear-electronic orbital approach: Incorporation of nuclear quantum effects in electronic structure calculations. *J. Chem. Phys.* **2002,** *117*, 4106-4118.

(6)   Pak, M. V.; Chakraborty, A.; Hammes-Schiffer, S., Density Functional Theory Treatment of Electron Correlation in the Nuclear−Electronic Orbital Approach. *J. Phys. Chem. A* **2007,** *111*, 4522-4526.

(7)   Yang, Y.; Brorsen, K. R.; Culpitt, T.; Pak, M. V.; Hammes-Schiffer, S., Development of a practical multicomponent density functional for electron-proton correlation to produce accurate proton densities. *J. Chem. Phys.* **2017,** *147*, 114113.

(8)   Brorsen, K. R.; Yang, Y.; Hammes-Schiffer, S., Multicomponent Density Functional Theory: Impact of Nuclear Quantum Effects on Proton Affinities and Geometries. *J. Phys. Chem. Lett.* **2017,** *8*, 3488-3493.

(9)   Pavošević, F.; Culpitt, T.; Hammes-Schiffer, S., Multicomponent Coupled Cluster Singles and Doubles Theory within the Nuclear-Electronic Orbital Framework. *J. Chem. Theory Comput.* **2019,** *15*, 338-347.

(10)   Sellers, H.; Pulay, P., The adiabatic correction to molecular potential surfaces in the SCF approximation. *Chem. Phys. Lett.* **1984,** *103*, 463-465.

(11)   Handy, N. C.; Yamaguchi, Y.; III, H. F. S., The diagonal correction to the Born–Oppenheimer approximation: Its effect on the singlet–triplet splitting of CH2 and other molecular effects. *J. Chem. Phys.* **1986,** *84*, 4481-4484.

(12)   Ioannou, A. G.; Amos, R. D.; Handy, N. C., The diagonal born-oppenheimer correction for He2+ and F+H2. *Chem. Phys. Lett.* **1996,** *251*, 52-58.

(13)   Valeev, E. F.; Sherrill, C. D., The diagonal Born–Oppenheimer correction beyond the Hartree–Fock approximation. *J. Chem. Phys.* **2003,** *118*, 3921-3927.

(14)   Schwenke, D. W., Beyond the Potential Energy Surface: Ab initio Corrections to the Born−Oppenheimer Approximation for H2O. *J. Phys. Chem. A* **2001,** *105*, 2352-2360.

(15)   Gauss, J.; Tajti, A.; Kállay, M.; Stanton, J. F.; Szalay, P. G., Analytic calculation of the diagonal Born-Oppenheimer correction within configuration-interaction and coupled-cluster theory. *J. Chem. Phys.* **2006,** *125*, 144111.

(16)   Tajti, A.; Szalay, P. G.; Gauss, J., Perturbative treatment of the electron-correlation contribution to the diagonal Born-Oppenheimer correction. *J. Chem. Phys.* **2007,** *127*, 014102.

(17)   Liévin, J.; Demaison, J.; Herman, M.; Fayt, A.; Puzzarini, C., Comparison of the experimental, semi-experimental and ab initio equilibrium structures of acetylene: Influence of relativisitic effects and of the diagonal Born–Oppenheimer corrections. *J. Chem. Phys.* **2011,** *134*, 064119.

(18)   Handy, N. C.; Lee, A. M., The adiabatic approximation. *Chem. Phys. Lett.* **1996,** *252*, 425-430.

(19)   Becke, A. D., Density-functional exchange-energy approximation with correct asymptotic behavior. *Phys. Rev. A* **1988,** *38*, 3098-3100.

(20)   Becke, A. D., Density-functional thermochemistry. III. The role of exact exchange. *J. Chem. Phys.* **1993,** *98*, 5648-5652.

(21)   Lee, C.; Yang, W.; Parr, R. G., Development of the Colle-Salvetti correlation-energy formula into a functional of the electron density. *Phys. Rev. B* **1988,** *37*, 785-789.

(22)   Brorsen, K. R.; Schneider, P. E.; Hammes-Schiffer, S., Alternative forms and transferability of electron-proton correlation functionals in nuclear-electronic orbital density functional theory. *J. Chem. Phys.* **2018,** *149*, 044110.

(23)   Dunning, T. H., Jr., Gaussian basis sets for use in correlated molecular calculations. I. The atoms boron through neon and hydrogen. *J. Chem. Phys.* **1989,** *90*, 1007-1023.

(24)   Feller, D. F.; Ruedenberg, K., Systematic approach to extended even-tempered orbital bases for atomic and molecular calculations. *Theor. Chim. Acta* **1979,** *52*, 231-251.

(25)   Schmidt, M. W.; Baldridge, K. K.; Boatz, J. A.; Elbert, S. T.; Gordon, M. S.; Jensen, J. H.; Koseki, S.; Matsunaga, N.; Nguyen, K. A.; Su, S.; Windus, T. L.; Dupuis, M.; Montgomery Jr, J. A., General atomic and molecular electronic structure system. *J. Comput. Chem.* **1993,** *14*, 1347-1363.

(26)   Tajti, A.; Szalay, P. G.; Császár, A. G.; Kállay, M.; Gauss, J.; Valeev, E. F.; Flowers, B. A.; Vázquez, J.; Stanton, J. F., HEAT: High accuracy extrapolated ab initio thermochemistry. *J. Chem. Phys.* **2004,** *121*, 11599-11613.

(27)   Mohallem, J. R., Semiempirical evaluation of post-Hartree–Fock diagonal-Born–Oppenheimer corrections for organic molecules. *J. Chem. Phys.* **2008,** *128*, 144113.

(28)   Yang, Y.; Schneider, P. E.; Culpitt, T.; Pavošević, F.; Hammes-Schiffer, S., Molecular Vibrational Frequencies within the Nuclear–Electronic Orbital Framework. *J. Phys. Chem. Lett.* **2019,** *10*, 1167-1172.

Chapter Three

Transition States, Reaction Paths, and Thermochemistry Using the Nuclear-Electronic
Orbital Analytic Hessian

Portions of this chapter are adapted and excerpted from the following reference with the

permission of the publisher:

Patrick E. Schneider, Zhen Tao, Fabijan Pavošević, Evgeny Epifanovsky, Xintian Feng,
and Sharon Hammes-Schiffer

Author contributions

P.E.S. and S.H.S. designed calculations. P.E.S. derived the theory. Z.T., F.P, E.E., and X.F. provided coding utilities. P.E.S. implemented the theory as code and performed the computations. P.E.S. created the figures and tables. P.E.S., Z.T., F.P., and S.H.S. wrote the manuscript.

Abstract

The nuclear-electronic orbital (NEO) method is a multicomponent quantum chemistry theory that describes electronic and nuclear quantum effects simultaneously while avoiding the Born-Oppenheimer approximation. Specified nuclei are treated quantum mechanically on the same level as the electrons, and the NEO potential energy surface depends on the classical nuclear coordinates. Herein theoretical methodology is developed to optimize and characterize stationary points on the NEO potential energy surface, to generate multicomponent minimum energy paths, and to compute thermochemical properties. For this purpose, the analytic coordinate Hessian is developed and implemented at the NEO Hartree-Fock level of theory. These NEO Hessians are used to study the S_N2 reaction of $ClCH_3Cl^-$ and the hydride transfer of $C_4H_9^+$. For each system, analysis of the single imaginary mode at the transition state and the intrinsic reaction coordinate along the minimum energy path identifies the dominant nuclear motions driving the chemical reaction. Visualization of the electronic and protonic orbitals along the minimum energy path illustrates the coupled electronic and protonic motions beyond the Born-Oppenheimer approximation. This work provides the foundation for applying the NEO approach at various correlated levels of theory to a wide range of chemical reactions.

Introduction

To incorporate nuclear quantum effects during the optimization of geometries and the generation of minimum energy paths for chemical systems in a computationally tractable manner, approaches beyond conventional quantum chemistry methods must be developed. One such approach is multicomponent quantum chemistry theory, where more than one type of particle is treated quantum mechanically on the same level with molecular orbital techniques.[1-7] The nuclear-electronic orbital (NEO) multicomponent theory[4, 8] treats specified nuclei, typically key protons, and all electrons quantum mechanically. This approach removes the Born-Oppenheimer separation between the electrons and the quantum nuclei but invokes a Born-Oppenheimer separation between the quantum portion of the system (i.e., the specified quantum nuclei and electrons) and the remaining nuclei, which are typically denoted "classical" for notational convenience.

Within the NEO framework, the potential energy surface (PES) and the associated coordinate NEO Hessian depend on only the classical nuclei. The NEO PES inherently includes the quantum mechanical effects associated with the specified quantum nuclei, such as zero-point energy and nuclear delocalization. The NEO optimized geometries are stationary points on the NEO PES. These optimized geometries can be characterized by a vibrational analysis based on diagonalization of the NEO Hessian.[9] In this manner, the stationary points can be identified as minima or transition states (i.e., first-order saddle points). Moreover, the imaginary mode associated with a NEO transition state can be analyzed to elucidate the dominant motions contributing to the chemical reaction. Related to this analysis, the minimum energy path (MEP) from a NEO transition state down to the reactant and product states

can also be computed on the NEO PES.

The nuclear motions associated with the imaginary mode at the NEO transition state and the intrinsic reaction coordinate along the MEP provide insight into the dominant motions of the classical nuclei that drive the chemical reaction. This framework is particularly relevant to hydrogen transfer (i.e., proton, hydride, and proton-coupled electron transfer), where the transferring hydrogen nucleus is treated quantum mechanically.[10-12] In this case, the NEO MEP elucidates the classical nuclear motions that drive hydrogen transfer, analogous to conventional electronic structure calculations probing the nuclear motions that drive electron transfer.[13-15] Due to the simultaneous quantum mechanical treatment of electrons and protons, analysis of the electronic and nuclear orbitals or densities along the MEP can provide mechanistic information, such as whether the electron and proton transfer synchronously or asynchronously in a proton-coupled electron transfer reaction.[16] Despite the conceptual simplicity and utility, NEO MEPs have not previously been implemented.

Although these types of analyses of the NEO PES provide useful insights, the calculation of full molecular vibrational frequencies requires inclusion of the coupling between the classical and quantum nuclei,[17-18] and a complete understanding of the chemical reaction path should also include this coupling. For this purpose, an extended NEO PES can be defined to include the expectation values of the quantum nuclei. All stationary points on the NEO PES are also stationary points on the extended NEO PES because of the variational principle, as discussed elsewhere.[17] Previously we developed the methodology to compute the extended NEO Hessian, which is defined in terms of second derivatives with respect to the classical nuclear coordinates and expectation

values of the quantum nuclei on the extended NEO PES.[17-18] The stationary points on the extended NEO PES can be characterized as minima or transition states by a vibrational analysis based on diagonalization of the extended NEO Hessian. Moreover, analysis of the imaginary mode at the transition state on the extended NEO PES provides insights into the role of the quantum protons in the chemical reaction. This extended Hessian approach has been shown to produce accurate molecular vibrational frequencies that incorporate significant anharmonic effects[17-18] but has not previously been used for the analysis of transition states.

The goal of this paper is to develop the methodology to characterize stationary points on the NEO PES and extended NEO PES, generate the NEO MEP, and perform thermochemistry calculations. All of these objectives require the NEO coordinate Hessian. Previous work has utilized either a semi-numerical or fully numerical implementation for calculations of the NEO Hessian.[9] However, as the field of multicomponent quantum chemistry expands and larger systems are studied, an analytic implementation of the NEO Hessian is necessary. Herein, we develop and implement analytic Hessians at the NEO-HF level of theory. We also use these analytic NEO Hessians to characterize stationary points, generate MEPs, and calculate thermochemical properties for two chemical systems: the self-exchange S_N2 reaction of $ClCH_3Cl^-$ and the intramolecular hydride shift in $C_4H_9^+$. This work provides the foundation for future extensions to compute NEO Hessians at correlated levels of theory, such as NEO coupled cluster singles and doubles (NEO-CCSD),[19] NEO orbital optimized second-order perturbation theory (NEO-OOMP2),[20] and NEO density functional theory (NEO-DFT).[21-25] Moreover, the results and analyses highlight the

fundamental conceptual insights obtained by computing MEPs within the NEO framework.

Theory

General Definition of the NEO Hessian

The Hamiltonian in the NEO framework is given by

$$
\begin{aligned}
H_{\mathrm{NEO}} = &-\frac{1}{2}\sum_{i}^{N_{\mathrm{e}}}\nabla_{i}^{2} - \sum_{i}^{N_{\mathrm{e}}}\sum_{A}^{N_{\mathrm{c}}}\frac{Z_{A}}{|\mathbf{r}_{i}^{\mathrm{e}}-\mathbf{r}_{A}^{\mathrm{c}}|} + \sum_{i>j}^{N_{\mathrm{e}}}\frac{1}{|\mathbf{r}_{i}^{\mathrm{e}}-\mathbf{r}_{j}^{\mathrm{e}}|} \\
&-\frac{1}{2m_{\mathrm{p}}}\sum_{i'}^{N_{\mathrm{p}}}\nabla_{i'}^{2} + \sum_{i'}^{N_{\mathrm{p}}}\sum_{A}^{N_{\mathrm{c}}}\frac{Z_{A}}{|\mathbf{r}_{i'}^{\mathrm{p}}-\mathbf{r}_{A}^{\mathrm{c}}|} + \sum_{i'>j'}^{N_{\mathrm{p}}}\frac{1}{|\mathbf{r}_{i'}^{\mathrm{p}}-\mathbf{r}_{j'}^{\mathrm{p}}|} \\
&-\sum_{i}^{N_{\mathrm{e}}}\sum_{i'}^{N_{\mathrm{p}}}\frac{1}{|\mathbf{r}_{i}^{\mathrm{e}}-\mathbf{r}_{i'}^{\mathrm{p}}|} + \sum_{A>B}^{N_{\mathrm{c}}}\frac{Z_{A}Z_{B}}{|\mathbf{r}_{A}^{\mathrm{c}}-\mathbf{r}_{B}^{\mathrm{c}}|}
\end{aligned} \tag{3.1}
$$

where electronic coordinates $\mathbf{r}^{\mathrm{e}}$ are indicated by lower-case indices i and j, quantum nuclear coordinates $\mathbf{r}^{\mathrm{p}}$ are indicated by primed versions of these indices, and the remaining classical nuclear coordinates $\mathbf{r}^{\mathrm{c}}$ are indicated by capital indices A and B. Moreover, N_{e}, N_{p}, and N_{c} denote the number of electrons, quantum nuclei, and classical nuclei, respectively. The proton mass is denoted by m_{p}. The Hamiltonian in Eq. (3.1) includes the standard electronic terms (i.e., the kinetic energy, interaction of the electrons with the classical nuclei, and electron-electron repulsion terms), the analogous quantum proton terms, the electron-proton attraction terms, and the classical nuclear repulsion term. For ease of presentation, the quantum nuclei are presumed to be protons, but this approach is generalizable for any type of particle and multiple types of particles. The NEO energy is computed as the expectation value of the NEO Hamiltonian in Eq. (3.1) with respect to the mixed nuclear-electronic wave function, which is typically expressed in terms of electronic and nuclear orbitals that are expanded in electronic and nuclear basis sets.

Within this framework, the NEO PES depends on only the positions of the classical nuclei, represented by the collective coordinate $\mathbf{r}^c$. However, in practice the quantum protons are typically associated with electronic and nuclear basis functions with centers represented by the collective coordinate $\mathbf{r}^b$. These basis function centers must be optimized for any given geometry of the classical nuclei to satisfy the variational principle. Thus, the energy for any geometry of the classical nuclei is variationally optimized with respect to the nuclear basis function center positions as well as the electronic and protonic orbital coefficients. In this case, the NEO PES can be expressed as $E_{\text{NEO}}\left(\mathbf{r}^c, \mathbf{r}^b\left(\mathbf{r}^c\right)\right)$. According to the variational procedure within the NEO framework, the equality

$$\frac{\partial E_{\text{NEO}}}{\partial \mathbf{r}^b} = 0 \tag{3.2}$$

is satisfied for any point on the NEO PES.[9] The dimensionality of the NEO PES will be lower than that of the conventional PES for the same system because certain nuclei are treated quantum mechanically. Similarly, the corresponding coordinate Hessian matrices will also be of lower dimensionality.

As shown in previous work,[17-18] the NEO gradient and Hessian elements on the NEO PES can be expressed as

$$\frac{\mathrm{d} E_{\text{NEO}}}{\mathrm{d} \mathbf{r}^c} = \left(\frac{\partial E_{\text{NEO}}}{\partial \mathbf{r}^c}\right)_{\mathbf{r}^b} + \left(\frac{\partial E_{\text{NEO}}}{\partial \mathbf{r}^b}\right)_{\mathbf{r}^c} \frac{\mathrm{d} \mathbf{r}^b}{\mathrm{d} \mathbf{r}^c} = \left(\frac{\partial E_{\text{NEO}}}{\partial \mathbf{r}^c}\right)_{\mathbf{r}^b} \tag{3.3}$$

and

$$\frac{\mathrm{d}^2 E_{\text{NEO}}}{\mathrm{d} \mathbf{r}^{c\,2}} = \left(\frac{\partial^2 E_{\text{NEO}}}{\partial \mathbf{r}^{c\,2}}\right)_{\mathbf{r}^b} - \frac{\partial^2 E_{\text{NEO}}}{\partial \mathbf{r}^c \partial \mathbf{r}^b} \left(\frac{\partial^2 E_{\text{NEO}}}{\partial \mathbf{r}^{b\,2}}\right)_{\mathbf{r}^c}^{-1} \frac{\partial^2 E_{\text{NEO}}}{\partial \mathbf{r}^b \partial \mathbf{r}^c}. \tag{3.4}$$

Eq. (3.4) shows that the Hessian elements require the calculation of not only the partial second derivatives of the NEO energy with respect to the classical coordinates, but also the pure and mixed derivatives with respect to the basis function centers. If N_c is the number of classical nuclei and N_b is the number of nuclear basis function centers, then $\dfrac{\partial^2 E_\text{NEO}}{\partial \mathbf{r}^{\text{c}\,2}}$ corresponds to a $3N_\text{c} \times 3N_\text{c}$ matrix, $\dfrac{\partial^2 E_\text{NEO}}{\partial \mathbf{r}^{\text{b}\,2}}$ corresponds to a $3N_\text{b} \times 3N_\text{b}$ matrix, and $\dfrac{\partial^2 E_\text{NEO}}{\partial \mathbf{r}^\text{c} \partial \mathbf{r}^\text{b}}$ corresponds to a $3N_\text{c} \times 3N_\text{b}$ matrix. Given that each quantum nucleus has at least one unique nuclear basis function center, the calculation of the NEO Hessian will require the calculation of at least as many second derivatives of the energy as required for the calculation of the conventional Hessian. These terms are combined as expressed in Eq. (3.4) to yield the final NEO Hessian elements.

NEO-HF Theory, Gradients, and Hessians

The equations for the analytic NEO-HF energy gradients were presented previously in Ref. [9]. However, as the analytic formulation of the Hessian extends that theory to a higher-order derivative, it is constructive to reproduce these expressions here. For the purposes of this paper, the theory is presented for closed-shell electronic and high-spin protonic configurations, but the extension to open-shell electronic configurations is straightforward. Moreover, the NEO-HF framework presented herein serves as the foundation for other multicomponent methods such as NEO-CCSD,[19] NEO-OOMP2,[20] and NEO-DFT.[21-25] Analogous to the conventional formulation of HF theory, NEO-HF[4] begins with a wave function ansatz of the form

$$\Psi_\text{tot}(\mathbf{r}^\text{e}, \mathbf{r}^\text{p}) = \Phi_0^\text{e}(\mathbf{r}^\text{e}) \Phi_0^\text{p}(\mathbf{r}^\text{p}) \tag{3.5}$$

which is a product of electronic and nuclear Slater determinants, $\Phi_0^e\left(\mathbf{r}^e\right)$ and $\Phi_0^p\left(\mathbf{r}^p\right)$, composed of electronic and nuclear orbitals, respectively. The electronic and nuclear spatial orbitals are expressed as linear combinations of Gaussian basis functions:

$$\psi_p^e\left(\mathbf{r}^e\right)=\sum_\mu c_{\mu p}^e \varphi_\mu^e\left(\mathbf{r}^e\right) \tag{3.6}$$

$$\psi_P^p\left(\mathbf{r}^p\right)=\sum_{\mu'} c_{\mu' P}^p \varphi_{\mu'}^p\left(\mathbf{r}^p\right). \tag{3.7}$$

In this notation, $\mu, \nu, \sigma, \ldots$ are the electronic Gaussian basis function indices, and the primed equivalents $\mu', \nu', \sigma', \ldots$ are the nuclear Gaussian basis function indices. Hereafter, the indices $i, j, k, \ldots$ denote occupied orbitals, $a, b, c, \ldots$ denote virtual orbitals, and $p, q, r, \ldots$ denote general orbitals for the electrons, and the upper case variants are used for the quantum nuclear indices. The NEO-HF Roothaan equations, which will be discussed below, are solved with a self-consistent-field (SCF) approach to yield the orbital coefficients.

The total closed-shell NEO-HF energy can be written in the form

$$
\begin{aligned}
E_{\text{NEO-HF}} = & \sum_{\mu\nu} P_{\mu\nu}^e H_{\mu\nu}^e + \frac{1}{2}\sum_{\mu\nu} P_{\mu\nu}^e G_{\mu\nu}^e - \frac{1}{2}\sum_{\mu\nu} P_{\mu\nu}^e G_{\mu\nu}^{ep} \\
& + \sum_{\mu'\nu'} P_{\mu'\nu'}^p H_{\mu'\nu'}^p + \frac{1}{2}\sum_{\mu'\nu'} P_{\mu'\nu'}^p G_{\mu'\nu'}^p - \frac{1}{2}\sum_{\mu'\nu'} P_{\mu'\nu'}^p G_{\mu'\nu'}^{pe} + V_{\text{nuc}}
\end{aligned}
\tag{3.8}
$$

where V_{nuc} is the Coulomb repulsion between the classical nuclei, the electronic and nuclear density matrices are defined as

$$P_{\mu\nu}^e = 2\sum_i^{N_e/2} c_{\mu i}^e c_{\nu i}^{e*} \tag{3.9}$$

$$P_{\mu'\nu'}^p = \sum_I^{N_p} c_{\mu' I}^p c_{\nu' I}^{p*} \tag{3.10}$$

and the integrals in the atomic orbital basis are given by

$$H_{\mu\nu}^{e} = \int d\mathbf{r}_1^e \varphi_\mu^e \left(\mathbf{r}_1^e \right) h^e \left(\mathbf{r}_1^e \right) \varphi_\nu^e \left(\mathbf{r}_1^e \right) \tag{3.11}$$

$$H_{\mu'\nu'}^{p} = \int d\mathbf{r}_1^p \varphi_{\mu'}^p \left(\mathbf{r}_1^p \right) h^p \left(\mathbf{r}_1^p \right) \varphi_{\nu'}^p \left(\mathbf{r}_1^p \right) \tag{3.12}$$

$$h^e \left(\mathbf{r}_1^e \right) = -\frac{1}{2} \nabla_1^2 - \sum_A^{N_c} \frac{Z_A}{|\mathbf{r}_1^e - \mathbf{r}_A^c|} \tag{3.13}$$

$$h^p \left(\mathbf{r}_1^p \right) = -\frac{1}{2m_p} \nabla_1^2 + \sum_A^{N_c} \frac{Z_A}{|\mathbf{r}_1^p - \mathbf{r}_A^c|} \tag{3.14}$$

$$G_{\mu\nu}^{e} = \sum_{\lambda\sigma} P_{\lambda\sigma}^e \left[(\mu\nu \mid \sigma\lambda) - \frac{1}{2}(\mu\sigma \mid \nu\lambda) \right] \tag{3.15}$$

$$G_{\mu'\nu'}^{p} = \sum_{\lambda'\sigma'} P_{\lambda'\sigma'}^p \left[(\mu'\nu' \mid \sigma'\lambda') - (\mu'\sigma' \mid \nu'\lambda') \right] \tag{3.16}$$

$$G_{\mu\nu}^{ep} = \sum_{\lambda'\sigma'} P_{\lambda'\sigma'}^p (\mu\nu \mid \sigma'\lambda') \tag{3.17}$$

$$G_{\mu'\nu'}^{pe} = \sum_{\lambda\sigma} P_{\lambda\sigma}^e (\mu'\nu' \mid \sigma\lambda) \tag{3.18}$$

$$(\mu\nu \mid \sigma\lambda) = \int d\mathbf{r}_1^e \int d\mathbf{r}_2^e \varphi_\mu^{e*} \left(\mathbf{r}_1^e \right) \varphi_\nu^e \left(\mathbf{r}_1^e \right) \frac{1}{|\mathbf{r}_1^e - \mathbf{r}_2^e|} \varphi_\sigma^{e*} \left(\mathbf{r}_2^e \right) \varphi_\lambda^e \left(\mathbf{r}_2^e \right) \tag{3.19}$$

with analogous definitions to Eq. (3.19) for the pure nuclear and mixed two-particle

integrals.

In the NEO-HF method, a set of Roothaan equations is solved variationally to

yield a single-configuration mixed nuclear-electronic wave function.[4] Specifically, the

equations for the electrons and quantum protons are given by

$$\mathbf{F}^e \mathbf{C}^e = \mathbf{S}^e \mathbf{C}^e \boldsymbol{\varepsilon}^e \tag{3.20}$$

$$\mathbf{F}^p \mathbf{C}^p = \mathbf{S}^p \mathbf{C}^p \boldsymbol{\varepsilon}^p \tag{3.21}$$

where orbital coefficients and energies are contained in the $\mathbf{C}$ and $\boldsymbol{\varepsilon}$ matrices,

respectively, the elements of the basis function overlap matrices are given by

$$S_{\mu\nu}^{\text{e}} = \int d\mathbf{r}_1^{\text{e}} \varphi_\mu^{\text{e}*}\left(\mathbf{r}_1^{\text{e}}\right)\varphi_\nu^{\text{e}}\left(\mathbf{r}_1^{\text{e}}\right) \tag{3.22}$$

$$S_{\mu'\nu'}^{\text{p}} = \int d\mathbf{r}_1^{\text{p}} \varphi_{\mu'}^{\text{p}*}\left(\mathbf{r}_1^{\text{p}}\right)\varphi_{\nu'}^{\text{p}}\left(\mathbf{r}_1^{\text{p}}\right) \tag{3.23}$$

and the elements of the Fock matrices are defined as

$$F_{\mu\nu}^{\text{e}} = H_{\mu\nu}^{\text{e}} + G_{\mu\nu}^{\text{e}} - G_{\mu\nu}^{\text{ep}} \tag{3.24}$$

$$F_{\mu'\nu'}^{\text{p}} = H_{\mu'\nu'}^{\text{p}} + G_{\mu'\nu'}^{\text{p}} - G_{\mu'\nu'}^{\text{pe}} \tag{3.25}$$

Notably, the electronic and nuclear Roothaan equations are coupled and influence each other through the electron-proton Coulomb terms. Furthermore, the solutions of these equations are subject to the orthonormality constraints

$$\mathbf{C}^{\text{e}\dagger}\mathbf{S}^{\text{e}}\mathbf{C}^{\text{e}} = \mathbf{I} \tag{3.26}$$

$$\mathbf{C}^{\text{p}\dagger}\mathbf{S}^{\text{p}}\mathbf{C}^{\text{p}} = \mathbf{I} \ . \tag{3.27}$$

As in the conventional electronic case,[26] application of the first derivative to the total energy given in Eq. (3.8) with respect to a geometric perturbation x and subsequent simplification to remove the density response terms yields an expression for the energy gradient:

$$\frac{\partial E_{\text{NEO-HF}}}{\partial x} = \sum_{\mu\nu} P_{\mu\nu}^{\text{e}}\left(H_{\mu\nu}^{\text{e}}\right)^x + \frac{1}{2}\sum_{\mu\nu} P_{\mu\nu}^{\text{e}}\left(G_{\mu\nu}^{\text{e}}\right)^x - \frac{1}{2}\sum_{\mu\nu} P_{\mu\nu}^{\text{e}}\left(G_{\mu\nu}^{\text{ep}}\right)^x - \sum_{\mu\nu} W_{\mu\nu}^{\text{e}}\left(S_{\mu\nu}^{\text{e}}\right)^x$$
$$+ \sum_{\mu'\nu'} P_{\mu'\nu'}^{\text{p}}\left(H_{\mu'\nu'}^{\text{p}}\right)^x + \frac{1}{2}\sum_{\mu'\nu'} P_{\mu'\nu'}^{\text{p}}\left(G_{\mu'\nu'}^{\text{p}}\right)^x - \frac{1}{2}\sum_{\mu'\nu'} P_{\mu'\nu'}^{\text{p}}\left(G_{\mu'\nu'}^{\text{pe}}\right)^x - \sum_{\mu'\nu'} W_{\mu'\nu'}^{\text{p}}\left(S_{\mu'\nu'}^{\text{p}}\right)^x + \left(V_{\text{nuc}}\right)^x \tag{3.28}$$

In this notation, terms such as $\left(H_{\mu\nu}^{\text{e}}\right)^x$ are the geometric derivative integrals, corresponding to the partial derivative of the integral in parentheses with respect to the geometric perturbation x (i.e., $\left(H_{\mu\nu}^{\text{e}}\right)^x \equiv \dfrac{\partial H_{\mu\nu}^{\text{e}}}{\partial x}$). The perturbation x can be either a

classical nuclear coordinate or a nuclear basis function center coordinate. The electronic and nuclear energy-weighted density matrices introduced in the above expression are defined as

$$W_{\mu\nu}^{e} = 2\sum_{i}^{N_e/2} c_{\mu i}^{e} c_{\nu i}^{e*} \varepsilon_i^{e} \qquad (3.29)$$

$$W_{\mu'\nu'}^{p} = \sum_{I}^{N_p} c_{\mu'I}^{p} c_{\nu'I}^{p*} \varepsilon_I^{p} \; . \qquad (3.30)$$

The calculation of the closed-shell NEO-HF gradient from Eq. (3.28) is straightforward. Most integral codes already include the analytic evaluation of the first-order electronic derivative integrals and with minor modification can provide the quantum nuclear analogs. In order to calculate $\dfrac{\partial^2 E_{\mathrm{NEO}}}{\partial \mathbf{r}^{c\,2}}$, $\dfrac{\partial^2 E_{\mathrm{NEO}}}{\partial \mathbf{r}^{b\,2}}$, and $\dfrac{\partial^2 E_{\mathrm{NEO}}}{\partial \mathbf{r}^c \partial \mathbf{r}^b}$, which are needed to compute the NEO Hessian, another derivative of Eq. (3.28) with respect to a second geometric perturbation, y, is taken, producing

$$
\begin{aligned}
\frac{\partial^2 E_{\mathrm{NEO\text{-}HF}}}{\partial x \partial y} =& \sum_{\mu\nu} P_{\mu\nu}^{e} \left(H_{\mu\nu}^{e} \right)^{xy} + \frac{1}{2} \sum_{\mu\nu} P_{\mu\nu}^{e} \left(G_{\mu\nu}^{e} \right)^{xy} - \frac{1}{2} \sum_{\mu\nu} P_{\mu\nu}^{e} \left(G_{\mu\nu}^{ep} \right)^{xy} - \sum_{\mu\nu} W_{\mu\nu}^{e} \left(S_{\mu\nu}^{e} \right)^{xy} \\
&+ \sum_{\mu'\nu'} P_{\mu'\nu'}^{p} \left(H_{\mu'\nu'}^{p} \right)^{xy} + \frac{1}{2} \sum_{\mu'\nu'} P_{\mu'\nu'}^{p} \left(G_{\mu'\nu'}^{p} \right)^{xy} - \frac{1}{2} \sum_{\mu'\nu'} P_{\mu'\nu'}^{p} \left(G_{\mu'\nu'}^{pe} \right)^{xy} - \sum_{\mu'\nu'} W_{\mu'\nu'}^{p} \left(S_{\mu'\nu'}^{p} \right)^{xy} + \left(V_{\mathrm{nuc}} \right)^{xy} \\
&+ \sum_{\mu\nu} \left(P_{\mu\nu}^{e} \right)^{y} \left(H_{\mu\nu}^{e} \right)^{x} + \frac{1}{2} \sum_{\mu\nu} \left(P_{\mu\nu}^{e} \right)^{y} \left(G_{\mu\nu}^{e} \right)^{x} - \frac{1}{2} \sum_{\mu\nu} \left(P_{\mu\nu}^{e} \right)^{y} \left(G_{\mu\nu}^{ep} \right)^{x} - \sum_{\mu\nu} \left(W_{\mu\nu}^{e} \right)^{y} \left(S_{\mu\nu}^{e} \right)^{x} \\
&+ \sum_{\mu'\nu'} \left(P_{\mu'\nu'}^{p} \right)^{y} \left(H_{\mu'\nu'}^{p} \right)^{x} + \frac{1}{2} \sum_{\mu'\nu'} \left(P_{\mu'\nu'}^{p} \right)^{y} \left(G_{\mu'\nu'}^{p} \right)^{x} - \frac{1}{2} \sum_{\mu'\nu'} \left(P_{\mu'\nu'}^{p} \right)^{y} \left(G_{\mu'\nu'}^{pe} \right)^{x} - \sum_{\mu'\nu'} \left(W_{\mu'\nu'}^{p} \right)^{y} \left(S_{\mu'\nu'}^{p} \right)^{x}
\end{aligned}
\qquad (3.31)
$$

The analytic evaluation of the electronic and nuclear terms that contain second-order derivative integrals has already been derived and implemented for Gaussian basis sets.[27] The response of the SCF solution quantities to geometric perturbations are manifested in the density and energy-weighted density matrix response terms $\left(P_{\mu\nu}^{e} \right)^{y}$,

$\left(P_{\mu'\nu'}^{\mathrm{p}} \right)^{y}$, $\left(W_{\mu\nu}^{\mathrm{e}} \right)^{y}$, and $\left(W_{\mu'\nu'}^{\mathrm{p}} \right)^{y}$. These quantities can be computed with coupled-

perturbed NEO-HF equations analogous to those derived and implemented for

conventional electronic HF theory.[26, 28-29] The formulations for the solution of these

equations at the restricted NEO-HF and unrestricted NEO-DFT levels are presented in

Appendix B.

Transition States and Minimum Energy Paths

Two of the most popular uses for coordinate Hessians in conventional quantum

chemistry are the optimization and characterization of transition state geometries and

the generation of MEPs. In the NEO formalism, these structures and paths are

computed on a lower-dimensional PES, which incorporates the zero-point energy,

anharmonicity, and nuclear delocalization of the quantum nuclei. Analogous to the

conventional electronic structure case, the transition state on the NEO PES is defined to

be a stationary point with a single imaginary vibrational frequency (i.e., a first-order

saddle point). For this reason, any algorithm that optimizes conventional transition state

geometries based on gradient and Hessian information[30-31] can be used to find a NEO

transition state with the NEO gradient and Hessian as input.

Also analogous to the conventional electronic structure case,[32] the NEO MEP

begins at the transition state and is guided by steepest descent steps with subsequent

corrective steps down to the reactant and product optimized geometries.[33-34] Analytic

Hessians are useful for MEP calculations because the energy gradient of the transition

state is zero, and the imaginary normal mode motion associated with the negative

eigenvalue of the Hessian is used for the first step of the reaction path. An additional

technical feature arises for the NEO MEP generation because the NEO energy must be

optimized with respect to the basis function centers as well as the orbital coefficients. As a result, after every steepest descent step and corrective step of the NEO MEP algorithm, the nuclear basis function center positions are optimized.

Results and Discussion

Implementation and model systems

The preceding theory was implemented in a development branch of the Q-Chem 5.3 quantum chemistry software.[35] This implementation built upon the existing NEO-HF framework in the release version of the software, and existing conventional electronic machinery was repurposed for the calculation of quantum nuclear derivative integrals, optimization of NEO-HF transition states, and determination of NEO-HF MEPs. The CP-NEO-HF equations are solved using the conjugate gradient algorithm for solutions of inhomogeneous linear systems.[36] The analytic Hessian was compared to numerical and semi-numerical Hessian calculations to validate the implementation. These validation tests, as well as more details on the implementation of the NEO analytic Hessian in Q-Chem, are provided in the supplementary material. All NEO-HF calculations herein utilized the 6-31G** electronic basis set[37] with the PB4-D nuclear basis set for the quantum protons,[38] and all conventional calculations were performed at the HF/6-31G** level of theory. The PB4-D basis set is composed of four s-type, three p-type, and two d-type primitive Gaussians ($4s3p2d$). For these applications, each quantum proton was represented by a single basis function center for both the electronic and nuclear basis functions, which were assumed to move together. The optimization of these nuclear basis function centers utilizes the energy gradients given in Eq. (3.28). Although the NEO-HF approach lacks electron-electron and electron-proton correlation, this

implementation illustrates the important fundamental concepts underlying NEO Hessians, transition states, and MEPs. Extensions to NEO-DFT, which includes these correlation effects,[21-25] are currently underway.

To illustrate the properties of transition states and MEPs at the NEO-HF level, two qualitatively different systems were studied. The S_N2 reaction of $ClCH_3Cl^-$ (Figure 3.1) provides an example of a transition state in which motion of the protons does not dominate the MEP. This system is intended to demonstrate the calculation of NEO transition states and reaction paths with multiple quantum protons, and it is expected to be qualitatively similar to the conventional analog because the quantum nuclei are predominantly spectators in the overall motion along the reaction path. For an example in which the quantum proton motion is expected to play a dominant role along the reaction path, the intramolecular hydride shift (i.e., carbocation rearrangement) between the middle two carbon atoms of the $C_4H_9^+$ species (Figure 3.1) was studied. In this application, only the transferring hydrogen was treated quantum mechanically to simplify the analysis.

Transition states

The transition states of both systems were found using the analytic Hessian and gradients in conjunction with an existing quasi-Newton like transition state search algorithm[30] with the NEO-HF and conventional HF methods. In this algorithm, the analytic Hessian is used at the first step. The conventional transition state of $C_4H_9^+$ was found to correspond to a single-well proton potential (i.e., the three-dimensional proton potential energy surface computed at the transition state geometry with all other nuclei fixed exhibited a single minimum, Figure B1 of Appendix B). This feature allows the use

of a single determinant NEO-HF description along the entire MEP, rather than requiring

multireference methods.[39] The transition states were verified to be first-order saddle

points because the gradients on the NEO PES were zero to within the specified

tolerance (3×10^{-5} Hartree/Bohr) and the vibrational analysis performed with the NEO

Hessian produced only a single imaginary frequency. The imaginary modes and

associated frequencies for the $ClCH_3Cl^-$ and $C_4H_9^+$ transition states are depicted in

Figure 3.2. The NEO and conventional calculations for the $ClCH_3Cl^-$ system produce

nearly identical imaginary frequencies of 412 cm^{-1} and 414 cm^{-1}, respectively. Even

when the proton motion dominates the normal mode in the $C_4H_9^+$ system, these

imaginary frequencies differ only by 5 cm^{-1}.

The visual comparisons shown in Figure 3.2 demonstrate that the motions of the

classical nuclei in the NEO-HF imaginary mode mirror the motions of those same atoms

in the conventional HF imaginary mode. To further analyze the differences between the

conventional and NEO imaginary normal mode vectors, we calculated the dot product

between these vectors, as given in Table 3.1. As the dimensionalities of the normal

mode vectors are different in the two cases, we excluded the normal mode elements in

the conventional HF vector that are associated with the quantum protons in the NEO-HF

calculation. We also computed this dot product after renormalizing the HF normal mode

vector when these elements are excluded. As the protons of $ClCH_3Cl^-$ do not contribute

significantly to the conventional HF imaginary mode (i.e., these coordinates correspond

to 6% of this normal mode vector), its dot product with the NEO-HF mode is nearly unity

before renormalization and is 1.000 after renormalization. In contrast, the conventional

$C_4H_9^+$ imaginary mode is dominated by the transferring proton motion (i.e., these

46

coordinates correspond to 74% of this normal mode vector), and its dot product with the NEO-HF mode is only 0.495. However, after renormalization, this dot product increases to 0.973, indicating that the motions of the classical nuclei are nearly identical in the NEO-HF and conventional HF imaginary modes for this system as well. These findings are consistent with the visual observation that the motions of the classical nuclei in the NEO imaginary mode are the same as the corresponding motions in the conventional description, even though the conventional mode is dominated by proton motion. The Cartesian coordinates associated with each imaginary normal mode are presented in Appendix B, Table B4.

The description of the imaginary mode obtained by diagonalizing the NEO Hessian does not include the motions of the quantum protons, which respond instantaneously to the motions of the classical nuclei due to the Born-Oppenheimer separation between the classical and quantum nuclei. This instantaneous response is analogous to the response of the electrons to the nuclei in conventional electronic structure calculations. In general, however, the molecular vibrational modes are mixtures of all nuclear coordinates, and a description of the full molecular vibrational frequencies requires coupling between the classical and quantum nuclei. To enable the calculation of molecular vibrational frequencies composed of both classical and quantum nuclei, we developed the NEO-DFT(V) method.[17-18] This approach involves the diagonalization of an extended NEO Hessian that is defined in terms of the second derivatives of the NEO energy with respect to the expectation values of the quantum nuclear coordinates as well as the classical nuclear coordinates. The extended portion of this Hessian is constructed with input from the proton vibrational excitations

computed with the NEO time-dependent DFT (NEO-TDDFT) method.[40-41] The NEO-DFT(V) approach has been shown to produce accurate molecular vibrational frequencies that incorporate the significant anharmonic effects associated with the quantum protons. The NEO-HF(V) method is the NEO-HF analog of the NEO-DFT(V) method.

We performed NEO-HF(V) calculations for the transition state geometry of $C_4H_9^+$ to compute the full molecular vibrational frequencies. Computational details for the NEO-HF(V) calculations are provided in the supplementary material. The optimized NEO-HF geometry is a stationary point in the extended NEO space corresponding to the classical nuclear coordinates and the expectation value of the quantum proton position coordinate because the derivatives of the NEO energy with respect to both types of coordinates are zero at this optimized geometry (see Ref. [17] for relevant derivation). Diagonalization of the extended Hessian produced a single imaginary frequency of 118 cm^{-1}, indicating that this geometry is a first-order saddle point in the extended NEO space. The resulting imaginary mode is nearly indistinguishable from the conventional HF mode, as depicted in Figure 3.3. To quantify this similarity, the dot product of the NEO-HF(V) and conventional HF imaginary normal mode vectors is 0.996. A similar NEO-HF(V) analysis was performed for the $ClCH_3Cl^-$ system (Table 3.1).

In addition to the imaginary mode, the majority of the other normal modes from the NEO-HF(V) calculation are nearly indistinguishable from their conventional counterparts at the $C_4H_9^+$ transition state geometry. The root-mean-square deviation between the NEO-HF(V) and conventional HF normal mode frequencies is 58 cm^{-1}, with

only six modes exhibiting differences greater than 10 cm^{-1}. These six modes, which

include the imaginary mode, correspond to vibrations with significant contributions from

the quantum proton. The quantum mechanical treatment of the proton in the NEO

framework incorporates anharmonic effects that are absent from the conventional HF

harmonic normal mode analysis. Thus, the NEO-HF(V) frequencies associated with the

quantum proton motion are expected to be more accurate than their conventional

counterparts. This anharmonicity is most likely responsible for the significantly lower

imaginary normal mode frequency produced by NEO-HF(V) than by conventional HF for

$C_4H_9^+$ (Table 3.1). The enhanced accuracy in the frequencies due to the inclusion of

anharmonic effects has been shown previously when comparing NEO-DFT(V)

calculations to second-order vibrational perturbation theory[42] calculations for a series of

molecules.[17-18] The complete results for this comparison are given in Appendix B, Table

B6. Furthermore, Appendix B also describes an additional test of the transition state

search algorithm for an asymmetric variant of the hydride transfer reaction shown in

Figure 3.1.

Minimum energy paths

Starting from the transition state structures, we calculated the MEPs for both

processes studied, as depicted in Figure 3.4. As expected, the multicomponent and

conventional MEPs for $ClCH_3Cl^-$ are virtually identical, with barrier heights that differ by

only 0.23 kcal/mol. The $C_4H_9^+$ reaction barrier is significantly lower than the $ClCH_3Cl^-$

barrier. Moreover, the difference in the barrier heights computed with the conventional

electronic and NEO methods is slightly larger (0.79 kcal/mol) for the $C_4H_9^+$ system,

presumably because the transferring proton is contributing more to the intrinsic reaction

coordinate.

The main origin of the slightly lower barrier for the NEO MEP compared to the conventional electronic MEP is that the NEO PES includes the zero-point energy of the quantum proton. To benchmark this effect, we performed Fourier Grid Hamiltonian (FGH) calculations[43-44] to compute the three-dimensional proton vibrational wave functions and zero-point energies at the conventional optimized transition state and reactant geometries of $C_4H_9^+$. Computational details for the FGH calculations are available in Appendix B. The proton zero-point energy at the transition state (5.79 kcal/mol) was found to be smaller than that at the reactant state (6.94 kcal/mol). Thus, including the zero-point energy of the quantum proton with the FGH method lowers the barrier height by 1.15 kcal/mol. This trend is similar to the lowering of the $C_4H_9^+$ barrier height by 0.79 kcal/mol for the NEO-HF method compared to the conventional HF method. The quantitative differences are most likely due to the lack of electron-proton correlation in the NEO-HF calculations, and the agreement is expected to be better with the NEO-DFT method[21-25] or with a higher level wave function-based method such as NEO-OOMP2 or NEO-CCSD.[19-20]

The MEP algorithm implemented in this study[33-34] uses the imaginary normal mode at the transition state as well as the energy gradients at points along the MEP to determine the pathway. Information from the Hessian is used only at the transition state. Steepest descent steps are taken, using energy gradients at points already determined to be on the pathway, and gradient bisector corrective steps or backup steps may be executed based on the local information of the surface. These backup steps can cause non-uniform spacing of points along the MEP, as observed in the conventional HF and

NEO-HF $C_4H_9^+$ MEPs shown in Figure 3.4. We have found that this behavior is typically more prevalent when the imaginary normal mode frequency is relatively low and the gradients along the MEP are relatively small. The points along the MEP will often become more evenly spaced when a smaller steepest descent step size is used, although small gradients along the MEP may require a sufficiently large step size for numerical reasons. Some of these technical issues may be alleviated by other algorithms, such as a Hessian based predictor-corrector integrator,[45] which utilizes information from the coordinate Hessian at each subsequently determined point along the MEP.

In the NEO framework, the intrinsic reaction coordinate is composed of only the classical nuclei. Analysis of the geometries along the MEP for a hydrogen atom transfer reaction, where the transferring hydrogen nucleus is treated quantum mechanically, provides insights into the classical nuclear reorganization that drives hydrogen transfer. This perspective is analogous to the nuclear reorganization that induces electron transfer in conventional calculations of electron transfer reactions. For the $C_4H_9^+$ system, analysis of the geometries along the NEO MEP illustrates that one of the two central carbon atoms adopts a tetrahedral geometry while the other remains planar with movement along the reaction path in either direction from the transition state, as depicted in Figure 3.5. Thus, the dominant reorganization that facilitates the movement of the quantum proton toward either carbon is the tetrahedral-to-planar (i.e., sp^3 to sp^2) rearrangement around the carbon atoms.

An advantage of the NEO approach is that the electronic and nuclear orbitals are computed simultaneously on equal footing. Figure 3.5 also presents a visualization of

the protonic orbital and the reactive electronic orbital along the MEP for the $C_4H_9^+$

hydride transfer reaction. The localization of the electronic wave function to produce

intrinsic bond orbitals and the visualization of these orbitals was performed with the

IboView software developed by Knizia and coworkers.[46-47] The protonic orbital appears

to be quite localized when using the same isovalue for both the electronic and protonic

orbitals, mainly due to the significant mass disparity. When a much smaller isovalue is

used, the protonic orbital displays the expected behavior of greater delocalization in the

transition state region of the MEP compared to the reactant and product state regions.

Moreover, the protonic orbital is expected to become more delocalized upon inclusion of

electron-proton correlation with an approach such as NEO-DFT.[8, 23] Our analysis based

on Figure 3.5 shows that the quantum proton moves between the two carbon atoms

concertedly with the shifting of the electronic orbital as one C-H bond breaks and

another C-H bond forms. This type of simultaneous visualization of quantum nuclear

and electronic orbitals during a chemical reaction provides insights beyond the previous

conventional electronic structure studies with this software. In particular, this analysis

will be able to classify proton-coupled electron transfer reactions as synchronous or

asynchronous mechanisms.[16]

Thermochemistry

The analytic NEO Hessian also enables the calculation of thermochemical

properties. As discussed above, the zero-point energies of the quantum nuclei are

already included in the NEO PES. The zero-point energies of the other nuclei can be

included by diagonalization of the NEO Hessian, analogous to the conventional

electronic structure vibrational analysis, although this approach neglects the coupling

between the classical and quantum nuclei in the vibrational modes. Similarly, the normal modes obtained from the NEO Hessian can be used to compute the entropic contributions to produce free energies, although these entropic contributions do not include the contributions from the quantum nuclei or the vibrational coupling between the classical and quantum nuclei. To account for the entropic contributions associated with all nuclei, including the vibrational coupling among all of them, the entropic contributions for both classical and quantum nuclei can be computed using the extended NEO Hessian within the NEO-HF(V) framework. Importantly, both the zero-point energies inherent to the NEO PES and the entropic contributions resulting from a NEO-HF(V) calculation include the anharmonicity of the quantum nuclei.

Table 3.2 provides the values for these various quantities for the two systems studied herein. The temperature used for inclusion of the vibrational entropy was 298.15 K. For the $ClCH_3Cl^-$ system, the barrier decreases when accounting for zero-point energy for both the NEO and conventional methods, and the addition of the respective vibrational entropy contributions increases each barrier by ~1.7 – 1.8 kcal/mol. For the $C_4H_9^+$ system, the zero-point energy contribution to the barrier of the hydride transfer process is nearly equal and opposite (±0.5 kcal/mol) for the HF and NEO-HF methods, yielding barrier heights closer in value. The vibrational entropy contributions are very similar for the HF and NEO-HF methods (0.8 – 0.9 kcal/mol). After addition of both zero-point energy and vibrational entropy contributions, the barrier heights are the same to within 0.5 kcal/mol for the $ClCH_3Cl^-$ system and to within 0.1 kcal/mol for the $C_4H_9^+$ system.

These results illustrate several general concepts relevant to thermochemistry

53

calculations within the NEO approach. The zero-point energy and vibrational entropy

corrections computed with the vibrational modes obtained from the NEO Hessian are

not expected to be the same as those obtained from the conventional Hessian because

the number of modes is different. However, inclusion of the zero-point energy

corrections from these Hessians for both conventional and NEO calculations is

expected to lead to more similar energy differences (i.e., barrier heights) because the

NEO PES already includes the zero-point energies associated with the quantum nuclei.

However, these energies will not be identical because the NEO approach includes the

anharmonic effects associated with the quantum nuclei, as well as the impact of the

nuclear quantum effects on the geometry optimization. Additionally, the vibrational

entropy contributions of the quantum nuclei can be included by obtaining the vibrational

modes from the extended NEO Hessian within the NEO-HF(V) framework. The

vibrational entropy contributions to the barriers of the $ClCH_3Cl^-$ and $C_4H_9^+$ systems

computed in this manner are 1.86 kcal/mol and 0.82 kcal/mol, respectively, compared to

the conventional HF values of 1.73 kcal/mol and 0.89 kcal/mol. The slight differences

between NEO-HF(V) and conventional HF vibrational entropy contributions are

attributable to the anharmonic effects of the quantum nuclei included in the NEO-HF(V)

approach. The neglect of correlation effects and limitations of the basis sets may also

contribute to these differences.

Conclusions

As multicomponent methods gain traction within the quantum chemistry

community, the development of tools to enable the multicomponent study of chemical

reactions becomes essential. Herein we developed and implemented the NEO-HF

analytic Hessian in the Q-Chem software package. We used this NEO Hessian to characterize stationary points as minima or transition states, analyze the imaginary mode at transition states, generate and analyze MEPs, and calculate thermochemical properties within the NEO framework. An advantage of the NEO approach is that the nuclear quantum effects, such as zero-point energy and nuclear delocalization, of specified nuclei are inherently included in the PES. Thus, these nuclear quantum effects are included during the optimizations of geometries and generation of MEPs rather than added subsequently as corrections. Analysis of the intrinsic reaction coordinate illustrates the dominant nuclear motions that drive the chemical reaction. Moreover, analysis of the electronic and nuclear orbitals along the MEP highlights the coupled motions of the electrons and quantum protons beyond the Born-Oppenheimer approximation. An extended NEO PES that depends on the expectation values of the quantum nuclei as well as the classical nuclei allows the inclusion of coupling between the classical and quantum nuclei.

In principle, the NEO framework can be used to treat all nuclei quantum mechanically. However, such a treatment requires the elimination of the overall rotations to allow the calculation of meaningful vibrational excitations.[48-49] Moreover, within the NEO-DFT framework, this treatment also requires the development of electron-nucleus correlation functionals for each type of nucleus. We have developed electron-proton correlation functionals that have been shown to provide accurate proton densities and energies within the NEO-DFT framework.[23-25] The development of more general electron-nucleus correlation functionals for other nuclei is an even more challenging task. On the other hand, the treatment of only specified protons quantum

mechanically enables the investigation of a wide range of chemical processes, particularly those involving hydrogen transfer. The extension of the NEO-HF analytic Hessian to the NEO-DFT analytic Hessian as a means of incorporating electron-proton correlation is currently underway. The description of hydrogen tunneling requires a multireference method such as NEO multistate DFT (NEO-MSDFT), which has been shown to produce bilobal, delocalized proton vibrational wave functions and accurate hydrogen tunneling splittings for systems such as malonaldehyde.[50] The combination of the NEO MEP methods presented herein with NEO-MSDFT will enable the incorporation of hydrogen tunneling effects into the reaction paths. Correlation effects could also be included in geometry optimizations and MEPs with wave function methods such as the NEO-CASSCF,[4] NEO-OOMP2, and NEO-CCSD[19-20] methods. This work provides the foundation for all of these future directions.

Figures and Tables
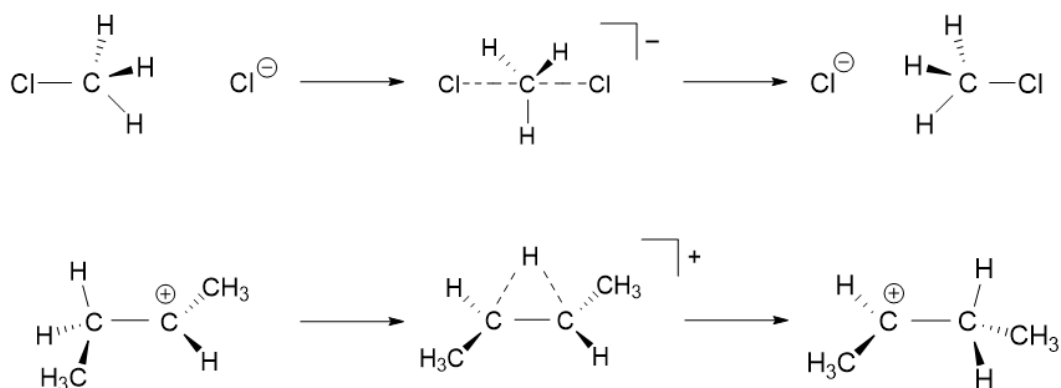
Figure 3.1. Schematic depiction of reactant (left), transition state (middle), and product (right) for the $ClCH_3Cl^-$ (top row) and $C_4H_9^+$ reactions.

57
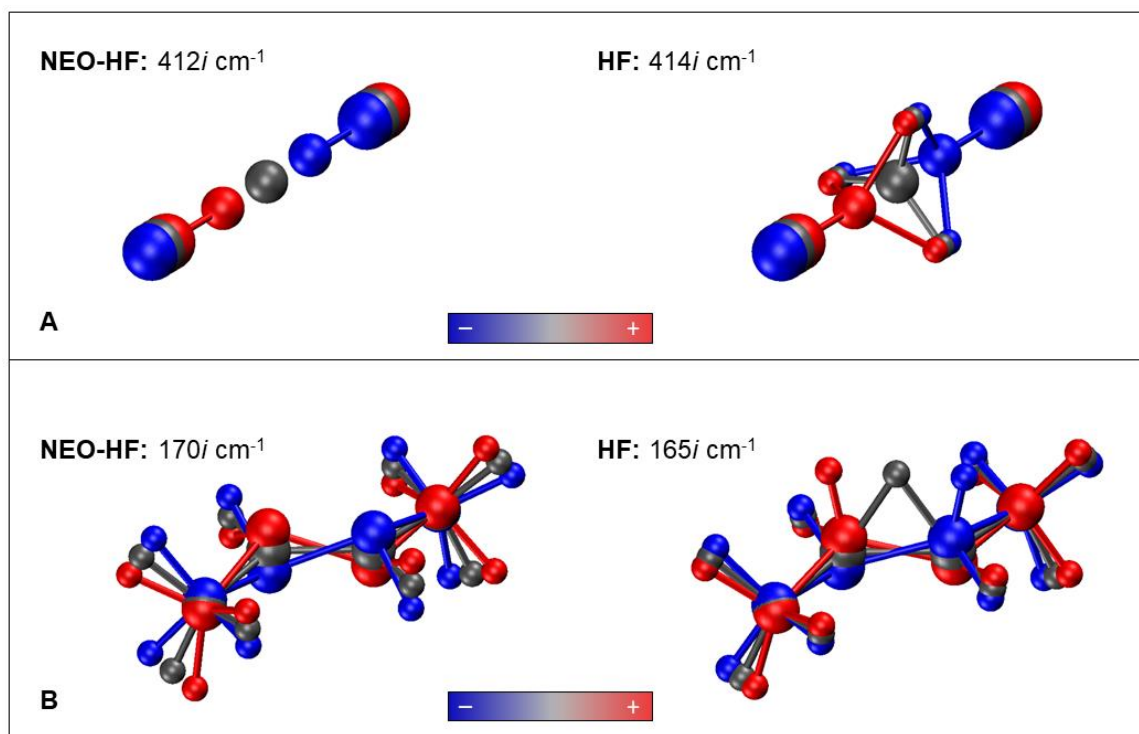
Figure 3.2. Depictions of the imaginary mode at the transition state for the (A) $ClCH_3Cl^-$ and (B) $C_4H_9^+$ systems calculated with the NEO-HF and HF methods[a]

[a]In the NEO cases, the quantum protons are excluded from the depiction, as their motion is not explicitly described by the normal mode. The transition state geometry is represented in gray, while positive and negative displacements of the nuclei along the imaginary mode are depicted with red and blue, respectively. (Multimedia view is available at DOI: 10.1063/5.0033540)

Table 3.1. NEO-HF, Conventional HF, and NEO-HF(V) Vibrational Frequencies Associated with the Imaginary Mode at the Optimized Transition States for the ClCH$_3$Cl$^-$ and C$_4$H$_9^+$ Systems[a]

	ClCH$_3$Cl$^-$	C$_4$H$_9^+$
NEO-HF Frequency	412	170
HF Frequency	414	165
NEO-HF(V) Frequency	410	118
HF and NEO-HF Dot Product[b]	0.968	0.495
HF and NEO-HF Dot Product after Renormalization[c]	1.000	0.973
HF and NEO-HF(V) Dot Product[d]	0.998	0.996

[a] All frequencies are given in wavenumbers and are imaginary.
[b] The dot product between the HF and NEO-HF normal mode vectors excludes the normal mode elements corresponding to the coordinates of the quantum protons.
[c] The dot product after renormalization entails renormalization of the HF vector after the normal mode elements corresponding to the coordinates of the quantum protons are excluded.
[d] The dot product between the HF and NEO-HF(V) normal mode vectors includes all elements.
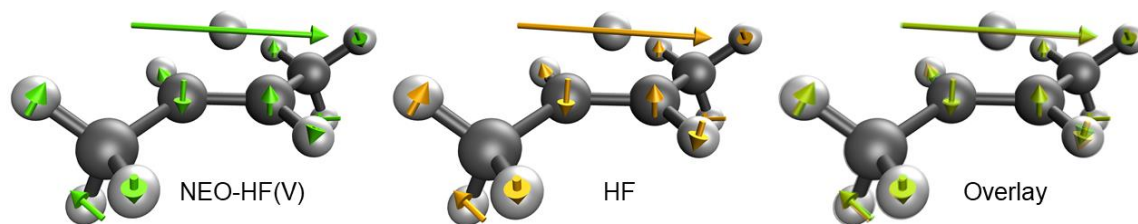
Figure 3.3. Depictions of imaginary vibrational normal modes at the transition state geometry of $C_4H_9^+$ computed with the NEO-HF(V) (teal arrows, left) and conventional HF (orange arrows, center) methods, as well as an overlay of the two depictions (right).
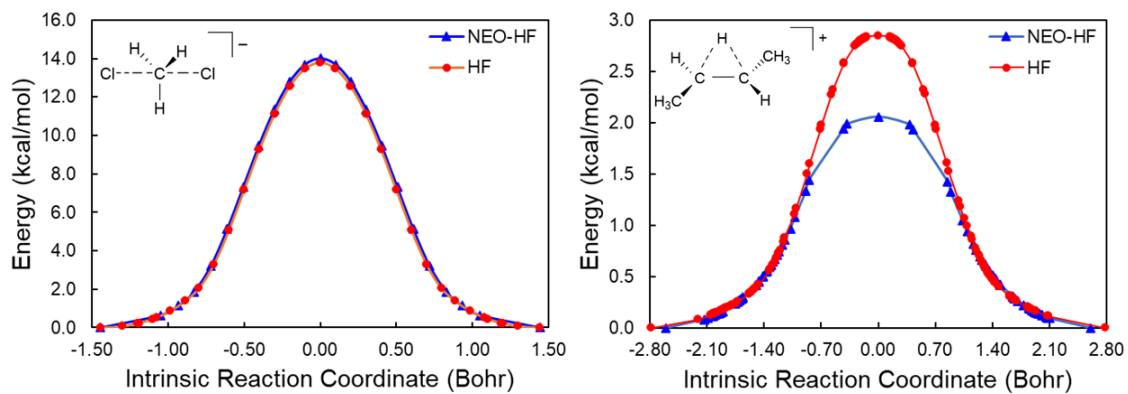
Figure 3.4. Minimum energy paths for ClCH$_3$Cl$^-$ (left) and C$_4$H$_9^+$ (right) calculated with NEO-HF/6-31G**/PB4-D (blue triangles) and conventional HF/6-31G** (red circles)[a]

[a]The intrinsic reaction coordinate is calculated in Cartesian coordinates.
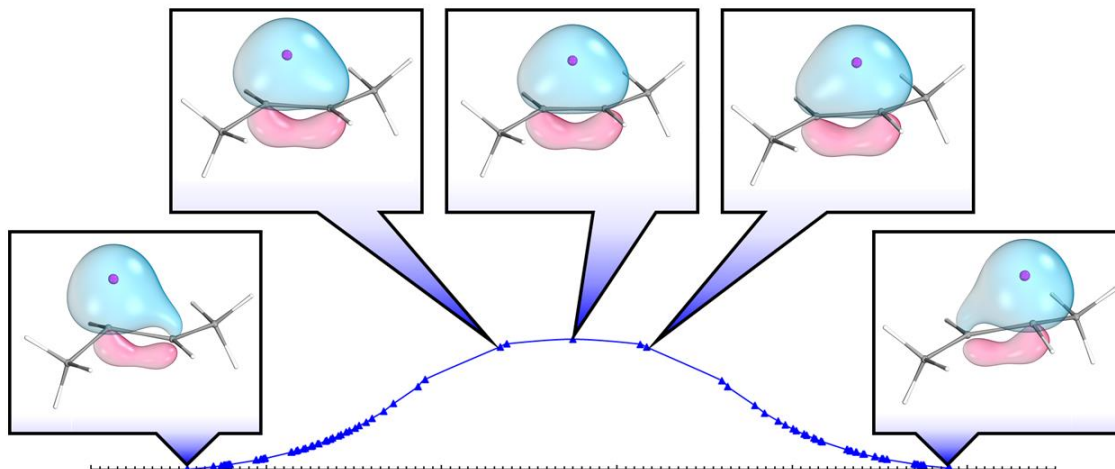
Figure 3.5. Depictions of protonic and electronic orbitals along the MEP for $C_4H_9^+$.[a]

[a]The protonic orbital is represented as the purple isosurface, and the reactive electronic intrinsic bond orbital is represented as blue (positive) and red (negative). The same isovalue is used for the protonic and electronic orbitals, indicating that the proton is significantly more localized. (Multimedia view is available at DOI: 10.1063/5.0033540)

Table 3.2. Barrier Heights (kcal/mol) for the ClCH$_3$Cl$^-$ and C$_4$H$_9^+$ Processes Calculated with NEO-HF and HF Methods Including Zero-Point Energy (ΔZPE) and Vibrational Entropy ($T\Delta S$) Contributions.

	ClCH$_3$Cl$^-$	C$_4$H$_9^+$
$\Delta E_{\text{NEO-HF}}$	14.01	2.06
$\Delta E_{\text{NEO-HF}} + \Delta ZPE_{\text{NEO-HF}}$	13.62	2.51
$\Delta E_{\text{NEO-HF}} + \Delta ZPE_{\text{NEO-HF}} - T\Delta S_{\text{NEO-HF}}$[a]	15.41	3.32
$\Delta E_{\text{NEO-HF}} + \Delta ZPE_{\text{NEO-HF}} - T\Delta S_{\text{NEO-HF(V)}}$[b]	15.47	3.32
ΔE_{HF}	13.78	2.85
$\Delta E_{\text{HF}} + \Delta ZPE_{\text{HF}}$	13.23	2.35
$\Delta E_{\text{HF}} + \Delta ZPE_{\text{HF}} - T\Delta S_{\text{HF}}$	14.96	3.24

[a]The vibrational entropy was computed with the NEO Hessian and therefore does not include contributions from the quantum nuclei.
[b]The vibrational entropy was computed with the extended NEO Hessian using the NEO-HF(V) method and therefore includes contributions from both quantum and classical nuclei.

Supplemental Information

The Supporting Information is available free of charge on the JCP website at

DOI: 10.1063/5.0033540. A comparison of semi-numerical and analytic Hessian

elements, the proton potential for the $C_4H_9^+$ transition state, a comparison of

conventional and NEO hydrogen motion along the MEP, imaginary normal mode

vectors for transition states, a comparison of NEO-HF(V) and HF frequencies, details on

the CP-NEO-HF equations, the unrestricted NEO-DFT formulation of the coupled-

perturbed equations, and additional computational details are found in Appendix B.

Acknowledgments

References

(1)   Thomas, I. L., Protonic Structure of Molecules. I. Ammonia Molecules. *Phys. Rev.* **1969,** *185*, 90-94.

(2)   Capitani, J. F.; Nalewajski, R. F.; Parr, R. G., Non-Born–Oppenheimer density functional theory of molecular systems. *J. Chem. Phys.* **1982,** *76*, 568-573.

(3)   Gidopoulos, N., Kohn-Sham equations for multicomponent systems: The exchange and correlation energy functional. *Phys. Rev. B* **1998,** *57*, 2146-2152.

(4)   Webb, S. P.; Iordanov, T.; Hammes-Schiffer, S., Multiconfigurational nuclear-electronic orbital approach: Incorporation of nuclear quantum effects in electronic structure calculations. *J. Chem. Phys.* **2002,** *117*, 4106-4118.

(5)   Ishimoto, T.; Tachikawa, M.; Nagashima, U., Review of multicomponent molecular orbital method for direct treatment of nuclear quantum effect. *Int. J. Quantum Chem.* **2009,** *109*, 2677-2694.

(6)   Hoshino, M.; Nishizawa, H.; Nakai, H., Rigorous non-Born-Oppenheimer theory: Combination of explicitly correlated Gaussian method and nuclear orbital plus molecular orbital theory. *J. Chem. Phys.* **2011,** *135*, 024111.

(7)   Bubin, S.; Pavanello, M.; Tung, W.-C.; Sharkey, K. L.; Adamowicz, L., Born–Oppenheimer and Non-Born–Oppenheimer, Atomic and Molecular Calculations with Explicitly Correlated Gaussians. *Chem. Rev.* **2013,** *113*, 36-79.

(8)   Pavošević, F.; Culpitt, T.; Hammes-Schiffer, S., Multicomponent Quantum Chemistry: Integrating Electronic and Nuclear Quantum Effects via the Nuclear–Electronic Orbital Method. *Chem. Rev.* **2020,** *120*, 4222-4253.

(9)   Iordanov, T.; Hammes-Schiffer, S., Vibrational analysis for the nuclear–electronic orbital method. *J. Chem. Phys.* **2003,** *118*, 9489-9496.

(10)   Borgis, D.; Hynes, J. T., Dynamical theory of proton tunneling transfer rates in solution: general formulation. *Chem. Phys.* **1993,** *170*, 315-346.

(11)   Hammes-Schiffer, S.; Soudackov, A. V., Proton-Coupled Electron Transfer in Solution, Proteins, and Electrochemistry. *J. Phys. Chem. B* **2008,** *112*, 14108-14123.

(12)   Layfield, J. P.; Hammes-Schiffer, S., Hydrogen Tunneling in Enzymes and Biomimetic Models. *Chem. Rev.* **2014,** *114*, 3466-3494.

(13)   Marcus, R. A.; Sutin, N., Electron transfers in chemistry and biology. *Biochim. Biophys. Acta* **1985,** *811*, 265-322.

(14)   Barbara, P. F.; Meyer, T. J.; Ratner, M. A., Contemporary Issues in Electron Transfer Research. *J. Phys. Chem.* **1996,** *100*, 13148-13168.

(15)   Blumberger, J., Recent Advances in the Theory and Molecular Simulation of Biological Electron Transfer Reactions. *Chem. Rev.* **2015,** *115*, 11191-11238.

(16)   Goings, J. J.; Hammes-Schiffer, S., Nonequilibrium Dynamics of Proton-Coupled Electron Transfer in Proton Wires: Concerted but Asynchronous Mechanisms. *ACS Cent. Sci.* **2020,** *6*, 1594-1601.

(17)   Yang, Y.; Schneider, P. E.; Culpitt, T.; Pavošević, F.; Hammes-Schiffer, S., Molecular Vibrational Frequencies within the Nuclear–Electronic Orbital Framework. *J. Phys. Chem. Lett.* **2019,** *10*, 1167-1172.

(18)   Culpitt, T.; Yang, Y.; Schneider, P. E.; Pavošević, F.; Hammes-Schiffer, S., Molecular Vibrational Frequencies with Multiple Quantum Protons within the Nuclear-Electronic Orbital Framework. *J. Chem. Theory Comput.* **2019,** *15*, 6840-6849.

(19)   Pavošević, F.; Culpitt, T.; Hammes-Schiffer, S., Multicomponent Coupled Cluster Singles and Doubles Theory within the Nuclear-Electronic Orbital Framework. *J. Chem. Theory Comput.* **2019,** *15*, 338-347.

(20)   Pavošević, F.; Rousseau, B. J. G.; Hammes-Schiffer, S., Multicomponent Orbital-Optimized Perturbation Theory Methods: Approaching Coupled Cluster Accuracy at Lower Cost. *J. Phys. Chem. Lett.* **2020,** *11*, 1578-1583.

(21)   Pak, M. V.; Chakraborty, A.; Hammes-Schiffer, S., Density Functional Theory Treatment of Electron Correlation in the Nuclear−Electronic Orbital Approach. *J. Phys. Chem. A* **2007,** *111*, 4522-4526.

(22)   Chakraborty, A.; Pak, M. V.; Hammes-Schiffer, S., Development of Electron-Proton Density Functionals for Multicomponent Density Functional Theory. *Phys. Rev. Lett.* **2008,** *101*, 153001.

(23)   Yang, Y.; Brorsen, K. R.; Culpitt, T.; Pak, M. V.; Hammes-Schiffer, S., Development of a practical multicomponent density functional for electron-proton correlation to produce accurate proton densities. *J. Chem. Phys.* **2017,** *147*, 114113.

(24)   Brorsen, K. R.; Yang, Y.; Hammes-Schiffer, S., Multicomponent Density Functional Theory: Impact of Nuclear Quantum Effects on Proton Affinities and Geometries. *J. Phys. Chem. Lett.* **2017,** *8*, 3488-3493.

(25)   Tao, Z.; Yang, Y.; Hammes-Schiffer, S., Multicomponent density functional theory: Including the density gradient in the electron-proton correlation functional for hydrogen and deuterium. *J. Chem. Phys.* **2019,** *151*, 124102.

(26)   Pople, J. A.; Krishnan, R.; Schlegel, H. B.; Binkley, J. S., Derivative studies in hartree-fock and møller-plesset theories. *Int. J. Quantum Chem.* **1979,** *16*, 225-241.

(27)   Gaw, J. F. Analytic evaluation of third and fourth derivatives for Hartree-Fock wave functions. United States, 1984.

(28)   Johnson, B. G.; Fisch, M. J., An implementation of analytic second derivatives of the gradient-corrected density functional energy. *J. Chem. Phys.* **1994,** *100*, 7429-7442.

(29)   Deglmann, P.; Furche, F.; Ahlrichs, R., An efficient implementation of second analytical derivatives for density functional methods. *Chem. Phys. Lett.* **2002,** *362*, 511-518.

(30)   Baker, J., An algorithm for the location of transition states. *J. Comput. Chem.* **1986,** *7*, 385-395.

(31)   Schlegel, H. B., Geometry optimization. *Wiley Interdiscip. Rev. Comput. Mol. Sci.* **2011,** *1*, 790-809.

(32)   Fukui, K., Formulation of the reaction coordinate. *J. Phys. Chem.* **1970,** *74*, 4161-4163.

(33)   Ishida, K.; Morokuma, K.; Komornicki, A., The intrinsic reaction coordinate. An ab initio calculation for HNC→HCN and H−+CH4→CH4+H− *J. Chem. Phys.* **1977,** *66*, 2153-2156.

(34)   Schmidt, M. W.; Gordon, M. S.; Dupuis, M., The intrinsic reaction coordinate and the rotational barrier in silaethylene. *J. Am. Chem. Soc.* **1985,** *107*, 2585-2589.

(35)   Shao, Y.; Gan, Z.; Epifanovsky, E.; Gilbert, A. T. B.; Wormit, M.; Kussmann, J.; Lange, A. W.; Behn, A.; Deng, J.; Feng, X.; Ghosh, D.; Goldey, M.; Horn, P. R.; Jacobson, L. D.; Kaliman, I.; Khaliullin, R. Z.; Kuś, T.; Landau, A.; Liu, J.; Proynov, E. I.; Rhee, Y. M.; Richard, R. M.; Rohrdanz, M. A.; Steele, R. P.; Sundstrom, E. J.; Woodcock, H. L.; Zimmerman, P. M.; Zuev, D.; Albrecht, B.; Alguire, E.; Austin, B.; Beran, G. J. O.; Bernard, Y. A.; Berquist, E.; Brandhorst, K.; Bravaya, K. B.; Brown, S. T.; Casanova, D.; Chang, C.-M.; Chen, Y.; Chien, S. H.; Closser, K. D.; Crittenden, D. L.; Diedenhofen, M.; DiStasio, R. A.; Do, H.; Dutoi, A. D.; Edgar, R. G.; Fatehi, S.; Fusti-Molnar, L.; Ghysels, A.; Golubeva-Zadorozhnaya, A.; Gomes, J.; Hanson-Heine, M. W. D.; Harbach, P. H. P.; Hauser, A. W.; Hohenstein, E. G.; Holden, Z. C.; Jagau, T.-C.; Ji, H.; Kaduk, B.; Khistyaev, K.; Kim, J.; Kim, J.; King, R. A.; Klunzinger, P.; Kosenkov, D.; Kowalczyk, T.; Krauter, C. M.; Lao, K. U.; Laurent, A. D.; Lawler, K. V.; Levchenko, S. V.; Lin, C. Y.; Liu, F.; Livshits, E.; Lochan, R. C.; Luenser, A.; Manohar, P.; Manzer, S. F.; Mao, S.-P.; Mardirossian, N.; Marenich, A. V.; Maurer, S. A.; Mayhall, N. J.; Neuscamman, E.; Oana, C. M.; Olivares-Amaya, R.; O'Neill, D. P.; Parkhill, J. A.; Perrine, T. M.; Peverati, R.; Prociuk, A.; Rehn, D. R.; Rosta, E.; Russ, N. J.; Sharada, S. M.; Sharma, S.; Small, D. W.; Sodt, A.; Stein, T.; Stück, D.; Su, Y.-C.; Thom, A. J. W.; Tsuchimochi, T.; Vanovschi, V.; Vogt, L.; Vydrov, O.; Wang, T.; Watson, M. A.;

Wenzel, J.; White, A.; Williams, C. F.; Yang, J.; Yeganeh, S.; Yost, S. R.; You, Z.-Q.; Zhang, I. Y.; Zhang, X.; Zhao, Y.; Brooks, B. R.; Chan, G. K. L.; Chipman, D. M.; Cramer, C. J.; Goddard, W. A.; Gordon, M. S.; Hehre, W. J.; Klamt, A.; Schaefer, H. F.; Schmidt, M. W.; Sherrill, C. D.; Truhlar, D. G.; Warshel, A.; Xu, X.; Aspuru-Guzik, A.; Baer, R.; Bell, A. T.; Besley, N. A.; Chai, J.-D.; Dreuw, A.; Dunietz, B. D.; Furlani, T. R.; Gwaltney, S. R.; Hsu, C.-P.; Jung, Y.; Kong, J.; Lambrecht, D. S.; Liang, W.; Ochsenfeld, C.; Rassolov, V. A.; Slipchenko, L. V.; Subotnik, J. E.; Van Voorhis, T.; Herbert, J. M.; Krylov, A. I.; Gill, P. M. W.; Head-Gordon, M., Advances in molecular quantum chemistry contained in the Q-Chem 4 program package. *Mol. Phys.* **2015,** *113*, 184-215.

(36)   O'Leary, D. P., The block conjugate gradient algorithm and related methods. *Linear Algebra Appl.* **1980,** *29*, 293-322.

(37)   Clark, T.; Chandrasekhar, J.; Spitznagel, G. W.; Schleyer, P. V. R., Efficient diffuse function-augmented basis sets for anion calculations. III. The 3-21+G basis set for first-row elements, Li–F. *J. Comput. Chem.* **1983,** *4*, 294-301.

(38)   Yu, Q.; Pavošević, F.; Hammes-Schiffer, S., Development of nuclear basis sets for multicomponent quantum chemistry methods. *J. Chem. Phys.* **2020,** *152*, 244123.

(39)   Pak, M. V.; Hammes-Schiffer, S., Electron-Proton Correlation for Hydrogen Tunneling Systems. *Phys. Rev. Lett.* **2004,** *92*, 103002.

(40)   Yang, Y.; Culpitt, T.; Hammes-Schiffer, S., Multicomponent Time-Dependent Density Functional Theory: Proton and Electron Excitation Energies. *J. Phys. Chem. Lett.* **2018,** *9*, 1765-1770.

(41)   Culpitt, T.; Yang, Y.; Pavošević, F.; Tao, Z.; Hammes-Schiffer, S., Enhancing the applicability of multicomponent time-dependent density functional theory. *J. Chem. Phys.* **2019,** *150*, 201101.

(42)   Barone, V., Anharmonic vibrational properties by a fully automated second-order perturbative approach. *J. Chem. Phys.* **2005,** *122*, 014108.

(43)   Marston, C. C.; Balint-Kurti, G. G., The Fourier grid Hamiltonian method for bound state eigenvalues and eigenfunctions. *J. Chem. Phys.* **1989,** *91*, 3571-3576.

(44)   Webb, S. P.; Hammes-Schiffer, S., Fourier grid Hamiltonian multiconfigurational self-consistent-field: A method to calculate multidimensional hydrogen vibrational wavefunctions. *J. Chem. Phys.* **2000,** *113*, 5214-5227.

(45)   Hratchian, H. P.; Schlegel, H. B., Accurate reaction paths using a Hessian based predictor–corrector integrator. *J. Chem. Phys.* **2004,** *120*, 9918-9924.

(46)   Knizia, G., Intrinsic Atomic Orbitals: An Unbiased Bridge between Quantum Theory and Chemical Concepts. *J. Chem. Theory Comput.* **2013,** *9*, 4834-4843.

(47)   Knizia, G.; Klein, J. E. M. N., Electron Flow in Reaction Mechanisms—Revealed from First Principles. *Angew. Chem. Int.* **2015,** *54*, 5518-5522.

(48)   Kreibich, T.; Gross, E. K. U., Multicomponent Density-Functional Theory for Electrons and Nuclei. *Phys. Rev. Lett.* **2001,** *86*, 2984-2987.

(49)   Bochevarov, A. D.; Valeev, E. F.; Sherrill, C. D., The electron and nuclear orbitals model: current challenges and future prospects. *Mol. Phys.* **2004,** *102*, 111-123.

(50)   Yu, Q.; Hammes-Schiffer, S., Nuclear-Electronic Orbital Multistate Density Functional Theory. *J. Phys. Chem. Lett.* **2020,** *11*, 10106-10113.

Chapter Four

Molecular Vibrational Frequencies within the Nuclear-Electronic Orbital Framework

Author contributions

All authors designed calculations. Y.Y., P.E.S., and T.C. derived the theory. P.E.S. and T.C. implemented the code for the computations and performed the calculations. P.E.S. created the figures and tables. All authors wrote the manuscript. Y.Y. and P.E.S. contributed equally to this work.

Abstract

A significant challenge of multicomponent quantum chemistry methods is the calculation of vibrational frequencies for comparison to experiment. The nuclear-electronic orbital (NEO) approach treats specified nuclei, typically key protons, quantum mechanically. The Born-Oppenheimer separation between the quantum and classical nuclei prevents the direct calculation of vibrational frequencies corresponding to modes composed of both types of nuclei. Herein an effective strategy for calculating the vibrational frequencies of the entire molecule within the NEO framework is devised and implemented. This strategy requires diagonalization of an extended NEO Hessian that depends on the expectation values of the quantum nuclei as well as the coordinates of the classical nuclei and is constructed with input from multicomponent time-dependent density functional theory (NEO-TDDFT). Application of this NEO-DFT(V) approach to molecular systems illustrates that it accurately incorporates the most significant anharmonic effects. This general theoretical formulation opens up a broad spectrum of new directions for multicomponent quantum chemistry.

Introduction

Multicomponent quantum chemistry, in which more than one type of particle is treated quantum mechanically with either wavefunction methods or density functional theory (DFT), is an emerging research field.[1-8] A significant advantage of multicomponent quantum chemistry is that electronic and nuclear quantum effects can be described simultaneously while avoiding the Born-Oppenheimer separation between the electrons and the quantum nuclei. The nuclear-electronic orbital (NEO) approach[3, 5-6, 9-11] balances chemical accuracy and computational practicality by treating all electrons and one or more nuclei, typically key protons, quantum mechanically, while treating at least two nuclei classically to avoid difficulties with translations and rotations. The NEO potential energy surface depends on only the coordinates of the classical nuclei,[12] predicated on the assumption that the electrons and quantum nuclei respond instantaneously to the motion of the classical nuclei. The characterization of stationary points on the NEO potential energy surface as minima or saddle points requires the computation of the NEO Hessian matrix within the coordinate space.[12] The Hessian matrix is also crucial for obtaining the intrinsic reaction coordinate (IRC) or the minimum energy path within the NEO framework. Thus, an efficient method for computing the NEO Hessian matrix is essential for a wide range of applications.

A significant challenge of multicomponent quantum chemistry methods is the calculation of meaningful vibrational frequencies. Molecular geometries can be described by representing the positions of the quantum nuclei by the expectation values of their coordinates. The Born-Oppenheimer separation between the quantum and classical nuclei, reflected by the instantaneous response of the former to the latter,

prevents the direct calculation of vibrational frequencies corresponding to modes composed of both types of nuclei. As a result, the vibrational modes obtained from diagonalizing the NEO Hessian matrix at a minimum on the NEO potential energy surface are not directly connected to those obtained from experimental infrared or Raman spectroscopy. In order to build this connection and enable the calculation of meaningful vibrational frequencies within the NEO framework, the quantum and classical nuclei must be coupled in a rigorous manner.

In this chapter, we derive the equations to efficiently calculate the NEO Hessian matrix and devise an effective strategy to enable the calculation of meaningful vibrational frequencies. The NEO Hessian is composed of second derivatives of the NEO energy with respect to only the classical nuclei, invoking the Born-Oppenheimer separation between the quantum and classical nuclei. The vibrational frequencies are calculated by diagonalizing an extended NEO Hessian that includes second derivatives of the NEO energy with respect to the expectation values of the quantum nuclei as well as the classical nuclei, thereby coupling these two types of nuclei. Diagonalization of this extended NEO Hessian produces vibrational modes that are composed of both types of nuclei and therefore can be directly connected to the vibrational modes measured spectroscopically. This strategy, denoted NEO-DFT(V), differs from conventional quantum chemistry calculations of vibrational frequencies because the delocalization and zero point energy effects of the quantum nuclei are included in the geometry optimizations, and anharmonic effects are included in the expectation values of the quantum nuclei used in the extended NEO Hessian. These differences are expected to improve the quantitative accuracy of the vibrational frequencies, particularly

72

those involving the quantum nuclei. After deriving the key equations, we apply this strategy to a set of molecular systems and compare the calculated vibrational frequencies to experimental data.

Theory

For a system with N_c classical nuclei and N_q quantum nuclei, the NEO potential energy surface depends on only the coordinates of the classical nuclei and therefore is $3N_c$-dimensional.[12] In practice, a single-point energy calculation within the NEO framework also depends on the positions of the electronic and nuclear basis function centers associated with the quantum nuclei. Here we assume that the quantum nuclei are described by a total of N_b basis function centers. Although often each quantum nucleus is represented by a single basis function center that is the same for both electronic and nuclear basis functions, leading to $N_b = N_q$, this assumption is not necessary. For a finite basis set, the positions of the basis function centers associated with the quantum nuclei must be optimized variationally to compute each point on the NEO potential energy surface (i.e., for each configuration of the classical nuclei). Mathematically, the NEO potential energy surface is defined by

$$E = E(\mathbf{r}_c, \mathbf{r}_b(\mathbf{r}_c)) \tag{4.1}$$

where $\mathbf{r}_c$ is a $3N_c$-dimensional vector denoting the combined coordinates of the classical nuclei and $\mathbf{r}_b$ is a $3N_b$-dimensional vector denoting the combined coordinates of the basis function centers associated with the quantum nuclei. According to the definition of the NEO potential energy surface, the coordinates $\mathbf{r}_b$ depend on the classical nuclear coordinates $\mathbf{r}_c$ and satisfy the condition

$$\frac{\partial E}{\partial \mathbf{r}_b} = 0 . \tag{4.2}$$

Using the chain rule, the gradient of the NEO energy, which is a $3N_c$-dimensional vector,

is

$$\frac{\mathrm{d}E}{\mathrm{d}\mathbf{r}_c} = \frac{\partial E}{\partial \mathbf{r}_c} + \frac{\partial E}{\partial \mathbf{r}_b} \frac{\mathrm{d}\mathbf{r}_b}{\mathrm{d}\mathbf{r}_c} = \frac{\partial E}{\partial \mathbf{r}_c} \tag{4.3}$$

where the second equality arises because Eq. (4.2) is satisfied.

The NEO Hessian matrix, a $3N_c \times 3N_c$ square matrix, can be obtained as

$$\frac{\mathrm{d}^2 E}{\mathrm{d}\mathbf{r}_c^2} = \frac{\partial^2 E}{\partial \mathbf{r}_c^2} + 2\frac{\partial^2 E}{\partial \mathbf{r}_b \partial \mathbf{r}_c}\frac{\mathrm{d}\mathbf{r}_b}{\mathrm{d}\mathbf{r}_c} + \frac{\partial^2 E}{\partial \mathbf{r}_b^2}\left(\frac{\mathrm{d}\mathbf{r}_b}{\mathrm{d}\mathbf{r}_c}\right)^2 + \frac{\partial E}{\partial \mathbf{r}_b}\frac{\mathrm{d}^2 \mathbf{r}_b}{\mathrm{d}\mathbf{r}_c^2} \tag{4.4}$$

where this compact notation does not explicitly indicate the order of matrix operations

and transpose of certain matrices for practical implementation. The direct evaluation of

this form is not straightforward because the function $\mathbf{r}_b = \mathbf{r}_b(\mathbf{r}_c)$ is not explicitly known.

However, this expression can be simplified by taking the derivative of Eq. (4.2) with

respect to $\mathbf{r}_c$, yielding:

$$\frac{\partial^2 E}{\partial \mathbf{r}_b \partial \mathbf{r}_c} + \frac{\partial^2 E}{\partial \mathbf{r}_b^2}\frac{\mathrm{d}\mathbf{r}_b}{\mathrm{d}\mathbf{r}_c} = 0 \tag{4.5}$$

and solving for $\dfrac{\mathrm{d}\mathbf{r}_b}{\mathrm{d}\mathbf{r}_c}$. Eqs. (4.2) and (4.5) lead to the simplification of the Hessian

matrix in Eq. (4.4) as

$$\frac{\mathrm{d}^2 E}{\mathrm{d}\mathbf{r}_c^2} = \frac{\partial^2 E}{\partial \mathbf{r}_c^2} - \frac{\partial^2 E}{\partial \mathbf{r}_b \partial \mathbf{r}_c}\left(\frac{\partial^2 E}{\partial \mathbf{r}_b^2}\right)^{-1}\frac{\partial^2 E}{\partial \mathbf{r}_b \partial \mathbf{r}_c} . \tag{4.6}$$

In this new form, only second-order energy derivatives remain, and all of these terms

can be evaluated numerically or analytically. Defining the three submatrices $\mathbf{H}_{cc} = \dfrac{\partial^2 E}{\partial \mathbf{r}_c^2}$,

$\mathbf{H}_{bc} = \dfrac{\partial^2 E}{\partial \mathbf{r}_b \partial \mathbf{r}_c}$, and $\mathbf{H}_{bb} = \dfrac{\partial^2 E}{\partial \mathbf{r}_b^2}$, as well as the NEO Hessian matrix $\mathbf{H}^{\mathrm{NEO}}$, Eq. (4.6) can

be expressed as

$$\mathbf{H}^{\mathrm{NEO}} = \mathbf{H}_{cc} - \mathbf{H}_{bc}^{\mathrm{T}} \mathbf{H}_{bb}^{-1} \mathbf{H}_{bc} . \tag{4.7}$$

This matrix folding process accounts for the effect of the optimization of the nuclear

basis function centers associated with the quantum nuclei.

Diagonalizing the NEO Hessian given in Eq. (4.7) leads to the vibrational modes

within the classical coordinate space, assuming that the quantum nuclei respond

instantaneously to the motion of classical nuclei. However, because the mass difference

between classical and quantum nuclei is not substantial, non-Born-Oppenheimer or

nonadiabatic effects between the two types of nuclei may be significant. Moreover, the

NEO framework does not provide frequencies that can be compared directly with

experimentally measured IR spectra because the normal modes obtained from the NEO

Hessian depend on only the classical nuclear coordinates and do not accurately

describe the coupling effects between the classical and quantum nuclear motions. To

address this issue, we propose and implement a practical strategy to recover the

experimentally meaningful vibrational modes by combining NEO Hessian and NEO-

TDDFT calculations.[13]

In a NEO calculation, the Hessian matrix is defined in the space of the N_c

classical nuclear coordinates, denoted by $\mathbf{r}_c$, and the normal modes obtained from this

Hessian do not depend explicitly on the quantum nuclear coordinates. However, an

extended NEO Hessian may be defined to depend on both the classical nuclear

coordinates, $\mathbf{r}_c$, and the expectation values of the quantum nuclear coordinates defined as

$$\mathbf{r}_{q_i} = \int \mathbf{r} \rho_{q_i}(\mathbf{r}) \mathrm{d}\mathbf{r} \ . \tag{4.8}$$

Here $\rho_{q_i}(\mathbf{r})$ and $\mathbf{r}_{q_i}$ denote the density and expectation value (i.e., average position), respectively, of the ith quantum nucleus. This extended NEO Hessian matrix can be divided into three submatrices: $\mathbf{H}_0 = \dfrac{\partial^2 E}{\partial \mathbf{r}_c^2}$, $\mathbf{H}_1 = \dfrac{\partial^2 E}{\partial \mathbf{r}_q \partial \mathbf{r}_c}$, $\mathbf{H}_2 = \dfrac{\partial^2 E}{\partial \mathbf{r}_q^2}$, where $\mathbf{r}_q$ is a $3N_q$-dimensional vector denoting the combined coordinates of the expectation values of the quantum nuclei. Analogous to conventional quantum chemistry calculations, the non-zero eigenvalues of the mass-weighted extended Hessian matrix correspond to the squares of the frequencies of the vibrational modes, and the associated eigenvectors correspond to the amplitudes of motion along the mass-weighted coordinates for these modes.

The $\dfrac{\partial^2 E}{\partial \mathbf{r}_q^2}$ term defined as $\mathbf{H}_2$ is the force constant matrix for the quantum nuclei while all classical nuclei are fixed within the harmonic oscillator approximation. Thus, this term is related to the harmonic vibrational excitation frequencies, which can be approximated by the vibrational excitation frequencies ω obtained from a NEO-TDDFT calculation.[13] In this case, the Hessian matrix elements can be calculated as

$$\frac{\partial^2 E}{\partial \mathbf{r}_q^2} = \mathbf{U}^\dagger \mathbf{\Omega} \mathbf{M} \mathbf{U} \tag{4.9}$$

where $\mathbf{M}$ is the diagonal mass matrix corresponding to the quantum nuclei, $\mathbf{\Omega}$ is the diagonal matrix with elements ω^2 corresponding to the NEO-TDDFT vibrational

76

frequencies for fixed classical nuclei, and $\mathbf{U}$ is a unitary matrix that transforms the

diagonal frequency matrix to a coordinate system consistent with the other molecular

vibrational modes. Note that nuclear delocalization and aharmonicity effects of the

quantum nuclei are included in the vibrational excitation frequencies ω, as well as in the

optimized geometries and expectation values of the quantum nuclear coordinates.

Although these anharmonic frequencies are incorporated as second-order harmonic

frequency terms in the extended Hessian, this procedure incorporates a portion of these

physically significant effects. This point will be discussed further below in the analysis of

the applications.

The $\dfrac{\partial^2 E}{\partial \mathbf{r}_c^2}$ term defined as $\mathbf{H}_0$ is the force constant matrix for the classical

nuclei with the expectation values of the quantum nuclei fixed. Therefore, it differs from

the elements of the NEO Hessian defined in Eq. (4.7), which requires the quantum

nuclei to respond instantaneously to the motion of the classical nuclei. The NEO energy

can be expressed as

$$E = E(\mathbf{r}_c, \mathbf{r}_q(\mathbf{r}_c)) \qquad (4.10)$$

where the expectation values of the quantum nuclei depend on the classical nuclear

coordinates. Because the NEO energy is computed by variationally optimizing the

densities of the quantum nuclei, the energy is stationary with respect to the expectation

values of the quantum nuclei (see Appendix C for details):

$$\frac{\partial E}{\partial \mathbf{r}_q} = 0 . \qquad (4.11)$$

Equations (4.10) and (4.11) have the same form as Eqs. (4.1) and (4.2), except that

the positions of the basis function centers, $\mathbf{r}_b$, have been substituted with the

expectation values of the quantum nuclei, $\mathbf{r}_q$. Following the same mathematical

derivations leads to

$$\frac{\mathrm{d}^2 E}{\mathrm{d}\mathbf{r}_c^2} = \frac{\partial^2 E}{\partial \mathbf{r}_c^2} - \frac{\partial^2 E}{\partial \mathbf{r}_q \partial \mathbf{r}_c} \left(\frac{\partial^2 E}{\partial \mathbf{r}_q^2} \right)^{-1} \frac{\partial^2 E}{\partial \mathbf{r}_q \partial \mathbf{r}_c} \tag{4.12}$$

$$\mathbf{H}^{\mathrm{NEO}} = \mathbf{H}_0 - \mathbf{H}_1^{\mathrm{T}} \mathbf{H}_2^{-1} \mathbf{H}_1 . \tag{4.13}$$

In this case, $\mathbf{H}_0$ is the target matrix that contains the $\dfrac{\partial^2 E}{\partial \mathbf{r}_c^2}$ matrix elements and can

be obtained by

$$\mathbf{H}_0 = \mathbf{H}^{\mathrm{NEO}} + \mathbf{H}_1^{\mathrm{T}} \mathbf{H}_2^{-1} \mathbf{H}_1 , \tag{4.14}$$

The NEO Hessian $\mathbf{H}^{\mathrm{NEO}}$ is already known from Eq. (4.7), $\mathbf{H}_2^{-1}$ can be calculated as

described above, and $\mathbf{H}_1$ will be derived in the next step.

The derivation of $\mathbf{H}_1$ utilizes the analog of Eq. (4.5) with $\mathbf{r}_b$ substituted by $\mathbf{r}_q$:

$$\frac{\partial^2 E}{\partial \mathbf{r}_q \partial \mathbf{r}_c} + \frac{\partial^2 E}{\partial \mathbf{r}_q^2} \frac{\mathrm{d}\mathbf{r}_q}{\mathrm{d}\mathbf{r}_c} = 0 , \tag{4.15}$$

Rearrangement of this equation provides the matrix elements in $\mathbf{H}_1$:

$$\frac{\partial^2 E}{\partial \mathbf{r}_q \partial \mathbf{r}_c} = -\frac{\partial^2 E}{\partial \mathbf{r}_q^2} \frac{\mathrm{d}\mathbf{r}_q}{\mathrm{d}\mathbf{r}_c} \tag{4.16}$$

$$\mathbf{H}_1 = -\mathbf{H}_2 \mathbf{R}$$

with the response of $\mathbf{r}_q$ to $\mathbf{r}_c$ defined as

$$\mathbf{R} = \frac{\mathrm{d}\mathbf{r}_q}{\mathrm{d}\mathbf{r}_c} = \frac{\mathrm{d}}{\mathrm{d}\mathbf{r}_c} \int \mathbf{r} \rho_{q_i}(\mathbf{r}) \mathrm{d}\mathbf{r} = \int \mathbf{r} \frac{\mathrm{d}\rho_{q_i}(\mathbf{r})}{\mathrm{d}\mathbf{r}_c} \mathrm{d}\mathbf{r} . \tag{4.17}$$

The matrix $\mathbf{R}$ can be calculated either numerically or analytically. For the applications

described below, we compute the numerical gradient of the expectation value of each

quantum nucleus with respect to each classical nucleus. Analytically, the density matrix response with respect to changes in the classical nuclear coordinates can be obtained by coupled perturbed NEO-Hartree-Fock equations, as described in Appendix C.

Combining all of these parts, the extended Hessian matrix can be calculated from the following expressions:

$$\mathbf{H}_2 = \mathbf{U}^\dagger \boldsymbol{\Omega} \mathbf{M} \mathbf{U} \tag{4.18}$$

$$\mathbf{H}_1 = -\mathbf{H}_2 \mathbf{R} \tag{4.19}$$

$$\mathbf{H}_0 = \mathbf{H}^{\text{NEO}} + \mathbf{H}_1^{\text{T}} \mathbf{H}_2^{-1} \mathbf{H}_1 = \mathbf{H}^{\text{NEO}} + \mathbf{R}^{\text{T}} \mathbf{H}_2 \mathbf{R} \tag{4.20}$$

Note that all of these quantities are straightforward to calculate. The two matrices $\mathbf{H}^{\text{NEO}}$ and $\mathbf{R}$ can be calculated numerically or analytically within the NEO-DFT method, while $\mathbf{H}_2$ is constructed from the results of a NEO-TDDFT calculation. These three matrices alone are sufficient for calculating the remaining required pieces for the full vibrational analysis, which is performed on the mass-weighted extended Hessian matrix. The construction of the extended Hessian matrix is depicted in Figure 4.1, and an example of this NEO-DFT(V) procedure applied to HCN is depicted in Figure 4.2.

Results and Discussion

Herein the NEO-DFT(V) method is used to compute the vibrational modes for a set of five molecular systems, each with a single proton. For each system, the geometries were optimized at the NEO-DFT level with the B3LYP electronic exchange-correlation functional[14-16] and the epc17-2 electron-proton correlation functional.[10] The cc-pVTZ[17] electronic basis set was used for all heavy nuclei, while the cc-pV6Z[18] basis set, excluding the *h*-function (denoted cc-pV6Z* herein), was employed for the protons. An even-tempered 8*s*8*p*8*d*8*f* proton basis set was used for all calculations with

$\alpha = 2\sqrt{2}$ and $\beta = \sqrt{2}$.[19] The NEO Hessian and the derivatives of the expectation value of the quantum proton with respect to the classical nuclei were computed numerically. The NEO-TDDFT calculations were performed at the same level of theory for these geometries with the exception that the cc-pVDZ[17] basis set was used for the oxygen and flurine atoms in HCFO and the fluorine atoms in HCF_3. For the TDDFT calculations, the proton basis function centers were placed at the covalent bond distance determined from conventional DFT; the results with the proton basis function centers placed at the expectation values are similar (Table C1 of Appendix C). The unitary matrix $\mathbf{U}$ in Eq. (4.9) is determined from the normal modes of the quantum proton, as obtained from the conventional DFT Hessian when all classical nuclei are assigned infinite masses. An alternative procedure based on NEO-TDDFT will be explored in future work. All of the NEO calculations and the conventional DFT calculations were performed with an in-house modified version of the GAMESS program.[20] For comparison, we also performed conventional DFT calculations including third and fourth order anharmonic terms using Gaussian09.[21] Although these molecules each contain only a single hydrogen nucleus, the extension to multiple protons is straightforward. For multiple protons, the extended Hessian depends on the expectation value of each proton orbital, and NEO-TDDFT is used to compute the vibrational frequencies for each proton.

The vibrational frequencies obtained from these calculations, as well as experimental data, are given in Table 4.1. The conventional harmonic DFT and NEO-DFT(V) methods provide similarly accurate vibrational frequencies, with the exception that the hydrogen stretch frequencies for terminal hydrogen nuclei are notably lower and closer to the experimental values when calculated with the NEO-DFT(V) method. This

decrease in the frequency of the hydrogen stretch is attributed to the anharmonic effects included directly in the NEO-DFT(V) calculations. Application of numerical third- and fourth-order corrections to the conventional DFT calculations supports this assertion, as the hydrogen stretch frequencies decrease by a similar amount. The hydrogen bending modes are more challenging to compute for linear molecules, as indicated by overestimates of these frequencies by vibrational self-consistent-field calculations (Table C2 of Appendix C). Thus, the NEO-DFT(V) method accurately incorporates the most significant anharmonic effects that lead to a substantial decrease in the hydrogen stretch frequencies.

A different trend is observed for the FHF^- system, where inclusion of anharmonic effects via NEO-DFT(V) or conventional DFT increases the hydrogen stretch frequency. This phenomonen of anharmonicity increasing the hydrogen stretch frequency for FHF^- is not uncommon for an internal hydrogen nucleus moving in a single well potential between two other nuclei, in contrast to the terminal hydrogen nuclei in the other molecules studied here. In this case, inclusion of anharmonicity increases the deviation of the calculated hydrogen stretch frequency compared to the experimental value. This deviation is attributed to limitations of the underlying DFT method on the basis of the similar trend observed in the conventional DFT calculations including anharmonic corrections. Moreover, coupled-cluster singles and doubles with perturbative triples (CCSD(T)) calculations[22] produce a hydrogen stretch frequency of 1195 cm^{-1} with a harmonic treatment and 1343 cm^{-1} with an anharmonic treatment, in good agreement with the experimental value. The magnitude of the increase in frequency due to anharmonic effects in these CCSD(T) calculations is similar to that observed with NEO-

DFT(V), confirming that the anharmonic effects are being described in a reasonable manner.

Conclusions

In this chapter, we presented an efficient method for computing the NEO Hessian matrix and a novel strategy for calculating the vibrational frequencies of the entire molecule. The NEO Hessian matrix is required for characterizing stationary points on the NEO potential energy surface and for generating the IRC or minimum energy path. However, the NEO Hessian matrix alone is not sufficient to compute vibrational frequencies composed of both classical and quantum nuclei. For this purpose, we devised an extended NEO Hessian that depends on the expectation values of the quantum nuclei as well as the coordinates of the classical nuclei. Diagonalization of this extended NEO Hessian, which relies on input from NEO-TDDFT, produces vibrational modes that are directly related to those measured spectroscopically. Application of this NEO-DFT(V) approach to a series of five molecules illustrates that this approach accurately includes anharmonic effects of the hydrogen nuclei. This general theoretical formulation opens up a broad spectrum of new directions for both DFT and wavefunction-based multicomponent quantum chemistry.

Figures and Tables

Figure 4.1: Schematic depiction of the extended Hessian matrix (upper left corner) associated with the coordinates of the classical nuclei and the expectation values of the quantum nuclei[a]

[a]The components $\mathbf{H}_0$, $\mathbf{H}_1$, and $\mathbf{H}_2$ are defined in Eqs. (4.18)-(4.20). $\mathbf{H}_{\text{NEO}}$ is the $3N_c \times 3N_c$ NEO Hessian matrix defined in Eq. (4.7), predicated on the instantaneous response of the quantum nuclei to the classical nuclei. $\mathbf{H}_2$ is the $3N_q \times 3N_q$ matrix computed from a unitary transform of the diagonal matrix composed of the NEO-TDDFT vibrational excitation frequencies associated with the quantum nuclei for fixed classical nuclei. $\mathbf{R}$ is the $3N_q \times 3N_c$ matrix defined in Eq. (4.17), corresponding to the derivatives of the expectation values of the quantum nuclei with respect to the classical nuclear coordinates.
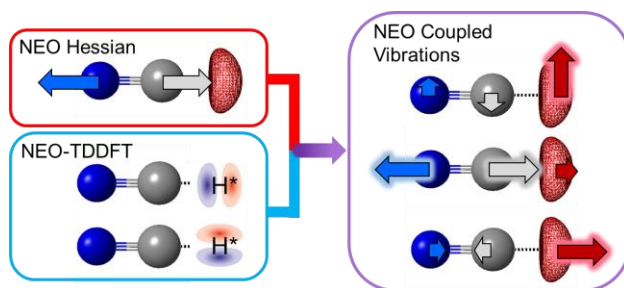
Figure 4.2: Schematic depiction of the application of the NEO-DFT(V) method to HCN, where the hydrogen nucleus and all electrons are treated quantum mechanically[a]

[a]The quantum proton is depicted in red mesh, and the classical nuclei carbon and nitrogen are depicted in gray and blue, respectively. The NEO Hessian calculation produces the CN vibrational stretch with the hydrogen nucleus responding instantaneously to this motion. The NEO-TDDFT calculation provides the vibrational excitation frequencies associated with the bend (doubly degenerate) and stretch for the hydrogen nucleus with the carbon and nitrogen nuclei fixed. This information is combined to construct the extended Hessian, as shown in Figure 4.1, to produce the four coupled vibrational motions shown on the right, where the bend is doubly degenerate.

Table 4.1: Vibrational Frequencies (in cm^{-1}) Calculated with Conventional DFT with Harmonic and Anharmonic Treatments and with NEO-DFT(V)

	Vibrational Mode	Experiment	NEO-DFT(V)[a]	Conv. Anharmonic[b]	Conv. Harmonic[b]
HCN [c]	CH stretch	3311	3317	3321	3439
	CN stretch	2097	2191	2177	2201
	CH bend	712	789	753	773
HNC [d]	NH stretch	3653	3645	3644	3814
	NC stretch	2024	2100	2073	2105
	NH bend	462	568	464	480
HCFO[e]	CH stretch	2976	2947	2942	3081
	CO stretch	1834	1885	1861	1891
	CH in-plane bend	1344	1329	1341	1370
	CF stretch	1070	1075	1049	1069
	CH out-of-plane bend	1000–1050	1061	1019	1039
	OCF scissor	661	665	659	665
HCF$_3$ [f]	CH stretch	3035	2988	2999	3119
	CH bend	1376	1353	1360	1388
	CF asymmetric stretch	1152	1134	1117	1139
	CF symmetric stretch	1137	1128	1118	1133
	CF simultaneous bend	700	693	688	694
	FCF scissor	508	501	497	501
FHF$^-$ [g]	FH stretch	1331	1695	1615	1451
	FH bend	1286	1302	1287	1360
	FF stretch	583	617	557	625

[a]NEO-DFT/B3LYP/epc17-2 with electronic and nuclear basis sets given in the text. [b]DFT/B3LYP; cc-pVTZ basis set for heavy nuclei and cc-pV6Z (cc-pV6Z*) basis set for the hydrogen for anharmonic (harmonic) treatment. [c]Experimental data from Ref. [23]. [d]Experimental data from Ref. [24]. [e]Experimental data from Ref. [25]. [f]Experimental data from Ref. [26]. [g]Experimental data from Ref. [27].

Supplemental Information

The Supporting Information is available free of charge on the ACS Publications

website at DOI: 10.1021/acs.jpclett.9b00299. Proof that derivative of NEO energy with

respect to expectation value of quantum nucleus vanishes, additional tables of

computed vibrational frequencies with different methods for comparison, and the

analytical expression for the R matrix are found in Appendix C.

Acknowledgments

References

(1)   Thomas, I. L., Protonic Structure of Molecules. I. Ammonia Molecules. *Physical Review* **1969,** *185*, 90-94.

(2)   Kreibich, T.; Gross, E. K. U., Multicomponent Density-Functional Theory for Electrons and Nuclei. *Phys. Rev. Lett.* **2001,** *86*, 2984-2987.

(3)   Webb, S. P.; Iordanov, T.; Hammes-Schiffer, S., Multiconfigurational nuclear-electronic orbital approach: Incorporation of nuclear quantum effects in electronic structure calculations. *J. Chem. Phys.* **2002,** *117*, 4106-4118.

(4)   Nakai, H., Simultaneous determination of nuclear and electronic wave functions without Born–Oppenheimer approximation: Ab initio NO+MO/HF theory. *Int. J. Quantum Chem.* **2002,** *86*, 511-517.

(5)   Pak, M. V.; Chakraborty, A.; Hammes-Schiffer, S., Density Functional Theory Treatment of Electron Correlation in the Nuclear−Electronic Orbital Approach. *J. Phys. Chem. A* **2007,** *111*, 4522-4526.

(6)   Chakraborty, A.; Pak, M. V.; Hammes-Schiffer, S., Development of Electron-Proton Density Functionals for Multicomponent Density Functional Theory. *Phys. Rev. Lett.* **2008,** *101*, 153001.

(7)   Ishimoto, T.; Tachikawa, M.; Nagashima, U., Review of multicomponent molecular orbital method for direct treatment of nuclear quantum effect. *Int. J. Quantum Chem.* **2009,** *109*, 2677-2694.

(8)   Bubin, S.; Pavanello, M.; Tung, W.-C.; Sharkey, K. L.; Adamowicz, L., Born–Oppenheimer and Non-Born–Oppenheimer, Atomic and Molecular Calculations with Explicitly Correlated Gaussians. *Chem. Rev.* **2013,** *113*, 36-79.

(9)   Yang, Y.; Brorsen, K. R.; Culpitt, T.; Pak, M. V.; Hammes-Schiffer, S., Development of a practical multicomponent density functional for electron-proton correlation to produce accurate proton densities. *J. Chem. Phys.* **2017,** *147*, 114113.

(10)   Brorsen, K. R.; Yang, Y.; Hammes-Schiffer, S., Multicomponent Density Functional Theory: Impact of Nuclear Quantum Effects on Proton Affinities and Geometries. *J. Phys. Chem. Lett.* **2017,** *8*, 3488-3493.

(11)   Pavošević, F.; Culpitt, T.; Hammes-Schiffer, S., Multicomponent Coupled Cluster Singles and Doubles Theory within the Nuclear-Electronic Orbital Framework. *Journal of Chemical Theory and Computation* **2019,** *15*, 338-347.

(12)   Iordanov, T.; Hammes-Schiffer, S., Vibrational analysis for the nuclear–electronic orbital method. *J. Chem. Phys.* **2003,** *118*, 9489-9496.

(13)   Yang, Y.; Culpitt, T.; Hammes-Schiffer, S., Multicomponent Time-Dependent Density Functional Theory: Proton and Electron Excitation Energies. *J. Phys. Chem. Lett.* **2018,** *9*, 1765-1770.

(14)   Becke, A. D., Density-functional exchange-energy approximation with correct asymptotic behavior. *Phys. Rev. A* **1988,** *38*, 3098-3100.

(15)   Becke, A. D., Density-functional thermochemistry. III. The role of exact exchange. *J. Chem. Phys.* **1993,** *98*, 5648-5652.

(16)   Lee, C.; Yang, W.; Parr, R. G., Development of the Colle-Salvetti correlation-energy formula into a functional of the electron density. *Phys. Rev. B* **1988,** *37*, 785-789.

(17)   Dunning, T. H., Jr., Gaussian basis sets for use in correlated molecular calculations. I. The atoms boron through neon and hydrogen. *J. Chem. Phys.* **1989,** *90*, 1007-1023.

(18)   Peterson, K. A.; Woon, D. E.; Dunning, T. H., Jr., Benchmark calculations with correlated molecular wave functions. IV. The classical barrier height of the H+H2→H2+H reaction. *J. Chem. Phys.* **1994,** *100*, 7410-7415.

(19)   Feller, D. F.; Ruedenberg, K., Systematic approach to extended even-tempered orbital

bases for atomic and molecular calculations. *Theor. Chim. Acta.* **1979,** *52*, 231-251.

(20)   Schmidt, M. W.; Baldridge, K. K.; Boatz, J. A.; Elbert, S. T.; Gordon, M. S.; Jensen, J. H.; Koseki, S.; Matsunaga, N.; Nguyen, K. A.; Su, S.; Windus, T. L.; Dupuis, M.; Montgomery Jr, J. A., General atomic and molecular electronic structure system. *J. Comput. Chem.* **1993,** *14*, 1347-1363.

(21)   Frisch, M. J.; Trucks, G. W.; Schlegel, H. B.; Scuseria, G. E.; Robb, M. A.; Cheeseman, J. R.; Scalmani, G.; Barone, V.; Petersson, G. A.; Nakatsuji, H.; Li, X.; Caricato, M.; Marenich, A. V.; Bloino, J.; Janesko, B. G.; Gomperts, R.; Mennucci, B.; Hratchian, H. P.; Ortiz, J. V.; Izmaylov, A. F.; Sonnenberg, J. L.; Williams; Ding, F.; Lipparini, F.; Egidi, F.; Goings, J.; Peng, B.; Petrone, A.; Henderson, T.; Ranasinghe, D.; Zakrzewski, V. G.; Gao, J.; Rega, N.; Zheng, G.; Liang, W.; Hada, M.; Ehara, M.; Toyota, K.; Fukuda, R.; Hasegawa, J.; Ishida, M.; Nakajima, T.; Honda, Y.; Kitao, O.; Nakai, H.; Vreven, T.; Throssell, K.; Montgomery Jr., J. A.; Peralta, J. E.; Ogliaro, F.; Bearpark, M. J.; Heyd, J. J.; Brothers, E. N.; Kudin, K. N.; Staroverov, V. N.; Keith, T. A.; Kobayashi, R.; Normand, J.; Raghavachari, K.; Rendell, A. P.; Burant, J. C.; Iyengar, S. S.; Tomasi, J.; Cossi, M.; Millam, J. M.; Klene, M.; Adamo, C.; Cammi, R.; Ochterski, J. W.; Martin, R. L.; Morokuma, K.; Farkas, O.; Foresman, J. B.; Fox, D. J. *Gaussian 16 Rev. B.01*, Wallingford, CT, 2016.

(22)   Hirata, S.; Yagi, K.; Perera, S. A.; Yamazaki, S.; Hirao, K., Anharmonic vibrational frequencies and vibrationally averaged structures and nuclear magnetic resonance parameters of FHF−. *J. Chem. Phys.* **2008,** *128*, 214305.

(23)   McBride, B. J.; Gordon, S., Thermodynamic Functions of Several Triatomic Molecules in the Ideal Gas State. *J. Chem. Phys.* **1961,** *35*, 2198-2206.

(24)   Burkholder, J. B.; Sinha, A.; Hammer, P. D.; Howard, C. J., High-resolution Fourier transform infrared spectroscopy of the fundamental bands of HNC. *J. Mol. Spectrosc.* **1987,** *126*, 72-77.

(25)   Morgan, H. W.; Staats, P. A.; Goldstein, J. H., Vibrational Spectra of Formyl Fluoride and d-Formyl Fluoride. *J. Chem. Phys.* **1956,** *25*, 337-342.

(26)   Long, D. A.; Gravenor, R. B.; Jones, D. T. L., Force constant calculations. Part 9.—CF3H and CF3D. *J. Chem. Soc. Faraday Trans.* **1964,** *60*, 1509-1514.

(27)   Kawaguchi, K.; Hirota, E., Diode laser spectroscopy of the v3 and v2 bands of FHF− in 1300 cm−1 region. *J. Chem. Phys.* **1987,** *87*, 6838-6841.

Chapter Five

Molecular Vibrational Frequencies with Multiple Quantum Protons within the Nuclear-Electronic Orbital Framework

Author contributions

All authors designed calculations. T.C., Y.Y., and P.E.S. derived the theory. T.C. implemented the code for the computations. T.C. and P.E.S. performed the calculations. T.C. and P.E.S. created the figures and tables. All authors wrote the manuscript. T.C. and Y.Y. contributed equally to this work.

Abstract

The nuclear-electronic orbital (NEO) approach treats all electrons and specified nuclei, typically protons, on the same quantum mechanical level. Proton vibrational excitations can be calculated using multicomponent time-dependent density functional theory (NEO-TDDFT) for fixed classical nuclei. Recently the NEO-DFT(V) approach was developed to enable the calculation of molecular vibrational frequencies for modes composed of both classical and quantum nuclei. This approach uses input from NEO-TDDFT to construct an extended NEO Hessian that depends on the expectation values of the quantum protons as well as the classical nuclear coordinates. Herein strategies are devised for extending these approaches to molecules with multiple quantum protons in a self-contained, effective, and computationally practical manner. The NEO-TDDFT method is shown to describe vibrational excitations corresponding to collective nuclear motions, such as linear combinations of proton vibrational excitations. The NEO-DFT(V) approach is shown to incorporate the most significant anharmonic effects in the molecular vibrations, particularly for the hydrogen stretching modes. These theoretical strategies pave the way for a wide range of multicomponent quantum chemistry applications.

91

Introduction

To enable the quantum mechanical treatment of more than one type of particle, a variety of multicomponent wave function theory[1-9] and density functional theory (DFT)[10-19] approaches have been developed. The nuclear-electronic orbital (NEO)[3, 5-7, 9, 14-15, 17-21] method is a multicomponent quantum chemistry method in which select nuclei, typically protons, are treated quantum mechanically at the same level as the electrons, while at least two other nuclei are treated classically to avoid difficulties with translations and rotations. The Born-Oppenheimer approximation between the electrons and quantum nuclei is avoided in this context, allowing for the simultaneous description of electronic and nuclear quantum effects. Within the NEO framework, NEO-DFT and NEO wave function methods have been demonstrated to accurately describe ground state properties such as proton densities[9, 17-19] and proton affinities.[9, 18-19] Expanding upon electronic time-dependent density functional theory (TDDFT)[22-27] and equation-of-motion coupled cluster (EOM-CC) theory,[28-31] advances have also been made in calculating vibrational and positronic excitation energies with NEO-TDDFT[20] and NEO-EOM-CCSD,[32] respectively.

Although the NEO approach does not invoke the Born-Oppenheimer separation between the quantum protons and the electrons, it does invoke the Born-Oppenheimer separation between the quantum protons and all classical nuclei. This separation leads to challenges in calculating vibrational frequencies that can be compared to spectroscopic data because the NEO potential energy surface depends on only the coordinates of the classical nuclei, and the quantum protons are assumed to respond instantaneously to the motion of the classical nuclei. As a result, diagonalization of the

NEO Hessian matrix produces vibrational modes that depend on only the classical nuclear coordinates without proper coupling to the quantum proton motions. Proton vibrational excitations can be calculated using NEO-TDDFT,[20] but these calculations are performed for fixed classical nuclei, resulting in proton vibrational excitations that are decoupled from the classical nuclei. Recently, the NEO-DFT(V) method was developed to overcome these difficulties and compute full molecular vibrational frequencies.[21]

The NEO-DFT(V) method is capable of calculating vibrational frequencies composed of both the classical and quantum nuclei via diagonalization of an extended NEO Hessian matrix that depends on second derivatives of the NEO energy with respect to the expectation values of the quantum nuclei as well as the coordinates of the classical nuclei. This extended NEO Hessian is constructed with input from NEO-TDDFT, which provides information about the proton vibrational excitations. The effects of zero-point energy and delocalization of the quantum nuclei are included in the geometry optimization, and anharmonic effects are incorporated into the molecular vibrational frequencies dominated by the quantum nuclei. The NEO-DFT(V) method was tested on a set of five molecules and found to produce results comparable to both experimental data and anharmonic calculations.[21] For all of these test systems, however, only a single proton was treated quantum mechanically. In this chapter, we extend the NEO-TDDFT method to molecules with multiple quantum protons, discuss the theoretical challenges associated with performing NEO-DFT(V) calculations with multiple quantum protons, and provide a generalization of the NEO-DFT(V) approach for any number of quantum nuclei.

The chapter is organized as follows. In the next section, we review the theory of

NEO-DFT(V) and NEO-TDDFT and then explain how properties calculated using NEO-TDDFT can be used to enable practical NEO-DFT(V) calculations with more than one quantum proton. We then calculate the vibrational frequencies for a set of four molecules, each with two quantum protons, using NEO-DFT(V). We compare the results to experimental data as well as anharmonic computational results. The final section contains concluding remarks.

Theory

Extended NEO Hessian

For a system with N_c classical nuclei and N_q quantum nuclei, the NEO potential energy surface (PES) depends on only the coordinates of the classical nuclei.[3] Because the NEO approach invokes the Born-Oppenheimer separation between the quantum and classical nuclei, the quantum nuclear densities are optimized variationally for a given configuration of the classical nuclei. As a consequence, diagonalization of the $3N_c \times 3N_c$ NEO Hessian matrix provides the harmonic vibrational excitation energies associated with only the classical nuclei. Additionally, these vibrational modes are not properly coupled to the quantum nuclei because the quantum nuclei are assumed to respond instantaneously to any perturbation of the classical nuclei. The strategy of the NEO-DFT(V) method is to compute and diagonalize an extended $3(N_c + N_q) \times 3(N_c + N_q)$ Hessian matrix that includes the proper coupling among all nuclei and produces full molecular vibrational excitation energies that can be compared to spectroscopic data.

The NEO energy can be expressed as

$$E = E(\mathbf{r}_c, \mathbf{r}_q(\mathbf{r}_c)) \ , \tag{5.1}$$

where $\mathbf{r}_c$ is a $3N_c$-dimensional vector denoting the combined coordinates of the classical

nuclei, and $\mathbf{r}_q$ is a $3N_q$-dimensional vector denoting the combined expectation values of the quantum nuclei. Specifically, $\mathbf{r}_q$ is a concatenation of $\mathbf{r}_{q_i}$ for each quantum nucleus, and $\mathbf{r}_{q_i}$ is defined as the expectation value of the ith quantum nucleus according to

$$\mathbf{r}_{q_i} = \int \mathbf{r} \, \Gamma_{q_i}(\mathbf{r}) \, d\mathbf{r} \,, \tag{5.2}$$

where $\Gamma_{q_i}(\mathbf{r})$ is the density of the ith quantum nucleus. This approach assumes that each quantum nucleus is spatially localized, rendering them effectively distinguishable. Consequently, each quantum nucleus corresponds to an occupied nuclear orbital that is localized in space, and $\Gamma_{q_i}(\mathbf{r})$ for a given nucleus is the square of this nuclear orbital.

Such an assumption is valid for most molecular systems of interest. From the definition of the NEO energy, which is calculated by variationally optimizing the densities of the electrons and quantum nuclei, the condition

$$\frac{\partial E}{\partial \mathbf{r}_q} = 0 \tag{5.3}$$

is satisfied for any geometry of the classical nuclei. Specifically, this condition must be satisfied under the constraint that the nuclear determinant used to construct the nuclear density $\Gamma_q(\mathbf{r})$ minimizes the total NEO energy in Eq. (5.1) (see the Supporting Information of Ref. [21] for details).

As mentioned above, the NEO-DFT(V) method requires the calculation and diagonalization of an extended Hessian that couples the classical and quantum nuclei. This extended Hessian is defined in terms of the $3N_c$ coordinates of the classical nuclei and the $3N_q$ expectation values (i.e., average positions) of the quantum nuclei. Mathematically, the extended Hessian matrix is defined as[21]

95

$$\mathbf{H}_{\text{NEO}}^{\text{ext}} = \begin{pmatrix} \mathbf{H}_0 & \mathbf{H}_1^{\text{T}} \\ \mathbf{H}_1 & \mathbf{H}_2 \end{pmatrix} . \tag{5.4}$$

where $\mathbf{H}_0 = \left(\dfrac{\partial^2 E}{\partial \mathbf{r}_c^2} \right)_{\mathbf{r}_q}$, $\mathbf{H}_1 = \dfrac{\P^2 E}{\P \mathbf{r}_q \, \P \mathbf{r}_c}$, and $\mathbf{H}_2 = \left(\dfrac{\partial^2 E}{\partial \mathbf{r}_q^2} \right)_{\mathbf{r}_c}$. Diagonalization of the mass-

weighted form of $\mathbf{H}_{\text{NEO}}^{\text{ext}}$ provides the full molecular vibrational excitation energies. The

remainder of this subsection will outline how each of these submatrices can be

calculated.

As a first step toward evaluating these three submatrices, we express the NEO

Hessian matrix $\mathbf{H}_{\text{NEO}}$ in terms of them. As discussed above, the $3N_c \times 3N_c$ NEO Hessian

matrix $\mathbf{H}_{\text{NEO}}$ depends on only the classical nuclear coordinates, assuming that the

quantum nuclei respond instantaneously to perturbations of the classical nuclei. In

practice, this Hessian matrix can be computed analytically or numerically while invoking

this Born-Oppenheimer separation between the classical and quantum nuclei.[21] An

alternative mathematically rigorous expression for the NEO Hessian matrix $\mathbf{H}_{\text{NEO}}$ can

be obtained by taking the second derivative of the NEO energy in Eq. (5.1) with respect

to the classical nuclei:

$$\frac{\mathrm{d}^2 E}{\mathrm{d}\mathbf{r}_c^2} = \left(\frac{\partial^2 E}{\partial \mathbf{r}_c^2} \right)_{\mathbf{r}_q} + 2 \frac{\partial^2 E}{\partial \mathbf{r}_c \partial \mathbf{r}_q} \frac{\mathrm{d}\mathbf{r}_q}{\mathrm{d}\mathbf{r}_c} + \left(\frac{\partial^2 E}{\partial \mathbf{r}_q^2} \right)_{\mathbf{r}_c} \left(\frac{\mathrm{d}\mathbf{r}_q}{\mathrm{d}\mathbf{r}_c} \right)^2 + \frac{\partial E}{\partial \mathbf{r}_q} \frac{\mathrm{d}^2 \mathbf{r}_q}{\mathrm{d}\mathbf{r}_c^2} . \tag{5.5}$$

This expression can be simplified after some straightforward mathematical

manipulations. Differentiating Eq. (5.3) with respect to the classical nuclei gives

$$\frac{\partial^2 E}{\partial \mathbf{r}_c \partial \mathbf{r}_q} + \frac{\mathrm{d}\mathbf{r}_q}{\mathrm{d}\mathbf{r}_c} \left(\frac{\partial^2 E}{\partial \mathbf{r}_q^2} \right)_{\mathbf{r}_c} = 0 , \tag{5.6}$$

and solving for $\dfrac{d\mathbf{r}_q}{d\mathbf{r}_c}$ yields

$$\frac{d\mathbf{r}_q}{d\mathbf{r}_c} = -\frac{\partial^2 E}{\partial \mathbf{r}_c \partial \mathbf{r}_q}\left(\frac{\partial^2 E}{\partial \mathbf{r}_q^2}\right)^{-1}_{\mathbf{r}_c} .$$
(5.7)

Using Eqs. (5.3) and (5.7) allows us to simplify Eq. (5.5) as

$$\frac{d^2 E}{d\mathbf{r}_c^2} = \left(\frac{\partial^2 E}{\partial \mathbf{r}_c^2}\right)_{\mathbf{r}_q} - \frac{\partial^2 E}{\partial \mathbf{r}_c \partial \mathbf{r}_q}\left(\frac{\partial^2 E}{\partial \mathbf{r}_q^2}\right)^{-1}_{\mathbf{r}_c}\frac{\partial^2 E}{\partial \mathbf{r}_q \partial \mathbf{r}_c} .$$
(5.8)

Eq. (5.8) can be expressed in terms of the submatrices defined above as[21]

$$\mathbf{H}_{\mathrm{NEO}} = \mathbf{H}_0 - \mathbf{H}_1^{\mathrm{T}}\mathbf{H}_2^{-1}\mathbf{H}_1 .$$
(5.9)

Given this mathematical expression for $\mathbf{H}_{\mathrm{NEO}}$, the three submatrices in Eq. (5.4) can be computed in a straightforward manner. The $\mathbf{H}_0$ submatrix is the force constant matrix for the classical nuclei with the expectation values of the quantum nuclei fixed, and it is obtained in practice through a rearrangement of Eq. (5.9):

$$\mathbf{H}_0 = \mathbf{H}_{\mathrm{NEO}} + \mathbf{H}_1^{\mathrm{T}}\mathbf{H}_2^{-1}\mathbf{H}_1 = \mathbf{H}_{\mathrm{NEO}} + \mathbf{R}^{\mathrm{T}}\mathbf{H}_2\mathbf{R} .$$
(5.10)

Here the $\mathbf{R}$ matrix is defined as

$$\mathbf{R} = \frac{d\mathbf{r}_q}{d\mathbf{r}_c} ,$$
(5.11)

where

$$\frac{d\mathbf{r}_{q_i}}{d\mathbf{r}_c} = \frac{d}{d\mathbf{r}_c}\int \mathbf{r}\rho_{q_i}(\mathbf{r})d\mathbf{r} = \int \mathbf{r}\frac{d\rho_{q_i}(\mathbf{r})}{d\mathbf{r}_c}d\mathbf{r} .$$
(5.12)

This $\mathbf{R}$ matrix can be calculated analytically or numerically from the gradient of the expectation value of each quantum nucleus with respect to each classical nucleus.

From Eq. (5.6), it is clear that the $\mathbf{H}_1$ submatrix can be expressed as[21]

$$\mathbf{H}_1 = -\mathbf{H}_2\mathbf{R} \ . \tag{5.13}$$

Eqs. (5.4), (5.10), and (5.13) indicate that if the $\mathbf{H}_2$ matrix is known, then the target

$\mathbf{H}_{\mathrm{NEO}}^{\mathrm{ext}}$ can be constructed and diagonalized. However, $\mathbf{H}_2$ is challenging to compute

directly using only information from the nuclear density because it contains second

derivatives of the NEO energy with respect to specific components of the combined

expectation values $\mathbf{r}_q$ that must vary while other components of $\mathbf{r}_q$ remain fixed.[21] It is

therefore desirable to formulate an alternative scheme for constructing $\mathbf{H}_2$.

As defined above, $\mathbf{H}_2$ is the Hessian matrix corresponding to the second

derivatives of the energy with respect to the expectation values of the quantum nuclei

with the classical nuclei fixed. Within the harmonic oscillator approximation, its

associated generalized eigenvalue equation is

$$\mathbf{H}_2\mathbf{U} = \mathbf{M}\mathbf{U}\mathbf{\Omega}, \tag{5.14}$$

with the orthonormalization condition

$$\mathbf{U}^\dagger\mathbf{M}\mathbf{U} = \mathbf{I} \tag{5.15}$$

where $\mathbf{\Omega}$ is the diagonal matrix of eigenvalues ω^2, $\mathbf{M}$ is the diagonal mass matrix

corresponding to the quantum nuclei, and $\mathbf{U}$ is composed of the eigenvectors, which are

denoted normal modes in this context. Typically the Hessian matrix is known and is

diagonalized to obtain the normal modes and vibrational frequencies. However, our

problem is the reverse in that $\mathbf{H}_2$ needs to be calculated from approximate normal

modes and frequencies. For this purpose, Eq. (5.14) can be rearranged to be

$$\mathbf{H}_2 = \left(\frac{\partial^2 E}{\partial \mathbf{r}_q^2} \right)_{\mathbf{r}_c} = \mathbf{MU\Omega U}^{-1} = \mathbf{MU\Omega U}^\dagger \mathbf{M} \ . \tag{5.16}$$

Thus, $\mathbf{H}_2$ can be constructed if we know the associated eigenvalues ω^2 and eigenvectors $\mathbf{U}$. In our strategy, the quantum proton vibrational frequencies w used to construct $\mathbf{\Omega}$ are approximated by the anharmonic frequencies calculated by NEO-TDDFT. As a result, this approach partially incorporates the anharmonic effects that naturally arise in NEO-TDDFT calculations of vibrational excitations. For single proton systems, the $\mathbf{U}$ matrix was previously constructed from the normal modes associated with the quantum proton as obtained from a conventional electronic Hessian matrix with all nuclei except the proton fixed.[21] While effective, this procedure is not self-contained and adds computational expense. An alternative construction of the $\mathbf{U}$ matrix based on the transition dipole moments obtained from NEO-TDDFT is introduced in the next subsection.

NEO-TDDFT and the U Matrix Construction

The NEO-DFT method was developed previously for a system composed of electrons and quantum nuclei in a field of fixed classical nuclei. To simplify the discussion, we only consider quantum protons, although the theory is easily extended to other types of quantum nuclei or particles such as positrons. Within the Kohn-Sham formalism, the reference state is defined as the product of electron and proton Slater determinants composed of electronic and protonic orbitals, respectively. The total energy depends on the electron and proton densities, r^e and r^p, respectively:

$$E[r^e, r^p] = E_{\text{ext}}[r^e, r^p] + E_{\text{ref}}[r^e, r^p] + E_{\text{exc}}[r^e] + E_{\text{pxc}}[r^p] + E_{\text{epc}}[r^e, r^p] \tag{5.17}$$

Here E denotes the interaction of the electron and proton densities with the external

potential due to the fixed classical nuclei, and E_{ref} includes the kinetic energies of the electrons and quantum protons and the classical Coulomb interactions for the reference state. In addition, E_{exc}, E_{pxc}, and E_{epc} denote the electron-electron exchange-correlation functional, the proton-proton exchange-correlation functional, and the electron-proton correlation functional. Application of the variational principle to this total energy functional leads to Kohn-Sham equations for the electrons and quantum protons that are solved iteratively. Our group has developed electron-proton correlation functionals,[19, 33] which can be used in conjunction with existing electronic exchange-correlation functionals. Because proton-proton exchange and correlation are negligible for molecular systems associated with localized proton densities, the proton-proton exchange-correlation functional is chosen to be the diagonal Hartree-Fock exchange terms to eliminate self-interaction energy.

The NEO-TDDFT approach was developed to compute electronic and proton vibrational excitations simultaneously in a computationally practical manner. The NEO-TDDFT equations have been derived previously,[20] and only the relevant working equations are presented here. The electronic and protonic excitation energies are calculated by solving

$$\begin{pmatrix} \mathbf{A}^e & \mathbf{B}^e & \mathbf{C} & \mathbf{C} \\ \mathbf{B}^e & \mathbf{A}^e & \mathbf{C} & \mathbf{C} \\ \mathbf{C}^T & \mathbf{C}^T & \mathbf{A}^p & \mathbf{B}^p \\ \mathbf{C}^T & \mathbf{C}^T & \mathbf{B}^p & \mathbf{A}^p \end{pmatrix} \begin{pmatrix} \mathbf{X}^e \\ \mathbf{Y}^e \\ \mathbf{X}^p \\ \mathbf{Y}^p \end{pmatrix} = \omega \begin{pmatrix} \mathbf{I} & 0 & 0 & 0 \\ 0 & -\mathbf{I} & 0 & 0 \\ 0 & 0 & \mathbf{I} & 0 \\ 0 & 0 & 0 & -\mathbf{I} \end{pmatrix} \begin{pmatrix} \mathbf{X}^e \\ \mathbf{Y}^e \\ \mathbf{X}^p \\ \mathbf{Y}^p \end{pmatrix} \qquad (5.18)$$

Within the adiabatic approximation, the matrix elements in Eq. (5.18) are,

$$A_{ia,jb}^{\text{e}} = (e_a - e_i)d_{ab}d_{ij} + \left(ia \mid bj\right) + \frac{d^2 E_{\text{exc}}}{dP_{jb}^{\text{e}}dP_{ai}^{\text{e}}} + \frac{d^2 E_{\text{epc}}}{dP_{jb}^{\text{e}}dP_{ai}^{\text{e}}} \,, \tag{5.19}$$

$$B_{ia,jb}^{\text{e}} = \left(ia \mid jb\right) + \frac{d^2 E_{\text{exc}}}{dP_{bj}^{\text{e}}dP_{ai}^{\text{e}}} + \frac{d^2 E_{\text{epc}}}{dP_{bj}^{\text{e}}dP_{ai}^{\text{e}}} \,, \tag{5.20}$$

$$A_{IA,JB}^{\text{p}} = \left(e_A - e_I\right)d_{AB}d_{IJ} + \left(IA \mid BJ\right) + \frac{d^2 E_{\text{pxc}}}{dP_{JB}^{\text{p}}dP_{AI}^{\text{p}}} + \frac{d^2 E_{\text{epc}}}{dP_{JB}^{\text{p}}dP_{AI}^{\text{p}}} \,, \tag{5.21}$$

$$B_{IA,JB}^{\text{p}} = \left(IA \mid JB\right) + \frac{d^2 E_{\text{pxc}}}{dP_{BJ}^{\text{p}}dP_{AI}^{\text{p}}} + \frac{d^2 E_{\text{epc}}}{dP_{BJ}^{\text{p}}dP_{AI}^{\text{p}}} \,, \tag{5.22}$$

$$C_{ia,JB} = -\left(ia \mid BJ\right) + \frac{d^2 E_{\text{epc}}}{dP_{JB}^{\text{p}}dP_{ai}^{\text{e}}} \,. \tag{5.23}$$

Here, P denotes the density matrix, e denotes the orbital energies, and the superscripts e and p denote electrons and protons, respectively. The lower case indices i and j denote occupied electronic orbitals, while the indices a and b denote virtual electronic orbitals. The upper case indices are defined analogously for protonic orbitals. The solution of Eq. (5.18) produces the excitation energies W.

In the current formulation of linear response NEO-TDDFT, only single excitations can be captured, and in principle these excitations could be of electronic, protonic, or mixed electron-proton vibronic character.[20] However, for electronically adiabatic systems, typically the excitations are either electronically or protonically dominated and thus can be described as pure electronic or vibrational excitations to a reasonable approximation. The character of the excitation can be evaluated by examination of the

corresponding eigenvector: electronic excitations are dominated by $\mathbf{X}^{\mathrm{e}}$, and protonic excitations are dominated by $\mathbf{X}^{\mathrm{p}}$. The eigenvectors are subject to the orthonormalization condition[20]

$$\left\langle \mathbf{X}_m^{\mathrm{e}} \middle| \mathbf{X}_n^{\mathrm{e}} \right\rangle - \left\langle \mathbf{Y}_m^{\mathrm{e}} \middle| \mathbf{Y}_n^{\mathrm{e}} \right\rangle + \left\langle \mathbf{X}_m^{\mathrm{p}} \middle| \mathbf{X}_n^{\mathrm{p}} \right\rangle - \left\langle \mathbf{Y}_m^{\mathrm{p}} \middle| \mathbf{Y}_n^{\mathrm{p}} \right\rangle = \pm d_{mn} \; . \tag{5.24}$$

In addition to calculating proton vibrational excitation energies, various other quantities can be calculated using information from NEO-TDDFT, such as transition densities, transition dipole moments, and oscillator strengths.[20, 34]

In the context of NEO-DFT(V), a quantity that is of particular interest is the transition dipole moment, which is defined for a general NEO excited state $\left| \mathsf{Y}_k \right\rangle$ as

$$\left\langle \Psi_0 \middle| \hat{r}_\gamma \middle| \Psi_k \right\rangle = \sum_{IA} \left[X_{IA}^{\mathrm{p}} \left\langle I \middle| r_\gamma \middle| A \right\rangle + Y_{IA}^{\mathrm{p}} \left\langle A \middle| r_\gamma \middle| I \right\rangle \right] + \sum_{ia} \left[X_{ia}^{\mathrm{e}} \left\langle i \middle| r_\gamma \middle| a \right\rangle + Y_{ia}^{\mathrm{e}} \left\langle a \middle| r_\gamma \middle| i \right\rangle \right] \; , \tag{5.25}$$

where $\hat{r}_\gamma = \hat{x}$, $\hat{y}$, or $\hat{z}$ for $g = 1, 2$, or 3, respectively, and $\mathbf{X}$ and $\mathbf{Y}$ are obtained from solving Eq. (5.18). For notational simplicity, the dependence of the elements of $\mathbf{X}$ and $\mathbf{Y}$ on k in Eq. (5.25) is omitted. As mentioned above, the excitations for electronically adiabatic systems can typically be characterized as purely electronic or vibrational. For the molecular vibrational analysis, $\left| \mathsf{Y}_k \right\rangle$ in Eq. (5.25) corresponds to the kth proton vibrational excited state, and the terms in the second summation vanish. The resulting transition dipole moment is a vector that reflects the polarization of the protonic transition. The kth transition dipole moment vector can be viewed as the "normal mode" associated with the kth proton vibrational excitation energy ω_k. These vectors are used to construct a rotation matrix $\mathbf{U}$ that in turn can be used in Eq. (5.16) for computing the submatrix $\mathbf{H}_2$. This approach provides the rotation matrix $\mathbf{U}$ in an effective, self-

contained, and generalizable manner.

As a simple conceptual example, consider the construction of the $\mathbf{H}_2$ matrix for HCN, which has a single quantum proton. To generate $\mathbf{H}_2$, we use NEO-TDDFT to calculate the $3N_p$ proton vibrational excitation energies W_1, W_2, and W_3 that comprise $\mathbf{\Omega}$:

$$\mathbf{\Omega} = \begin{pmatrix} \omega_1^2 & 0 & 0 \\ 0 & \omega_2^2 & 0 \\ 0 & 0 & \omega_3^2 \end{pmatrix}. \tag{5.26}$$

We then use Eq. (5.25) to calculate the transition dipole moment vectors associated with each excitation. The transition densities and transition dipole moment vectors associated with the three proton vibrational excitations for HCN are shown in Figure 5.1.

In Figure 5.1, the three orthogonal transition dipole moment vectors $\left| W_k \right\rangle$ associated with the three protonic excitations are represented along axes in a primed coordinate system that may be viewed as the "normal mode" coordinate system for the quantum proton. In most cases, the primed coordinate system will not be coincident with the unprimed coordinate system associated with the lab frame, as observed in Fig. 5.1. The vectors $\left| W_k \right\rangle$ can be represented in the lab frame coordinates using Eq. (5.25) according to

$$\left| W_k \right\rangle = u_x^k \left| x \right\rangle + u_y^k \left| y \right\rangle + u_z^k \left| z \right\rangle \tag{5.27}$$

where

$$u_\gamma^k = \frac{\langle \Psi_0 | \hat{r}_\gamma | \Psi_k \rangle}{\sqrt{m_p \sum_{\gamma=1}^{3} \left| \langle \Psi_0 | \hat{r}_\gamma | \Psi_k \rangle \right|^2}} \quad . \tag{5.28}$$

Here m_p is the mass of the proton and $\hat{r}_\gamma = \hat{x}$, $\hat{y}$, or $\hat{z}$ for g = 1, 2, or 3. Each $|W_k\rangle$ vector forms a column of the transformation matrix $\mathbf{U}$

$$\mathbf{U} = \begin{pmatrix} u_x^1 & u_x^2 & u_x^3 \\ u_y^1 & u_y^2 & u_y^3 \\ u_z^1 & u_z^2 & u_z^3 \end{pmatrix}. \tag{5.29}$$

This matrix corresponds to a transformation or rotation from the normal mode coordinate system to the lab frame coordinate system. Note that this $\mathbf{U}$ matrix satisfies the orthonormalization condition in Eq. (5.15).

At this point, we have generated the $\mathbf{U}$ and $\mathbf{\Omega}$ matrices for the case of a single quantum proton and are now equipped to calculate $\mathbf{H}_2$ according to Eq. (5.16). In the special case where the "normal mode" coordinate system is coincident with the lab frame coordinate system, the matrix given in Eq. (5.29) becomes the $\mathbf{M}^{-1/2}$ matrix, and the $\mathbf{H}_2$ matrix given in Eq. (16) has the simple diagonal representation

$$\mathbf{H}_2 = \begin{pmatrix} m_p \omega_1^2 & 0 & 0 \\ 0 & m_p \omega_2^2 & 0 \\ 0 & 0 & m_p \omega_3^2 \end{pmatrix}. \tag{5.30}$$

However, this situation is not typical, particularly for non-linear molecules with multiple protons.

Building on the single proton case, the $\mathbf{U}$ matrix can be constructed for a system with multiple quantum protons. A system of N_p quantum protons will have N_p occupied

protonic orbitals that are assumed to be spatially localized. A NEO-TDDFT calculation will yield $3N_\mathrm{p}$ protonic excitation energies of interest, where each excitation energy W will be associated with collective protonic motions. For a given collective mode, we calculate N_p individual transition dipole moment vectors, where each vector is associated with a singly occupied protonic orbital. In the single proton case, each column of the $\mathbf{U}$ matrix was constructed according to Eqs. (5.27) and (5.28). In the multiproton case, a given excitation is now associated with N_p individual transition dipole moment vectors, which may be conceptualized as

$$|\omega_k\rangle \begin{cases} u_x^{k1}|x\rangle + u_y^{k1}|y\rangle + u_z^{k1}|z\rangle\} \rightarrow \text{proton } 1 \\ u_x^{k2}|x\rangle + u_y^{k2}|y\rangle + u_z^{k2}|z\rangle\} \rightarrow \text{proton } 2 \\ \quad \vdots \\ u_x^{kN_p}|x\rangle + u_y^{kN_p}|y\rangle + u_z^{kN_p}|z\rangle\} \rightarrow \text{proton } N_p \end{cases} \tag{5.31}$$

For a system composed of N_p quantum protons, the general $3N_\mathrm{p} \times 3N_\mathrm{p}$ $\mathbf{U}$ matrix used in NEO-DFT(V) is constructed according to

$$U = \begin{pmatrix} u_x^{11} & u_x^{21} & u_x^{31} & & u_x^{(k-2)1} & u_x^{(k-1)1} & u_x^{k1} \\ u_y^{11} & u_y^{21} & u_y^{31} & \cdots & u_y^{(k-2)1} & u_y^{(k-1)1} & u_y^{k1} \\ u_z^{11} & u_z^{21} & u_z^{31} & & u_z^{(k-2)1} & u_z^{(k-1)1} & u_z^{k1} \\ & \vdots & & \ddots & & \vdots & \\ u_x^{1N_p} & u_x^{2N_p} & u_x^{3N_p} & & u_x^{(k-2)N_p} & u_x^{(k-1)N_p} & u_x^{kN_p} \\ u_y^{1N_p} & u_y^{2N_p} & u_y^{3N_p} & \cdots & u_y^{(k-2)N_p} & u_y^{(k-1)N_p} & u_y^{kN_p} \\ u_z^{1N_p} & u_z^{2N_p} & u_z^{3N_p} & & u_z^{(k-2)N_p} & u_z^{(k-1)N_p} & u_z^{kN_p} \end{pmatrix} \tag{5.32}$$

where

$$u_g^{kQ} = \frac{\left\langle \Upsilon_0 \left| \hat{r}_g^Q \right| \Upsilon_k \right\rangle}{\sqrt{\sum_Q^{N_p} m_Q \sum_{g=1}^{3} \left| \left\langle \Upsilon_0 \left| \hat{r}_g^Q \right| \Upsilon_k \right\rangle \right|^2}} \ . \tag{5.33}$$

In Eq. (5.33), k is the index specifying a proton vibrational excited state, Q is the index

specifying a quantum proton, and m_Q is the mass of the Qth quantum proton. For

notational clarity in Eq. (5.32), $u_g^{kQ} = u_x^{kQ}$, u_y^{kQ}, u_z^{kQ} for g = 1, 2, and 3, respectively. The

operator $\hat{r}_g^Q$ appearing in Eq. (5.33) acts on only the Qth quantum proton, which

occupies the Qth nuclear orbital in the ground state, and the corresponding matrix

element is defined as

$$\left\langle \Psi_0 \left| \hat{r}_\gamma^Q \right| \Psi_k \right\rangle = \sum_A \left[X_{QA}^p \left\langle Q \left| r_\gamma \right| A \right\rangle + Y_{QA}^p \left\langle A \left| r_\gamma \right| Q \right\rangle \right] \ . \tag{5.34}$$

The resulting $\mathbf{U}$ matrix is composed of column vectors, each associated with a

specific proton vibrational excited state k. These column vectors are themselves

composed of N_p concatenated sets of x, y, z transition dipole moment vector

components, where each set is associated with an occupied protonic orbital Q. Note

that in the case of a single type of quantum nucleus, the mass m_Q in the expression for

u_g^{kQ} can be factored out in the denominator because it is the same for all quantum

nuclei. However, the expression for u_g^{kQ} in Eq. (5.33) is general and is valid for the case

of multiple types of quantum nuclei with different masses. This procedure can be used

to construct the $\mathbf{U}$ matrix, which in conjunction with the associated $\mathbf{\Omega}$ matrix can be

used to compute the $\mathbf{H}_2$ matrix given in Eq. (5.16). The $\mathbf{H}_2$ matrix can be used to

compute the $\mathbf{H}_0$ and $\mathbf{H}_1$ matrices for the construction of $\mathbf{H}_{NEO}^{ext}$. The eigenvalues and

eigenvectors of this extended Hessian provide the molecular vibrational frequencies and normal modes coupling the classical and quantum nuclei.

Overview of NEO-DFT(V) for Multiple Protons

The overall NEO-DFT(V) procedure described above is well-defined and systematic. Given the reasonable definition of the extended Hessian in terms of the classical nuclear coordinates and the expectation values of the quantum nuclei, the expressions for the $\mathbf{H}_0$ and $\mathbf{H}_1$ matrices are mathematically rigorous. The main approximation of this approach lies in the physically motivated construction of the $\mathbf{H}_2$ matrix from the NEO-TDDFT proton vibrational excitation energies and transition dipole moment vectors. A significant advantage of this procedure is that the anharmonicities of the proton vibrational modes are naturally included in the NEO-TDDFT proton vibrational excitation energies used to construct the $\mathbf{H}_2$ matrix. Thus, even though the use of a Hessian to produce vibrational frequencies is based on the harmonic oscillator approximation, the matrix elements of the extended Hessian incorporate the anharmonic effects associated with the quantum protons. As will be shown below, the resulting molecular vibrational frequencies reflect this incorporation of anharmonic effects.

Results and Discussion

We used the NEO-DFT(V) method described above to compute the molecular vibrational frequencies for a set of four molecules, each containing two protons. All molecular geometries were optimized using NEO-DFT with the B3LYP[35-36] electronic exchange-correlation functional and the epc17-2 electron-proton correlation functional,[18] which has been shown to provide accurate proton affinities[18] and accurate NEO-TDDFT

excitations.[20, 34] The cc-pVDZ electronic basis set[37] was used for the heavy atoms, and the cc-pV5Z electronic basis set[37-38] was used for the quantum protons. An even tempered $6s6p6d6f$ nuclear basis set with exponents spanning the range from $4\sqrt{2}$ to 32 was used for the quantum protons. This combination of nuclear and electronic basis sets for the quantum proton has been demonstrated to be effective in calculating accurate proton vibrational excitation energies with the NEO-TDDFT/B3LYP/epc17-2 method.[34] The NEO-DFT(V) and conventional harmonic calculations were performed using a developer version of the GAMESS program.[39] The anharmonic calculations were performed using Gaussian09.[40]

For the ground state NEO-DFT calculations, the nuclear and electronic basis function centers were chosen to be the same for each quantum proton, and the positions of these centers were optimized variationally. For the NEO-TDDFT calculations, the variational ground state positions of the nuclear/electronic basis function centers may not be optimal for calculating accurate proton vibrational excitation energies. The impact of the nuclear/electronic basis function center position on proton vibrational excitation energies calculated with NEO-TDDFT has been investigated in previous work.[34] These previous results indicate that two possible choices for the positions of the nuclear/electronic basis function centers yield accurate and comparable results: (1) the conventional electronic XH bond distance and angle (where X represents an arbitrary heavy atom), and (2) the expectation value of the quantum proton obtained from a ground state NEO-DFT calculation, where the nuclear/electronic basis function centers are optimized variationally.[34] In the present work, the NEO-TDDFT proton vibrational excitation energies used in Eq. (5.16) were calculated with the

nuclear/electronic basis function centers placed at the expectation values of the quantum protons. This choice has the benefit of being self-contained and therefore more computationally practical, as all information necessary for performing the NEO-TDDFT calculation is obtained from the ground state NEO-DFT calculation.

The procedure for calculating vibrational modes with the NEO-DFT(V) approach is summarized as follows. First, a NEO-DFT geometry optimization is performed on the system of interest. The matrix $\mathbf{H}_{\text{NEO}}$ is then calculated numerically by perturbing the classical nuclear coordinates and optimizing the basis function centers for the quantum protons at each perturbed geometry. Using the NEO-DFT optimized geometry for the classical nuclei and the expectation values of the quantum nuclei for the nuclear/electronic basis function center positions, a NEO-TDDFT calculation is performed. The $\mathbf{U}$ matrix is constructed according to Eqs. (5.32) and (5.33), and this matrix is used in conjunction with the proton vibrational excitation energies to obtain the $\mathbf{H}_2$ matrix given by Eq. (5.16). The $\mathbf{H}_2$ matrix is then used together with the $\mathbf{R}$ matrix to calculate the $\mathbf{H}_0$ and $\mathbf{H}_1$ matrices according to Eqs. (5.10) and (5.13), respectively. Finally, $\mathbf{H}_0$, $\mathbf{H}_1$, and $\mathbf{H}_2$ are used to construct the extended NEO Hessian $\mathbf{H}_{\text{NEO}}^{\text{ext}}$ in Eq. (5.4). Diagonalization of the mass-weighted form of $\mathbf{H}_{\text{NEO}}^{\text{ext}}$ gives the full molecular vibrational modes.

An important aspect of the NEO-DFT(V) scheme is the use of NEO-TDDFT to compute the proton vibrational excitations for fixed classical nuclei. In our previous work,[20, 34] the NEO-TDDFT method was applied to molecular systems with only a single quantum proton. Herein, we implement the NEO-TDDFT method for molecular systems

with multiple quantum protons. Interestingly, the NEO-TDDFT method produces collective proton vibrational modes that combine motions of multiple quantum nuclei. These collective proton vibrational modes correspond to linear combinations of singly excited determinants and thus are described by linear response NEO-TDDFT. For example, Figure 5.2 shows the six NEO-TDDFT proton vibrational modes and excitation energies calculated for HCCH with fixed carbon nuclei, where two of the modes are doubly degenerate. Arrows indicating the direction of the transition dipole vector associated with each quantum proton are shown for each mode. Table 5.1 provides the full $\mathbf{U}$ matrix, which contains the values of all components of the transition dipole moment vectors shown in Figure 5.2. As mentioned previously, the NEO Hessian depends on only the classical nuclei, assuming the instantaneous response of the quantum nuclei. Thus, the NEO Hessian is one-dimensional in the case of HCCH, with a CC frequency of 2207 cm^{-1}.

The NEO-DFT(V) approach mixes the CC frequency from the NEO Hessian with the NEO-TDDFT modes shown in Figure 5.2 to produce the coupled molecular vibrational modes shown in Figure 5.3. Given the three translational and two rotational modes for this linear molecule, this approach provides seven vibrational modes, where two of these modes are doubly degenerate. The TDDFT proton vibrational excitation energies for the other three molecules studied, namely H_2O_2, H_2CO, and H_2NF, are provided in Appendix D. All of these molecules contain only two classical nuclei and therefore correspond to linear geometries in the NEO framework. However, when the quantum nuclei do not maintain this linearity (i.e., the molecule is not linear in a conventional electronic structure calculation), the NEO-DFT(V) approach produces one

rotational mode that is associated with a negligible NEO-TDDFT excitation energy. Thus, this approach provides six vibrational modes for the other three molecules.

The NEO-DFT(V) vibrational frequencies for the four molecular systems studied are given in Table 5.2. Experimental data are provided, along with results obtained from a conventional Hessian calculation within the harmonic oscillator approximation, as well as results obtained from perturbative anharmonic calculations.[41] The average mean unsigned error (MUE) relative to experiment is also reported. Note that the average MUE is virtually the same for the NEO-DFT(V) and the conventional perturbative anharmonic calculations, and both of these methods are more accurate than the conventional harmonic calculations. The errors for specific modes vary, with NEO-DFT(V) typically overestimating bending modes, as well as low energy modes such as the H_2O_2 torsion, to a greater extent than the perturbative anharmonic calculations. Conversely, the conventional perturbative anharmonic calculations typically underestimate the hydrogen stretching modes to a greater extent than do the NEO-DFT(V) calculations, with the largest deviations observed for the asymmetric CH stretch and the NH stretch in H_2CO and H_2NF, respectively. The overall comparability of the NEO-DFT(V) and conventional perturbative anharmonic methods is reasonable because the anharmonicity associated with the hydrogen nuclei is partially incorporated into the NEO-DFT(V) procedure through the NEO-TDDFT proton vibrational excitation energies that are used to construct the $\mathbf{H}_2$ matrix.

Conclusions

In this chapter, we have developed and implemented the formalism for treating multiple quantum protons within the NEO-DFT(V) scheme. In this approach, proton

vibrational excitation energies and transition dipole moment vectors calculated with NEO-TDDFT are used to construct an extended NEO Hessian matrix, which is defined in terms of the expectation values of the quantum protons as well as the classical nuclear coordinates. Diagonalization of this extended Hessian provides the molecular vibrational frequencies associated with coupled motions of both classical and quantum nuclei. The underlying assumptions of this molecular vibrational analysis are: (1) the harmonic approximation inherent to the Hessian framework; (2) the representation of the quantum nuclei by their expectation values; and (3) the use of the NEO-TDDFT proton vibrational excitation energies and transition dipole moment vectors to construct the submatrix associated with the quantum nuclei, thereby partially including the corresponding anharmonicities.

The results indicate that NEO-TDDFT is capable of capturing vibrational excitation energies associated with collective nuclear motion. Moreover, the NEO-DFT(V) calculations for molecules with multiple quantum protons are accurate and comparable to conventional perturbative anharmonic calculations. Anharmonicity is included in NEO-DFT(V) calculations through the NEO-DFT geometry optimizations and the NEO-TDDFT vibrational excitation energies, leading to significantly more accurate hydrogen stretching modes, as well as an overall improvement in accuracy compared to conventional harmonic calculations. The NEO-DFT(V) approach incorporates anharmonicities associated with the quantum nuclei, and the anharmonicities associated with the classical nuclei could be included perturbatively if they are expected to be significant. This formalism lays the foundation for a wide range of applications for multicomponent quantum chemistry methods.

112

Figures and Tables
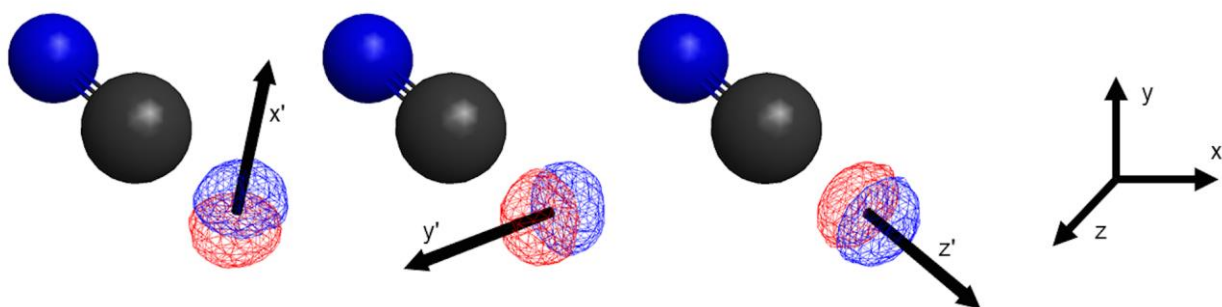
Figure 5.1. Protonic transition densities and associated transition dipole moment vectors (primed axes) for the three excitations with energies W_1 (left), W_2 (center), and W_3 (right)[a]

[a]The lab frame coordinate system is depicted as the unprimed coordinate system at the far right of the figure. Each transition dipole moment vector is defined along a primed coordinate axis which is, in general, different than the lab frame.
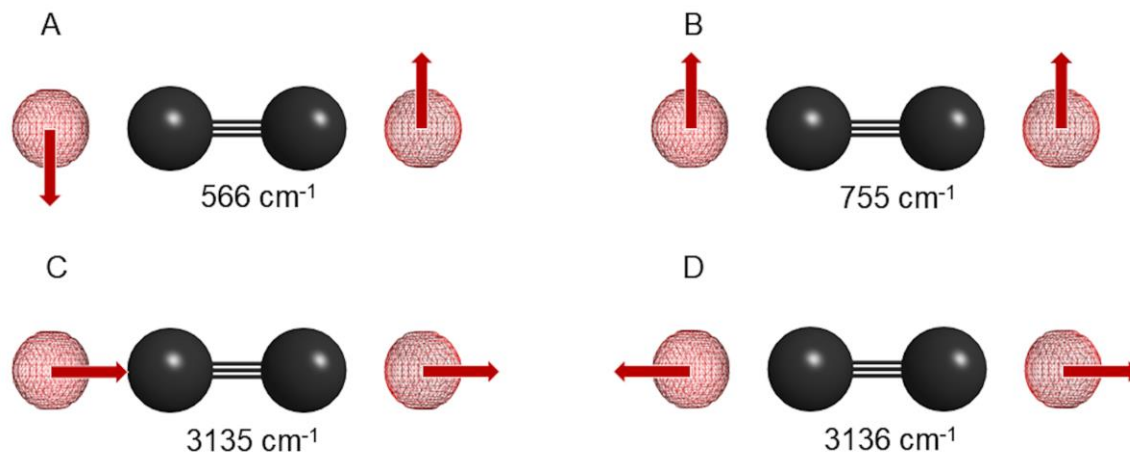
Figure 5.2. Proton vibrational modes and excitation energies calculated with NEO-TDDFT for HCCH with fixed carbon nuclei[a]

[a]The red mesh indicates the quantum proton density. The molecule is oriented on the z-axis with one carbon placed at the origin and a C–C bond distance of 1.207 Å. The expectation values of the quantum protons are −1.086 Å and 2.293 Å. For each mode, the red arrows indicate the direction of the transition dipole moment vector associated with each quantum proton. Mode (A) is a doubly degenerate CH symmetric bend, mode (B) is a doubly degenerate asymmetric CH bend, mode (C) is an asymmetric CH stretch, and mode (D) is a symmetric CH stretch.

Table 5.1: U Matrix for HCCH Constructed from the Transition Dipole Moments Computed with NEO-TDDFT[a]

	A	A	B	B	C	D
1x	-0.707	0.000	0.707	0.000	0.000	0.000
1y	0.000	0.707	0.000	-0.707	0.000	0.000
1z	0.000	0.000	0.000	0.000	0.705	-0.710
2x	0.707	0.000	0.707	0.000	0.000	0.000
2y	0.000	-0.707	0.000	-0.707	0.000	0.000
2z	0.000	0.000	0.000	0.000	0.710	0.705

[a]Each column corresponds to a concatenation of transition dipole moment vectors associated with a given NEO-TDDFT vibrational mode, as defined in Eqs. (5.32)-(5.34). The labels A, B, C, and D correspond to the modes presented in Figure 5.1. The left-most column indicates the quantum proton (1 or 2) and the Cartesian component (x, y, or z). The slight asymmetry in the z components of protons 1 and 2 for columns C and D arises from numerical error and does not impact the NEO-DFT(V) frequencies given in Figure 5.2.
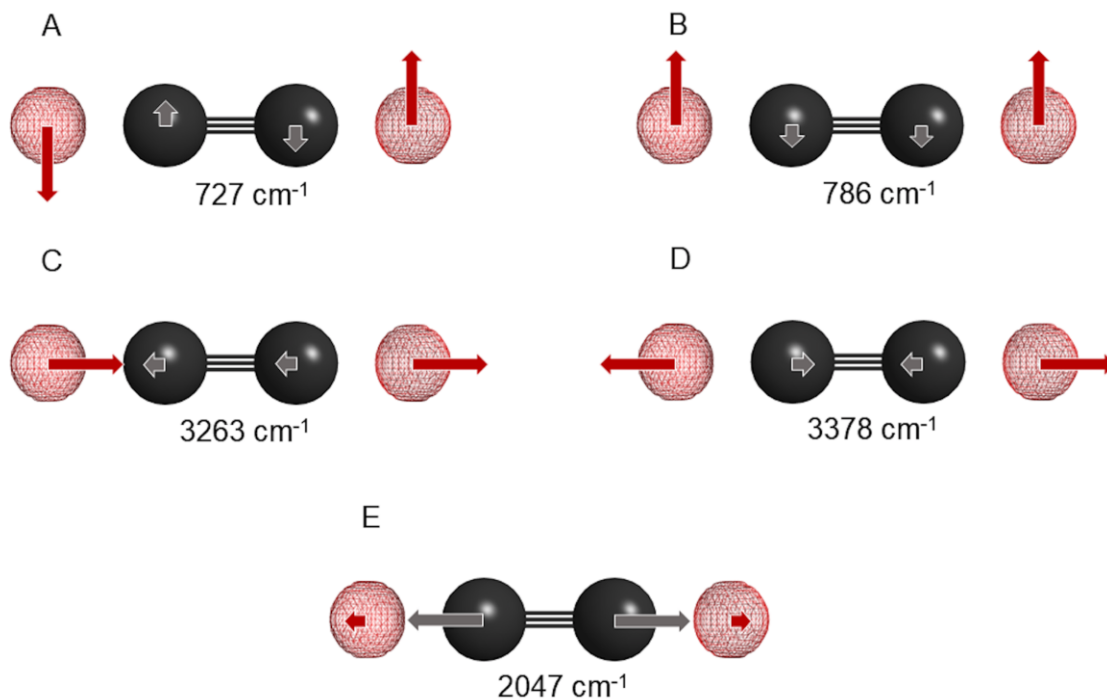
Figure 5.3. Molecular vibrational modes and excitation energies calculated with NEO-DFT(V) for HCCH[a]

[a]The red mesh indicates the quantum proton density. For each mode, the red and gray arrows indicate the directions of the motions of the quantum protons and carbon atoms, respectively. Mode (A) is a doubly degenerate CH symmetric bend, mode (B) is a doubly degenerate asymmetric CH bend, mode (C) is an asymmetric CH stretch, mode (D) is a symmetric CH stretch, and mode (E) is a symmetric CC stretch.

Table 5.2: Proton Vibrational Frequencies Calculated with the NEO-DFT(V), Conventional Harmonic, and Conventional Perturbative Anharmonic Methods, as well as Comparison to Experimental Data.[a]

	Mode	Experiment	NEO-DFT(V)	Conv Anharmonic	Conv Harmonic
C_2H_2[b]	Symmetric CH bend (2)	612	727	700	569
	Aymmetric CH bend (2)	730	786	753	777
	CC stretch	1974	2047	2040	2070
	Asymmetric CH stretch	3289	3263	3294	3388
	Symmetric CH stretch	3374	3378	3390	3503
H_2O_2[c]	HOOH torsion	254-370	523	248	424
	OO stretch	865-877	957	921	957
	Asymmetric OH bend	1265-1274	1314	1249	1332
	Symmetric OH bend	1393	1425	1397	1435
	Asymmetric OH stretch	3610-3619	3596	3522	3789
	Symmetric OH stretch	3609-3618	3599	3528	3792
H_2CO[d]	CH2 wag	1167	1190	1167	1239
	CH2 rock	1249	1254	1233	1278
	CH2 scissor	1500	1477	1484	1567
	CO stretch	1746	1812	1808	1824
	Symmetric CH stretch	2783	2724	2706	2882
	Asymmetric CH stretch	2843	2772	2651	2935
H_2NF[e]	NF stretch	891	936	910	941
	NH2 wag	1233	1257	1225	1271
	NH2 wag	1241	1310	1294	1338
	NH2 scissor	1564	1556	1550	1638
	Symmetric NH stretch	3234	3241	3192	3420
	Asymmetric NH stretch	3346	3336	3266	3506
	MUE[f]		47	48	92

[a]All frequencies given in cm^{-1}. The average mean unsigned error (MUE) relative to experiment is reported for all methods. All calculations were performed with the B3LYP electronic exchange-correlation functional, and the NEO-DFT(V) excitation energies were computed with the epc17-2 electron-proton correlation functional. The electronic and nuclear basis sets are given in the text.
[b]Experimental data from ref.[42].
[c]Experimental data from ref.[43] (HOOH torsion), ref.[44] (OO stretch), ref.[45] (OH stretches, OH asym. bend),   ref.[46] (OH sym. bend) .
[d]Experimental data from ref.[42].
[e]Experimental data from ref.[47].
[f]For H_2O_2 the average of the reported experimental range was used for the calculation of the MUE.

Supplemental Information

The Supporting Information is available free of charge on the ACS Publications website at DOI: 10.1021/acs.jctc.9b00665. A table of TDDFT vibrational excitation energies is found in Appendix D.

Acknowledgments

References

(1)   Thomas, I. L., Protonic Structure of Molecules. I. Ammonia Molecules. *Physical Review* **1969,** *185*, 90-94.

(2)   Tachikawa, M.; Mori, K.; Nakai, H.; Iguchi, K., An extension of ab initio molecular orbital theory to nuclear motion. *Chem. Phys. Lett.* **1998,** *290*, 437-442.

(3)   Webb, S. P.; Iordanov, T.; Hammes-Schiffer, S., Multiconfigurational nuclear-electronic orbital approach: Incorporation of nuclear quantum effects in electronic structure calculations. *J. Chem. Phys.* **2002,** *117*, 4106-4118.

(4)   Nakai, H.; Sodeyama, K., Many-body effects in nonadiabatic molecular theory for simultaneous determination of nuclear and electronic wave functions: Ab initio NOMO/MBPT and CC methods. *J. Chem. Phys.* **2003,** *118*, 1119-1127.

(5)   Swalina, C.; Pak, M. V.; Hammes-Schiffer, S., Alternative formulation of many-body perturbation theory for electron-proton correlation. *Chem. Phys. Lett.* **2005,** *404*, 394-399.

(6)   Chakraborty, A.; Pak, M. V.; Hammes-Schiffer, S., Inclusion of explicit electron-proton correlation in the nuclear-electronic orbital approach using Gaussian-type geminal functions. *J. Chem. Phys.* **2008,** *129*, 014101.

(7)   Sirjoosingh, A.; Pak, M. V.; Swalina, C.; Hammes-Schiffer, S., Reduced explicitly correlated Hartree-Fock approach within the nuclear-electronic orbital framework: Theoretical formulation. *J. Chem. Phys.* **2013,** *139*, 034102.

(8)   Bubin, S.; Pavanello, M.; Tung, W.-C.; Sharkey, K. L.; Adamowicz, L., Born–Oppenheimer and Non-Born–Oppenheimer, Atomic and Molecular Calculations with Explicitly Correlated Gaussians. *Chem. Rev.* **2013,** *113*, 36-79.

(9)   Pavošević, F.; Culpitt, T.; Hammes-Schiffer, S., Multicomponent Coupled Cluster Singles and Doubles Theory within the Nuclear-Electronic Orbital Framework. *J. Chem. Theory Comput.* **2019,** *15*, 338-347.

(10)   Capitani, J. F.; Nalewajski, R. F.; Parr, R. G., Non-Born–Oppenheimer density functional theory of molecular systems. *J. Chem. Phys.* **1982,** *76*, 568-573.

(11)   Gidopoulos, N., Kohn-Sham equations for multicomponent systems: The exchange and correlation energy functional. *Phys. Rev. B.* **1998,** *57*, 2146-2152.

(12)   Kreibich, T.; Gross, E. K. U., Multicomponent Density-Functional Theory for Electrons and Nuclei. *Phys. Rev. Lett.* **2001,** *86*, 2984-2987.

(13)   Udagawa, T.; Tachikawa, M., H/D isotope effect on porphine and porphycene molecules with multicomponent hybrid density functional theory. *J. Chem. Phys.* **2006,** *125*, 244105.

(14)   Pak, M. V.; Chakraborty, A.; Hammes-Schiffer, S., Density Functional Theory Treatment of Electron Correlation in the Nuclear−Electronic Orbital Approach. *J. Phys. Chem. A.* **2007,** *111*, 4522-4526.

(15)   Chakraborty, A.; Pak, M. V.; Hammes-Schiffer, S., Development of Electron-Proton Density Functionals for Multicomponent Density Functional Theory. *Phys. Rev. Lett.* **2008,** *101*, 153001.

(16)   Chakraborty, A.; Pak, M. V.; Hammes-Schiffer, S., Properties of the exact universal functional in multicomponent density functional theory. *J. Chem. Phys.* **2009,** *131*, 124115.

(17)   Yang, Y.; Brorsen, K. R.; Culpitt, T.; Pak, M. V.; Hammes-Schiffer, S., Development of a practical multicomponent density functional for electron-proton correlation to produce accurate proton densities. *J. Chem. Phys.* **2017,** *147*, 114113.

(18)   Brorsen, K. R.; Yang, Y.; Hammes-Schiffer, S., Multicomponent Density Functional Theory: Impact of Nuclear Quantum Effects on Proton Affinities and Geometries. *J. Phys. Chem. Lett.* **2017,** *8*, 3488-3493.

(19)   Brorsen, K. R.; Schneider, P. E.; Hammes-Schiffer, S., Alternative forms and transferability of electron-proton correlation functionals in nuclear-electronic orbital density functional theory. *J. Chem. Phys.* **2018,** *149*, 044110.

(20)   Yang, Y.; Culpitt, T.; Hammes-Schiffer, S., Multicomponent Time-Dependent Density Functional Theory: Proton and Electron Excitation Energies. *J. Phys. Chem. Lett.* **2018,** *9*, 1765-1770.

(21)   Yang, Y.; Schneider, P. E.; Culpitt, T.; Pavošević, F.; Hammes-Schiffer, S., Molecular Vibrational Frequencies within the Nuclear–Electronic Orbital Framework. *J. Phys. Chem. Lett.* **2019,** *10*, 1167-1172.

(22)   Casida, M. E., Time-dependent density functional response theory of molecular systems: theory, computational methods, and functionals. In *Recent Developments and Applications of Modern Density Functional Theory*, Seminario, J., Ed. Elsevier Science: 1996; Vol. 4, pp 391-439.

(23)   Dreuw, A.; Head-Gordon, M., Single-Reference ab Initio Methods for the Calculation of Excited States of Large Molecules. *Chem. Rev.* **2005,** *105*, 4009-4037.

(24)   Burke, K.; Werschnik, J.; Gross, E. K. U., Time-dependent density functional theory: Past, present, and future. *J. Chem. Phys.* **2005,** *123*, 062206.

(25)   Ulrich, C. A., *Time-Dependent Density-Functional Theory: Concepts and Applications*. Oxford University Press: Oxford, 2012.

(26)   Maitra, N. T., Perspective: Fundamental aspects of time-dependent density functional theory. *J. Chem. Phys.* **2016,** *144*, 220901.

(27)   Goings, J. J.; Lestrange, P. J.; Li, X., Real-time time-dependent electronic structure theory. *Wiley Interdisciplinary Reviews: Computational Molecular Science* **2018,** *8*, e1341.

(28)   Stanton, J. F.; Bartlett, R. J., The equation of motion coupled-cluster method. A systematic biorthogonal approach to molecular excitation energies, transition probabilities, and excited state properties. *J. Chem. Phys.* **1993,** *98*, 7029-7039.

(29)   Comeau, D. C.; Bartlett, R. J., The equation-of-motion coupled-cluster method. Applications to open- and closed-shell reference states. *Chem. Phys. Lett.* **1993,** *207*, 414-423.

(30)   Levchenko, S. V.; Krylov, A. I., Equation-of-motion spin-flip coupled-cluster model with single and double substitutions: Theory and application to cyclobutadiene. *J. Chem. Phys.* **2003,** *120*, 175-185.

(31)   Krylov, A. I., Equation-of-Motion Coupled-Cluster Methods for Open-Shell and Electronically Excited Species: The Hitchhiker's Guide to Fock Space. *Annu. Rev. Phys. Chem.* **2008,** *59*, 433-462.

(32)   Pavošević, F.; Hammes-Schiffer, S., Multicomponent equation-of-motion coupled cluster singles and doubles: Theory and calculation of excitation energies for positronium hydride. *J. Chem. Phys.* **2019,** *150*, 161102.

(33)   Yang, Y.; Kurt, R. B.; Tanner, C.; Michael, V. P.; Sharon, H.-S., Development of a practical multicomponent density functional for electron-proton correlation to produce accurate proton densities. *J. Chem. Phys.* **2017,** *147*, 114113.

(34)   Culpitt, T.; Yang, Y.; Pavošević, F.; Tao, Z.; Hammes-Schiffer, S., Enhancing the applicability of multicomponent time-dependent density functional theory. *J. Chem. Phys.* **2019,** *150*, 201101.

(35)   Lee, C.; Yang, W.; Parr, R. G., Development of the Colle-Salvetti correlation-energy formula into a functional of the electron density. *Phys. Rev. B.* **1988,** *37*, 785-789.

(36)   Becke, A. D., Density-functional thermochemistry. III. The role of exact exchange. *J. Chem. Phys.* **1993,** *98*, 5648-5652.

(37)   Dunning, T. H., Gaussian basis sets for use in correlated molecular calculations. I. The atoms boron through neon and hydrogen. *J. Chem. Phys.* **1989,** *90*, 1007-1023.

(38)   Peterson, K. A.; Woon, D. E.; Dunning, T. H., Benchmark calculations with correlated molecular wave functions. IV. The classical barrier height of the H+H2→H2+H reaction. *J. Chem. Phys.* **1994,** *100*, 7410-7415.

(39)   Schmidt, M. W.; Baldridge, K. K.; Boatz, J. A.; Elbert, S. T.; Gordon, M. S.; Jensen, J. H.; Koseki, S.; Matsunaga, N.; Nguyen, K. A.; Su, S., General atomic and molecular electronic structure system. *J. Comput. Chem.* **1993,** *14*, 1347-1363.

(40)   Frisch, M. J.; Trucks, G. W.; Schlegel, H. B.; Scuseria, G. E.; Robb, M. A.; Cheeseman, J. R.; Scalmani, G.; Barone, V.; Mennucci, B.; Petersson, G. A.; Nakatsuji, H.; Caricato, M.; Li, H.; Hratchian, H. P.; Izmaylov, A. F.; Bloino, J.; Zheng, G.; Sonnenberg, J. L.; Hada, M.; Ehara, M.; Toyota, K.; Fukuda, R.; Hasegawa, J.; Ishida, M.; Nakajima, T.; Honda, Y.; Kitao, O.; Nakai, H.; Vreven, T.; Montgomery, J., J. A.; Peralta, J. E.; Ogliaro, F.; Bearpark, M. J.; Heyd, J. J.; Brothers, E. N.; Kudin, K. N.; Staroverov, V. N.; Kobayashi, R.; Normand, J.; Raghavachari, K.; Rendell, A.; Burant, J. C.; Iyengar, S. S.; Tomasi, J.; Cossi, M.; Rega, N.; Millam, J. M.; Klene, M.; Knox, J. E.; Cross, J. B.; Bakken, V.; Adamo, C.; Jaramillo, J.; Gomperts, R.; Stratmann, R. E.; Yazyev, O.; Austin, A. J.; Cammi, R.; Pomelli, C.; Ochterski, J. W.; Martin, R. L.; Morokuma, K.; Zakrzewski, V. G.; Voth, G. A.; Salvador, P.; Dannenberg, J. J.; Dapprich, S.; Daniels, A. D.; Farkas, O.; Foresman, J. B.; Ortiz, J. V.; Cioslowski, J.; Fox, D. J. *Gaussian 09 Rev. D.01*, Wallingford, CT, 2009.

(41)   Barone, V., Anharmonic vibrational properties by a fully automated second-order perturbative approach. *J. Chem. Phys.* **2004,** *122*, 014108.

(42)   Shimanouchi, T., Tables of Molecular Vibrational Frequencies Consolidated Volume I. National Bureau of Standards: 1972; pp 1-160.

(43)   Hunt, R. H.; Leacock, R. A.; Peters, C. W.; Hecht, K. T., Internal-Rotation in Hydrogen Peroxide: The Far-Infrared Spectrum and the Determination of the Hindering Potential. *J. Chem. Phys.* **1965,** *42*, 1931-1946.

(44)   Camy-Peyret, C.; Flaud, J. M.; Johns, J. W. C.; Noël, M., Torsion-vibration interaction in H2O2: First high-resolution observation of v3. *Journal of Molecular Spectroscopy* **1992,** *155*, 84-104.

(45)   Bain, O.; Giguère, P. A., HYDROGEN PEROXIDE AND ITS ANALOGUES: VI. INFRARED SPECTRA OF H2O2, D2O2, AND HDO2. *Canadian Journal of Chemistry* **1955,** *33*, 527-545.

(46)   Giguére, P. A.; Srinivasan, T. K. K., A Raman study of H2O2 and D2O2 vapor. *Journal of Raman Spectroscopy* **1974,** *2*, 125-132.

(47)   Baumgärtel, H.; Jochims, H. W.; Rühl, E.; Bock, H.; Dammel, R.; Minkwitz, J.; Nass, R., *Photoelectron and photoionization mass spectra of the fluoramines NH3-nFn1*. 1989; Vol. 28, p 943-949.

Chapter Six

Conclusion

In the preceding chapters, the development of several functionalities of the nuclear-electronic orbital (NEO) method were presented, all related to the NEO potential energy surface (PES). As the PES concept is foundational in a computational approach to chemical reactions, the findings of this dissertation have helped to solidify the basis and practicality of these multicomponent methods. As will be demonstrated, the previous chapters have opened the door to several novel opportunities for applications of the NEO method.

In chapter 2, the diagonal Born-Oppenheimer correction for NEO-DFT was derived and employed to validate the separation of quantum and classical nuclei intrinsic to the NEO method. The DBOC was calculated in a numerical fashion and it was found to not appreciably change equilibrium bond lengths and heavy atom vibrational frequencies for a set of simple molecular systems, demonstrating that the difference between the NEO energy surface and the adiabatic surface including the DBOC is negligible in these situations. Much like the conventional electronic DBOC, the NEO DBOC was found to increase in value based on the number of particles being treated quantum mechanically. Ultimately, the results presented in chapter 2 confirmed the validity of the NEO method's separation between light and heavy nuclei for the systems that were studied.

Chapter 3 was concerned with the development and implementation of analytical Hessian functionality for the NEO method, particularly in its utility for transition state searches and minimum energy path calculations. The analytical equations for Hessian elements were given and the implementation was verified by comparison to numerical benchmarks. Transition states for both an S_N2 and a hydride transfer reaction were then located on the PES using a transition state optimization based on surface characterization from the analytical Hessian. The heavy atom motion of the imaginary vibrational mode defining each transition state was shown to align with the corresponding atomic motion of the conventionally calculated transition states.

Differences between conventional and multicomponent computed minimum energy paths were elucidated by demonstrating the fact that the zero-point energy of the quantum nuclei is included directly into the NEO surface, accounting for most of the difference in calculated barrier height. Lastly, modeling software was used to animate the change in both the reactive electronic orbital and the quantum nuclear orbital along the reaction coordinate.

In chapters 4 and 5, the NEO-DFT(V) method for the calculation of molecular vibrational frequencies within the NEO framework was presented. Chapter 4 concerned the application to systems where a single proton was treated quantum mechanically, and chapter 5 generalized the formalism for treatment of any number of quantum nuclei. These studies found that quantities concerning the vibrational excitations of the classical modes from the NEO Hessian needed to be coupled with the quantum nuclear vibrational excitations from NEO-TDDFT in order to yield a complete set of molecular vibrational frequencies. In both chapters, the resulting NEO-DFT(V) vibrational analysis yielded highly accurate results relative to experimental data on par in accuracy with conventional anharmonic vibrational analysis calculations.

In light of the advances in the NEO method presented in this dissertation, a survey on the future outlook of the method's applicability can be made. Analysis of the DBOC verified the central approximation of the method, which is also now outfitted with a tool for vibrational analysis and PES characterization via the analytical Hessian. The vibrational analysis has been used to compute differences in free energy, and a protocol for calculation of IR spectra in the NEO method was developed. With this work, significant strides have been made in preparing the method for meaningful application to larger systems of interest, notably molecular electrocatalysts. In the future, this multicomponent method can be used in conjunction with proton-coupled electron transfer (PCET) theory[1-2] to improve the capabilities

of charge transfer models and help distinguish between asynchronous and synchronous concerted electron-proton transfer.[3] As a final concrete example, previously studied N_2O_2-ligated Co-centered oxygen reduction reaction catalysts[4] could be revisited computationally with this multicomponent method. A preliminary calculation of the peroxide species in the catalytic pathway is presented in Figure 6.1, with the distal proton treated quantum mechanically. The quantum proton orbital is depicted as an isosurface with yellow mesh. With the advances described in this dissertation, novel studies of such complexes using multicomponent quantum chemical theory are on the horizon.
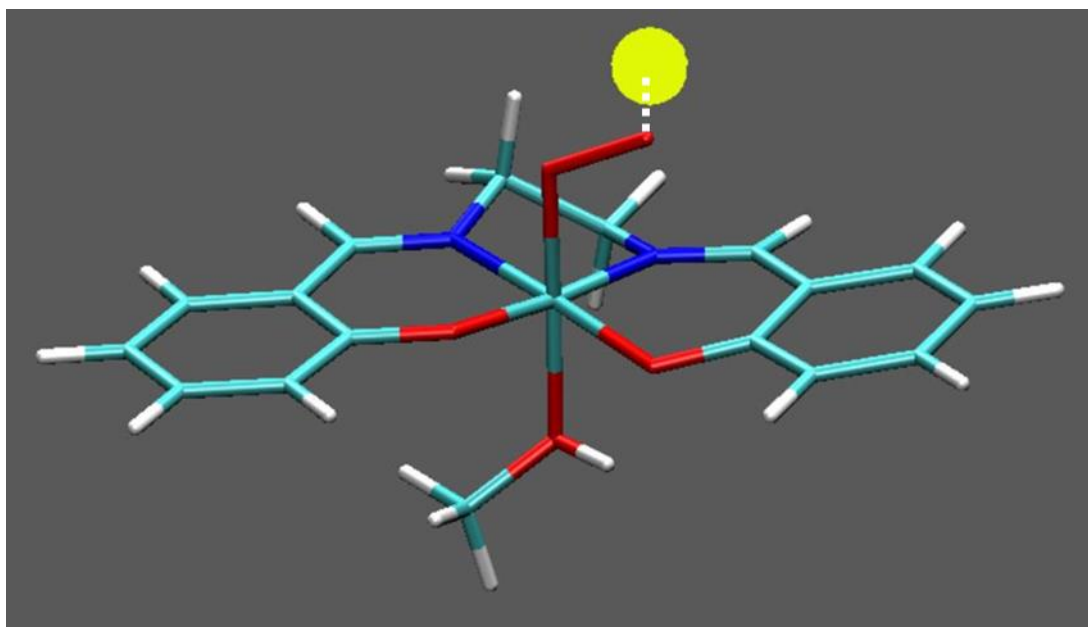
Figure 6.1 Structure of the peroxo species of an N_2O_2-ligated Co-centered molecular electrocatalyst[a]

[a]The proton on the distal oxygen of the peroxo moiety was treated quantum mechanically using NEO-DFT, and the protonic orbital is depicted as an isosurface with yellow mesh.

References

(1)   Soudackov, A.; Hammes-Schiffer, S., Derivation of rate expressions for nonadiabatic proton-coupled electron transfer reactions in solution. *J. Chem. Phys.* **2000,** *113*, 2385-2396.

(2)   Hammes-Schiffer, S.; Stuchebrukhov, A. A., Theory of Coupled Electron and Proton Transfer Reactions. *Chem. Rev.* **2010,** *110*, 6939-6960.

(3)   Goings, J. J.; Hammes-Schiffer, S., Nonequilibrium Dynamics of Proton-Coupled Electron Transfer in Proton Wires: Concerted but Asynchronous Mechanisms. *ACS Cent. Sci.* **2020,** *6*, 1594-1601.

(4)   Wang, Y.-H.; Goldsmith, Z. K.; Schneider, P. E.; Anson, C. W.; Gerken, J. B.; Ghosh, S.; Hammes-Schiffer, S.; Stahl, S. S., Kinetic and Mechanistic Characterization of Low-Overpotential, H2O2-Selective Reduction of O2 Catalyzed by N2O2-Ligated Cobalt Complexes. *J. Am. Chem. Soc.* **2018,** *140*, 10890-10899.

Appendices

A.   Supplemental Information for Chapter 2

Supporting Information for Diagonal Born-Oppenheimer Corrections within the Nuclear-Electronic Orbital Framework

Patrick E. Schneider, Fabijan Pavošević, and Sharon Hammes-Schiffer*

Department of Chemistry, Yale University

225 Prospect Street, New Haven, Connecticut 06520 USA

*Corresponding author: sharon.hammes-schiffer@yale.edu

Derivation of protonic DBOC for simple harmonic oscillator model system

The analog of the hydrogen atom for the protonic DBOC is a diatomic molecule, where the heavy atom has mass M_C and the hydrogen atom has mass m_p. This molecule has a single vibrational mode of frequency v described as a harmonic oscillator that depends on the distance x between the two atoms: $x = |r_p - r_C|$. The harmonic oscillator ground state wavefunction is given by

$$\psi_p = (\alpha/\pi)^{1/4} e^{-\alpha x^2/2} \ , \ \alpha = 2\pi v m/\hbar \ . \tag{A1}$$

Here we assume that $m = m_p$, although the results will be similar if we use the reduced mass instead. The protonic DBOC is given by

$$E_{DBOC}^p = -\frac{\hbar^2}{2M_C} \langle \psi_p | \nabla_C^2 \psi_p \rangle \ . \tag{A2}$$

Because the proton vibrational wavefunction depends on x, which is defined to be the distance between the two coordinates, the second derivative with respect to r_p is the same as the second derivative with respect to r_C. Then the quantity in Eq. (A2) is just the expectation value of the kinetic energy T of the proton multiplied by the mass ratio:

$$E_{DBOC}^p = \frac{m_p}{M_C} \langle T \rangle = \frac{m_p}{M_C} \frac{hv}{4} = \frac{m_p}{2M_C} \frac{hv}{2} \ . \tag{A3}$$

Testing the Numerical Precision of the DBOC

When including the DBOC in the calculation of vibrational frequencies, a finite-difference numerical second derivative of the DBOC with respect to the distance between the heavy nuclei must be calculated. As the DBOC is also calculated via a finite-difference second derivative method (see Eqs. 2.5-2.7 of chapter 2), its contribution to the vibrational frequencies is effectively a numerical fourth derivative with

two finite-difference parameters: δ for the initial DBOC calculation and Δ for the second derivative of the DBOC with respect to the heavy nuclei. An additional numerical challenge is that the positions of the quantum proton basis function centers must be optimized variationally for each position of the heavy nuclei. An extra tight value, 10^{-6} Hartree/Bohr, was used as the geometry optimization convergence criterion, where both the magnitude of the maximal gradient element must be smaller than the threshold and the root-mean-square of all gradient element magnitudes must be smaller than one third of the threshold. The precision of these numerical fourth derivatives was determined by examining the dependence of the vibrational frequencies on these two parameters, as given in Tables A1 and A2. For chapter 2, values of $\delta=10^{-3}$ Bohr and $\Delta=10^{-2}$ Bohr were employed. Note that increasing or decreasing these chosen values by a factor of two can change the vibrational frequency by less than 1 cm^{-1} in some cases or as much as 6 cm^{-1} in one case, although the typical change is ~1 cm^{-1}. When these parameters become too small, the energy differences become smaller than the numerical precision, and consequently the numerical derivatives are no longer meaningful. Thus, the numerical precision of these calculations is presumed to be ~1 cm^{-1} with a more conservative estimate of ~6 cm^{-1}.

Effect of DBOC on Equilibrium Distance and Vibrational Frequency at the NEO-HF Level

Analogous to the analysis in chapter 2, the effects of including the DBOC in the calculation of the vibrational stretching frequencies of the heavy nuclei was performed at the NEO-HF level of theory for HCN. The vibrational frequency of the CN stretching mode was found to change from 2514 cm^{-1} to 2518 cm^{-1}, a somewhat larger change

than that observed at the NEO-DFT/epc17-2 level. The NEO-HF equilibrium CN

distance for HCN was found to change from 1.125116 Å to 1.125719 Å, corresponding

to an increase of 6.03×10^{-4} Å with an energy stabilization of -2.20 µH. The changes in

the equilibrium distance and vibrational frequency of HCN upon inclusion of the DBOC

are greater at the NEO-HF level of theory than at the NEO-DFT/epc17-2 level of theory.

This trend is consistent with the larger value of $E_{\mathrm{DBOC}}^{\mathrm{p}}$ computed with NEO-HF, as seen

in Table 2.2 of chapter 2.

Table A1: Effect of Changing the DBOC Finite Difference Parameter δ on the Magnitude of the DBOC and its Components for HCN and HCC^{-} [a]

		δ (parameter for computing DBOC; Bohr)						
		1×10^{-2}	5×10^{-3}	2×10^{-3}	1×10^{-3}	5×10^{-4}	2×10^{-4}	1×10^{-4}
HCN	$E_{\text{DBOC}}^{\text{tot}}$	1328.7	1333.4	1334.8	1335.1	1335.1	1335.1	1335.0
	$E_{\text{DBOC}}^{\text{e}}$	800.4	803.6	804.5	804.7	804.7	804.7	804.7
	$E_{\text{DBOC}}^{\text{p}}$	528.2	529.8	530.3	530.4	530.4	530.4	530.3
HCC^{-}	$E_{\text{DBOC}}^{\text{tot}}$	1245.2	1249.1	1250.2	1250.4	1250.3	1250.1	1250.4
	$E_{\text{DBOC}}^{\text{e}}$	725.2	727.6	728.3	728.4	728.4	728.4	728.4
	$E_{\text{DBOC}}^{\text{p}}$	520.0	521.5	521.9	522.0	521.9	521.7	522.0

[a]All calculations were performed at the NEO-DFT/B3LYP/epc17-2 level of theory with the basis sets given in the text. All values are given in units of cm^{-1}. The value of $\delta=10^{-3}$ Bohr was used for the calculations in the main text.

Table A2: Effect of Changing the DBOC Finite Difference Parameter δ on the Vibrational Frequency of HCN and HCC⁻ [a]

			δ (parameter for computing DBOC; Bohr)						
			1×10^{-2}	5×10^{-3}	2×10^{-3}	1×10^{-3}	5×10^{-4}	2×10^{-4}	1×10^{-4}
$\Delta=10^{-2}$ (Bohr)	HCN	No DBOC				2293			
		With $E^{\mathrm{p}}_{\mathrm{DBOC}}$	2294	2294	2293	2293	2293	2287	2297
	HCC⁻	No DBOC				1963			
		With $E^{\mathrm{p}}_{\mathrm{DBOC}}$	1963	1963	1964	1962	1968	1967	1965

[a]For both molecules, the NEO potential energy surface is one-dimensional with a single vibrational mode because all protons are treated quantum mechanically and each molecule has only two heavy atoms. All calculations were performed at the NEO-DFT/B3LYP/epc17-2 level of theory with the basis sets given in the text. All frequencies are given in units of cm⁻¹. The values of $\delta=10^{-3}$ Bohr and $\Delta=10^{-2}$ Bohr were used for the calculations in the main text.

Table A3: Effect of Changing the Vibrational Analysis Parameter Δ on the Vibrational Frequency of HCN and HCC^{-a}

			Δ (parameter for computing second derivative of DBOC; Bohr)						
			1×10^{-1}	5×10^{-2}	2×10^{-2}	1×10^{-2}	5×10^{-3}	2×10^{-3}	1×10^{-3}
$\delta=10^{-3}$ (Bohr)	HCN	No DBOC	2330	2302	2294	2293	2292	2292	2292
		With $E^{\mathrm{p}}_{\mathrm{DBOC}}$	2331	2303	2294	2293	2288	2259	2106
	HCC$^-$	No DBOC	1989	1969	1963	1963	1962	1962	1962
		With $E^{\mathrm{p}}_{\mathrm{DBOC}}$	1991	1970	1965	1962	1963	1951	1930

^{a}For both molecules, the NEO potential energy surface is one-dimensional with a single vibrational mode because all protons are treated quantum mechanically and each molecule has only two heavy atoms. All calculations were performed at the NEO-DFT/B3LYP/epc17-2 level of theory with the basis sets given in the text. All frequencies are given in units of cm^{-1}. The values of $\delta=10^{-3}$ Bohr and $\Delta=10^{-2}$ Bohr were used for the calculations in the main text.

Table A4: Effect of Including the DBOC on the Equilibrium Heavy Atom Distances and Energies

	HCN	HNC	HCC$^-$	FHF$^-$
Bond length (Å)	1.146979	1.165022	1.238879	2.321623
Bond length with $E_{\mathrm{DBOC}}^{\mathrm{tot}}$ (Å)	1.147471	1.165561	1.239244	2.321735
Change (Å)	0.000492	0.00054	0.000365	0.000111
Energy Change (µHa)	-0.884	-0.435	-0.617	-0.015
Heavy atom vibrational frequency without DBOC (cm^{-1})^a	2293	2160	1962	606
Heavy atom vibrational frequency with $E_{\mathrm{DBOC}}^{\mathrm{tot}}$ (cm^{-1})^b	2291	2158	1963	606

^{a}Frequency calculated at the NEO equilibrium geometry without considering $E_{\mathrm{DBOC}}^{\mathrm{tot}}$.

^{b}Frequency calculated with $E_{\mathrm{DBOC}}^{\mathrm{tot}}$ at the equilibrium bond length determined with $E_{\mathrm{DBOC}}^{\mathrm{tot}}$.

Table A5: Effect of Changing the DBOC Finite Difference Parameter δ on the Vibrational Frequency of HCN and HCC$^-$ at Equilibrium Bond Length Determined with $E_{\text{DBOC}}^{\text{tot}}$ *[a]*

			δ (parameter for computing DBOC; Bohr)						
			1×10^{-2}	5×10^{-3}	2×10^{-3}	1×10^{-3}	5×10^{-4}	2×10^{-4}	1×10^{-4}
$\Delta=10^{-2}$ (Bohr)	HCN	No DBOC				2293			
		With $E_{\text{DBOC}}^{\text{tot}}$	2290	2290	2290	2291	2290	2282	2282
	HCC$^-$	No DBOC				1963			
		With $E_{\text{DBOC}}^{\text{tot}}$	1961	1961	1962	1963	1962	1954	1965

*[a]*For both molecules, the NEO potential energy surface is one-dimensional with a single vibrational mode because all protons are treated quantum mechanically and each molecule has only two heavy atoms. All calculations were performed at the NEO-DFT/B3LYP/epc17-2 level of theory with the basis sets given in the text. All frequencies are given in units of cm^{-1}. The values of $\delta=10^{-3}$ Bohr and $\Delta=10^{-2}$ Bohr were used for the calculations in the main text.

Table A6: Effect of Changing the Vibrational Analysis Parameter Δ on the Vibrational Frequency of HCN and HCC⁻ at Equilibrium Bond Length Determined with $E_{\text{DBOC}}^{\text{tot}}$ [a]

			Δ (parameter for computing second derivative of DBOC; Bohr)						
			1×10^{-1}	5×10^{-2}	2×10^{-2}	1×10^{-2}	5×10^{-3}	2×10^{-3}	1×10^{-3}
$\delta=10^{-3}$ (Bohr)	HCN	No DBOC	2330	2302	2294	2293	2292	2292	2292
		With $E_{\text{DBOC}}^{\text{tot}}$	2327	2299	2291	2291	2291	2308	2327
	HCC⁻	No DBOC	1989	1969	1963	1963	1962	1962	1962
		With $E_{\text{DBOC}}^{\text{tot}}$	1988	1968	1963	1963	1965	1998	2051

[a]For both molecules, the NEO potential energy surface is one-dimensional with a single vibrational mode because all protons are treated quantum mechanically and each molecule has only two heavy atoms. All calculations were performed at the NEO-DFT/B3LYP/epc17-2 level of theory with the basis sets given in the text. All frequencies are given in units of cm⁻¹. The values of $\delta=10^{-3}$ Bohr and $\Delta=10^{-2}$ Bohr were used for the calculations in the main text.

B.   Supplemental Information for Chapter 3

Supporting Information for Transition States, Reaction Paths, and Thermochemistry Using the Nuclear-Electronic Orbital Analytic Hessian

Patrick E. Schneider,[1] Zhen Tao,[1] Fabijan Pavošević,[1] Evgeny Epifanovsky,[2] Xintian Feng,[2] and Sharon Hammes-Schiffer[1]*

[1]Department of Chemistry, Yale University

225 Prospect Street, New Haven, Connecticut 06520 USA

[2]Q-Chem, Inc.

6601 Owens Drive, Suite 105, Pleasanton, California 94588 USA

*Corresponding author: sharon.hammes-schiffer@yale.edu

Comparison of Analytic Hessian with Semi-Numerical Implementation

The implementation of the analytic Hessian was benchmarked by comparing semi-numerical and analytic Hessians for a set of molecules. One representative example is the HCN molecule. The geometry of HCN was optimized to the desired tolerance (3×10^{-5} Hartree/Bohr for gradient elements) at the NEO-HF level with the STO-3G electronic basis set and a minimal *sp* nuclear basis set and is given in Table B1. The *sp* nuclear basis set is composed of a single *s*-type Gaussian function and a single *p*-type Gaussian function both with exponent 4.00 for each basis function center. The semi-numerical Hessian and analytic Hessian for this HCN system are given in Tables B2 and B3, respectively. All Hessians discussed in the main text were computed fully analytically.

Coupled-Perturbed NEO-HF Equations

To calculate the density matrix response terms and orbital energy response terms needed for the Hessian element evaluation, the Roothaan equations and orthonormality constraints given in Eqs. (3.20), (3.21), (3.26), and (3.27) from chapter 3 are written under a general geometric perturbation y as[1]

$$\mathbf{F}^{e}(y)\mathbf{C}^{e}(y)=\mathbf{S}^{e}(y)\mathbf{C}^{e}(y)\boldsymbol{\varepsilon}^{e}(y) \tag{B1}$$

$$\mathbf{F}^{p}(y)\mathbf{C}^{p}(y)=\mathbf{S}^{p}(y)\mathbf{C}^{p}(y)\boldsymbol{\varepsilon}^{p}(y) \tag{B2}$$

$$\mathbf{C}^{e\dagger}(y)\mathbf{S}^{e}(y)\mathbf{C}^{e}(y)=\mathbf{I} \tag{B3}$$

$$\mathbf{C}^{p\dagger}(y)\mathbf{S}^{p}(y)\mathbf{C}^{p}(y)=\mathbf{I}\ . \tag{B4}$$

Note that in the limit of y approaching zero, the original Roothaan equations and solutions are reproduced. The perturbed orbital coefficients can be written as a unitary transformation of the unperturbed coefficients,

$$\mathbf{C}^{\mathrm{e}}(y) = \mathbf{C}^{\mathrm{e}}(0)\mathbf{U}^{\mathrm{e}}(y) \tag{B5}$$

$$\mathbf{C}^{\mathrm{p}}(y) = \mathbf{C}^{\mathrm{p}}(0)\mathbf{U}^{\mathrm{p}}(y) \tag{B6}$$

which can be used to recast the relations given in Eqs. (B1)–(B4) in terms of orbital rotations:

$$\bar{\mathbf{F}}^{\mathrm{e}}(y)\mathbf{U}^{\mathrm{e}}(y) = \bar{\mathbf{S}}^{\mathrm{e}}(y)\mathbf{U}^{\mathrm{e}}(y)\boldsymbol{\varepsilon}^{\mathrm{e}}(y) \tag{B7}$$

$$\bar{\mathbf{F}}^{\mathrm{p}}(y)\mathbf{U}^{\mathrm{p}}(y) = \bar{\mathbf{S}}^{\mathrm{p}}(y)\mathbf{U}^{\mathrm{p}}(y)\boldsymbol{\varepsilon}^{\mathrm{p}}(y) \tag{B8}$$

$$\mathbf{U}^{\mathrm{e}\dagger}(y)\bar{\mathbf{S}}^{\mathrm{e}}(y)\mathbf{U}^{\mathrm{e}}(y) = \mathbf{I} \tag{B9}$$

$$\mathbf{U}^{\mathrm{p}\dagger}(y)\bar{\mathbf{S}}^{\mathrm{p}}(y)\mathbf{U}^{\mathrm{p}}(y) = \mathbf{I}. \tag{B10}$$

In this form, the Fock and overlap matrices have now been transformed to the orbital basis and are represented by the notation

$$\bar{\mathbf{F}}^{\mathrm{e}}(y) = \mathbf{C}^{\mathrm{e}\dagger}(0)\mathbf{F}^{\mathrm{e}}(y)\mathbf{C}^{\mathrm{e}}(0) \tag{B11}$$

$$\bar{\mathbf{F}}^{\mathrm{p}}(y) = \mathbf{C}^{\mathrm{p}\dagger}(0)\mathbf{F}^{\mathrm{p}}(y)\mathbf{C}^{\mathrm{p}}(0) \tag{B12}$$

$$\bar{\mathbf{S}}^{\mathrm{e}}(y) = \mathbf{C}^{\mathrm{e}\dagger}(0)\mathbf{S}^{\mathrm{e}}(y)\mathbf{C}^{\mathrm{e}}(0) \tag{B13}$$

$$\bar{\mathbf{S}}^{\mathrm{p}}(y) = \mathbf{C}^{\mathrm{p}\dagger}(0)\mathbf{S}^{\mathrm{p}}(y)\mathbf{C}^{\mathrm{p}}(0). \tag{B14}$$

To solve for the orbital rotations and perturbed energies of Eq. (B7)–(B10), the Fock matrix, overlap matrix, orbital rotations, and energy matrix are expressed as Taylor expansions in terms of the perturbation:

$$\overline{\mathbf{F}}^{\xi}(y) = \overline{\mathbf{F}}_0^{\xi} + \left(\overline{\mathbf{F}}^{\xi}\right)^y y + \cdots \tag{B15}$$

$$\overline{\mathbf{S}}^{\xi}(y) = \mathbf{1} + \left(\overline{\mathbf{S}}^{\xi}\right)^y y + \cdots \tag{B16}$$

$$\mathbf{U}^{\xi}(y) = \mathbf{1} + \left(\mathbf{U}^{\xi}\right)^y y + \cdots \tag{B17}$$

$$\boldsymbol{\varepsilon}^{\xi}(y) = \boldsymbol{\varepsilon}_0^{\xi} + \left(\boldsymbol{\varepsilon}^{\xi}\right)^y y + \cdots \tag{B18}$$

where the superscript $\xi \in \{e, p\}$ refers to the electron or proton terms. The only unknown

quantities in the first-order Taylor expansions are the first-order derivatives of the orbital

energy, orbital rotations, and Fock matrix, the last of which is only unknown due to a

dependence on the orbital rotations. The first-order overlap matrix, $\left(\overline{\mathbf{S}}^{\xi}\right)^y$, is related to

the basis function overlap derivative integrals by a transformation to the orbital basis,

$$\left(\overline{\mathbf{S}}^{\xi}\right)^y = \mathbf{C}^{\xi\dagger}(0)\left(\mathbf{S}^{\xi}\right)^y \mathbf{C}^{\xi}(0). \tag{B19}$$

The first-order Fock matrix, $\left(\overline{\mathbf{F}}^{\xi}\right)^y$, is similarly related to other first-order derivative

integrals but also depends on the orbital rotations. After combining Eqs. (B15)–(B18)

with Eqs. (B7)–(B10) and rearranging terms, an expression is found for $\left(\boldsymbol{\varepsilon}^{\xi}\right)^y$ that

depends on the diagonal elements of the Fock and overlap matrices:

$$\left(\varepsilon^{\xi}\right)^y_{pp} = \left(\overline{F}^{\xi}\right)^y_{pp} - \left(\overline{S}^{\xi}\right)^y_{pp} \varepsilon^{\xi}_{pp}. \tag{B20}$$

The occupied-occupied block of the first-order orbital rotations is determined to be

$$\left(U^{\xi}\right)^y_{ij} = -\frac{1}{2}\left(\overline{S}^{\xi}\right)^y_{ij} \tag{B21}$$

through similar mathematical manipulations, and the virtual-virtual block is zero. Now

the only remaining unknown is the occupied-virtual block, $\left(U^{\xi}\right)^y_{ai}$.

143

These rotations are solutions of the well-known coupled-perturbed HF equations,[1-3] which are expressed in the multicomponent framework as

$$\left(\varepsilon_i^e - \varepsilon_a^e\right)\left(U^e\right)_{ai}^y - 4\tilde{G}_{ai}^e\left[\left(U^e\right)_{bj}^y,\left(U^p\right)_{BJ}^y\right] = \left(Q^e\right)_{ai}^y \tag{B22}$$

$$\left(\varepsilon_I^p - \varepsilon_A^p\right)\left(U^p\right)_{AI}^y - 4\tilde{G}_{AI}^p\left[\left(U^p\right)_{BJ}^y,\left(U^e\right)_{bj}^y\right] = \left(Q^p\right)_{AI}^y \tag{B23}$$

with

$$\left(Q^e\right)_{ai}^y = \left(\bar{H}^e\right)_{ai}^y + \left(\bar{G}^e\right)_{ai}^y - \left(\bar{G}^{ep}\right)_{ai}^y - \varepsilon_i^e\left(\bar{S}^e\right)_{ai}^y - 2\tilde{G}_{ai}^e\left[\left(\bar{S}^e\right)_{jk}^y,\left(\bar{S}^p\right)_{JK}^y\right] \tag{B24}$$

$$\left(Q^p\right)_{AI}^y = \left(\bar{H}^p\right)_{AI}^y + \left(\bar{G}^p\right)_{AI}^y - \left(\bar{G}^{pe}\right)_{AI}^y - \varepsilon_I^p\left(\bar{S}^p\right)_{AI}^y - 2\tilde{G}_{AI}^p\left[\left(\bar{S}^p\right)_{JK}^y,\left(\bar{S}^e\right)_{jk}^y\right] \tag{B25}$$

In these coupled-perturbed NEO-HF (CP-NEO-HF) equations, $\left(\bar{H}^\xi\right)^y$, $\left(\bar{G}^\xi\right)^y$, $\left(\bar{G}^{ep}\right)^y$, and $\left(\bar{G}^{pe}\right)^y$ are defined in terms of basis function derivative integrals analogous to $\left(\bar{S}^\xi\right)^y$ given in Eq. (B19). The matrices $\tilde{G}$, given general electronic and nuclear inputs M_{rs}^e and M_{RS}^p, are defined as

$$\tilde{G}_{pq}^e\left[M_{rs}^e, M_{RS}^p\right] = \sum_{\mu\nu} c_{\mu p}^e c_{\nu q}^e\left(\tilde{G}_{\mu\nu}^e\left[M_{rs}^e\right] - \frac{1}{2}\tilde{G}_{\mu\nu}^{ep}\left[M_{RS}^p\right]\right) \tag{B26}$$

$$\tilde{G}_{PQ}^p\left[M_{RS}^p, M_{rs}^e\right] = \sum_{\mu'\nu'} c_{\mu'P}^p c_{\nu'Q}^p\left(\frac{1}{2}\tilde{G}_{\mu'\nu'}^p\left[M_{RS}^p\right] - \tilde{G}_{\mu'\nu'}^{pe}\left[M_{rs}^e\right]\right) \tag{B27}$$

$$\tilde{G}_{\mu\nu}^e\left[M_{rs}^e\right] = \sum_{rs\sigma\lambda} c_{\sigma r}^e M_{rs}^e c_{\lambda s}^e\left[\left(\mu\nu\mid\sigma\lambda\right) - \frac{1}{2}\left(\mu\sigma\mid\nu\lambda\right)\right] \tag{B28}$$

$$\tilde{G}_{\mu\nu}^{ep}\left[M_{RS}^p\right] = \sum_{RS\sigma'\lambda'} c_{\sigma'R}^p M_{RS}^p c_{\lambda'S}^p\left[\left(\mu\nu\mid\sigma'\lambda'\right)\right] \tag{B29}$$

$$\tilde{G}_{\mu'\nu'}^p\left[M_{RS}^p\right] = \sum_{RS\sigma'\lambda'} c_{\sigma'R}^p M_{RS}^p c_{\lambda'S}^p\left[\left(\mu'\nu'\mid\sigma'\lambda'\right) - \left(\mu'\sigma'\mid\nu'\lambda'\right)\right] \tag{B30}$$

$$\tilde{G}^{\mathrm{pe}}_{\mu'\nu'}\left[M^{\mathrm{e}}_{rs}\right]=\sum_{rs\sigma\lambda}c^{\mathrm{e}}_{\sigma r}M^{\mathrm{e}}_{rs}c^{\mathrm{e}}_{\lambda s}\left[\left(\mu'\nu'\mid\sigma\lambda\right)\right]. \tag{B31}$$

The matrices M^{e}_{rs} and M^{p}_{RS} will be either $\left(U^{\mathrm{e}}\right)^{y}_{bj}$ and $\left(U^{\mathrm{p}}\right)^{y}_{BJ}$ as in Eqs. (B22) and (B23)

or $\left(S^{\mathrm{e}}\right)^{y}_{ij}$ and $\left(S^{\mathrm{p}}\right)^{y}_{IJ}$ as in Eqs. (B24) and (B25). Now the occupied-virtual first-order

orbital rotations $\left(U^{\mathrm{e}}\right)^{y}_{ai}$ and $\left(U^{\mathrm{p}}\right)^{y}_{AI}$ are the unknowns for a system of coupled

inhomogeneous linear equations. By solving these CP-NEO-HF equations for every

geometric perturbation y, the derivative density and derivative energy-weighted density

matrices of Eq. (31) are obtained, providing the complete analytic expression for the

NEO-HF coordinate Hessian elements.

Unrestricted NEO-DFT Coupled-Perturbed Equations

The analytical unrestricted NEO-DFT energy coordinate Hessian elements are

given by

$$
\begin{aligned}
\frac{\partial^{2}E_{\mathrm{NEO\text{-}HF}}}{\partial x\partial y}=&\sum_{\mu\nu\sigma}P^{\mathrm{e}}_{\mu\nu\sigma}\left(H^{\mathrm{e}}_{\mu\nu}\right)^{xy}+\sum_{\mu'\nu'}P^{\mathrm{p}}_{\mu'\nu'}\left(H^{\mathrm{p}}_{\mu'\nu'}\right)^{xy}-\sum_{\mu\nu\sigma}W^{\mathrm{e}}_{\mu\nu\sigma}\left(S^{\mathrm{e}}_{\mu\nu}\right)^{xy}-\sum_{\mu'\nu'}W^{\mathrm{p}}_{\mu'\nu'}\left(S^{\mathrm{p}}_{\mu'\nu'}\right)^{xy}\\
&+\sum_{\mu\nu\sigma\lambda\kappa\sigma'}G^{\mathrm{ee}}_{\mu\nu\sigma,\lambda\kappa\sigma'}\left(\mu\nu\mid\lambda\kappa\right)^{xy}+\sum_{\mu'\nu'\lambda'\kappa'}G^{\mathrm{pp}}_{\mu'\nu',\lambda'\kappa'}\left(\mu'\nu'\mid\lambda'\kappa'\right)^{xy}\\
&+\sum_{\mu\nu\sigma}\left(P^{\mathrm{e}}_{\mu\nu\sigma}\right)^{y}\left(H^{\mathrm{e}}_{\mu\nu}\right)^{x}+\sum_{\mu'\nu'}\left(P^{\mathrm{p}}_{\mu'\nu'}\right)^{y}\left(H^{\mathrm{p}}_{\mu'\nu'}\right)^{x}-\sum_{\mu\nu\sigma}\left(W^{\mathrm{e}}_{\mu\nu\sigma}\right)^{y}\left(S^{\mathrm{e}}_{\mu\nu}\right)^{x}-\sum_{\mu'\nu'}\left(W^{\mathrm{p}}_{\mu'\nu'}\right)^{y}\left(S^{\mathrm{p}}_{\mu'\nu'}\right)^{x}\\
&+\sum_{\mu\nu\sigma\lambda\kappa\sigma'}\left(G^{\mathrm{ee}}_{\mu\nu\sigma,\lambda\kappa\sigma'}\right)^{y}\left(\mu\nu\mid\lambda\kappa\right)^{x}+\sum_{\mu'\nu'\lambda'\kappa'}\left(G^{\mathrm{pp}}_{\mu'\nu',\lambda'\kappa'}\right)^{y}\left(\mu'\nu'\mid\lambda'\kappa'\right)^{x}\\
&-\sum_{\mu\nu\sigma\mu'\nu'}G^{\mathrm{ep}}_{\mu\nu\sigma,\mu'\nu'}\left(\mu\nu\mid\mu'\nu'\right)^{xy}-\sum_{\mu\nu\sigma\mu'\nu'}\left(G^{\mathrm{ep}}_{\mu\nu\sigma,\mu'\nu'}\right)^{y}\left(\mu\nu\mid\mu'\nu'\right)^{x}\\
&+\left(E^{\mathrm{exc}}\right)^{(x)(y)}+\left(E^{\mathrm{epc}}\right)^{(x)(y)}+\left(E^{\mathrm{exc}}\right)^{(x)[y]}+\left(E^{\mathrm{epc}}\right)^{(x)[y]}+\left(V_{\mathrm{nuc}}\right)^{xy}
\end{aligned} \tag{B32}
$$

using notation from chapter 3, with

$$G^{\mathrm{ee}}_{\mu\nu\sigma,\lambda\kappa\sigma'}=\frac{1}{2}\left(P^{\mathrm{e}}_{\mu\nu\sigma}P^{\mathrm{e}}_{\lambda\kappa\sigma'}-c_{\mathrm{x}}\delta_{\sigma\sigma'}P^{\mathrm{e}}_{\mu\kappa\sigma}P^{\mathrm{e}}_{\lambda\nu\sigma}\right) \tag{B33}$$

$$G^{\text{pp}}_{\mu'\nu',\lambda'\kappa'} = \frac{1}{2}\left(P^{\text{p}}_{\mu'\nu'} P^{\text{p}}_{\lambda'\kappa'} - P^{\text{e}}_{\mu'\kappa'} P^{\text{e}}_{\lambda'\nu'} \right) \tag{B34}$$

$$G^{\text{ep}}_{\mu\nu\sigma,\mu'\nu'} = P^{\text{e}}_{\mu\nu\sigma} P^{\text{p}}_{\mu'\nu'} \tag{B35}$$

where σ denotes electron spin and c_{x} is the exchange coefficient for hybrid electronic

exchange-correlation functionals. The notation for the derivatives of functional

contributions is borrowed from previous work,[2] which uses parentheses around the

perturbation to denote the explicit derivative and square brackets to denote the implicit

derivative. In short, the explicit derivative is attributed to only the geometric perturbation

of the basis functions with no response of the SCF quantities, whereas the implicit

derivative contains a first-order response of the wavefunction. This response of the

wavefunction is also present in the derivatives of the **P**, **W**, and **G** matrices.

The first-order wavefunction response can be completely described by occupied-

virtual orbital rotations as well as the derivatives of overlap integrals, the latter of which

have an analytical form. The occupied-virtual rotations U are solutions of the coupled-

perturbed NEO-SCF equations:

$$
\begin{aligned}
\left(\varepsilon^{\text{e}}_{i\sigma} - \varepsilon^{\text{e}}_{a\sigma} \right)\left(U^{\text{e}}_{ai\sigma} \right)^{y} - \left(\tilde{G}^{\text{e}}_{ai\sigma} \right)^{y} \left[\left(U^{\text{e}}_{bj\alpha} \right)^{y}, \left(U^{\text{e}}_{bj\beta} \right)^{y}, \left(U^{\text{p}}_{BJ} \right)^{y} \right] &= \left(Q^{\text{e}}_{ai\sigma} \right)^{y} \\
\left(\varepsilon^{\text{p}}_{I} - \varepsilon^{\text{p}}_{A} \right)\left(U^{\text{p}}_{AI} \right)^{y} - \left(\tilde{G}^{\text{p}}_{AI} \right)^{y} \left[\left(U^{\text{e}}_{bj\alpha} \right)^{y}, \left(U^{\text{e}}_{bj\beta} \right)^{y}, \left(U^{\text{p}}_{BJ} \right)^{y} \right] &= \left(Q^{\text{p}}_{AI} \right)^{y}
\end{aligned}
\tag{B36}
$$

The right-hand sides of the equations are given by

$$\left(Q_{ai\sigma}^{e}\right)^{y} = \left(H_{ai\sigma}^{e}\right)^{y} + \sum_{j\sigma'}\left[\left(ai\sigma \mid jj\sigma'\right)^{y} - c_{x}\delta_{\sigma\sigma'}\left(aj\sigma \mid ji\sigma\right)^{y}\right] - \sum_{I}\left(ai\sigma \mid II\right)^{y}$$

$$+ \left(v_{ai\sigma}^{exc}\right)^{(y)} + \left(v_{ai\sigma}^{epc,e}\right)^{(y)} - \varepsilon_{i\sigma}^{e}\left(S_{ai\sigma}^{e}\right)^{y} - \frac{1}{2}\left(\tilde{G}_{ai\sigma}^{e}\right)^{y}\left[\left(S_{jk\alpha}^{e}\right)^{y},\left(S_{jk\beta}^{e}\right)^{y},\left(S_{JK}^{p}\right)^{y}\right]$$

$$\left(Q_{AI}^{p}\right)^{y} = \left(H_{AI}^{p}\right)^{y} + \sum_{J}\left[\left(AI \mid JJ\right)^{y} - \left(AJ \mid JI\right)^{y}\right] - \sum_{i\sigma}\left(AI \mid ii\sigma\right)^{y}$$

$$+ \left(v_{AI}^{epc,p}\right)^{(y)} - \varepsilon_{I}^{p}\left(S_{AI}^{p}\right)^{y} - \frac{1}{2}\left(\tilde{G}_{AI}^{p}\right)^{y}\left[\left(S_{jk\alpha}^{e}\right)^{y},\left(S_{jk\beta}^{e}\right)^{y},\left(S_{JK}^{p}\right)^{y}\right]$$

(B37)

where the functional potentials are given as $v_{\sigma}^{exc} = \delta E^{exc}/\delta\rho_{\sigma}^{e}$, $v_{\sigma}^{epc,e} = \delta E^{epc}/\delta\rho_{\sigma}^{e}$, and

$v^{epc,p} = \delta E^{epc}/\delta\rho^{p}$. For general electronic and protonic derivative quantities $\left(\Theta_{rs\sigma'}^{e}\right)^{y}$ and

$\left(\Theta_{RS}^{p}\right)^{y}$, here $\left(\tilde{G}_{ai\sigma}^{e}\right)^{y}$ and $\left(\tilde{G}_{AI}^{p}\right)^{y}$ are defined as

$$\left(\tilde{G}_{ai\sigma}^{e}\right)^{y} = \sum_{\sigma'}\sum_{rs\kappa\lambda}C_{r\kappa\sigma'}^{e}\left(\Theta_{rs\sigma'}^{e}\right)^{y}C_{s\lambda\sigma'}^{e}\begin{cases}2\left(ia\sigma \mid \lambda\kappa\sigma'\right)\\-c_{x}\delta_{\sigma\sigma'}\left[\left(\lambda a\sigma \mid i\kappa\sigma\right)+\left(a\kappa\sigma \mid i\lambda\sigma\right)\right]\\+2f_{ia\sigma,\lambda\kappa\sigma'}^{exc}+2f_{ia\sigma,\lambda\kappa\sigma'}^{epc,ee}\end{cases}$$

$$- \sum_{RS\kappa'\lambda'}C_{R\kappa'}^{p}\left(\Theta_{RS}^{p}\right)^{y}C_{S\lambda'}^{p}\left[2\left(ia\sigma \mid \lambda'\kappa'\right)-2f_{ia\sigma,\lambda'\kappa'}^{epc,ep}\right]$$

(B38)

$$\left(\tilde{G}_{AI}^{p}\right)^{y} = \sum_{RS\kappa'\lambda'}C_{R\kappa'}^{p}\left(\Theta_{RS}^{p}\right)^{y}C_{S\lambda}^{p}\begin{bmatrix}2\left(IA \mid \lambda'\kappa'\right)-\left(\lambda'A \mid I\kappa'\right)\\-\left(A\kappa' \mid I\lambda'\right)+2f_{IA,\lambda'\kappa'}^{epc,pp}\end{bmatrix}$$

$$- \sum_{\sigma'}\sum_{rs\kappa\lambda}C_{r\kappa\sigma'}^{e}\left(\Theta_{rs\sigma'}^{e}\right)^{y}C_{s\lambda\sigma'}^{e}\left[2\left(IA \mid \lambda\kappa\sigma'\right)-2f_{IA,\lambda\kappa\sigma'}^{epc,pe}\right]$$

with the functional kernels defined as $f_{\sigma,\sigma'}^{exc} = \delta^{2}E^{exc}/\delta\rho_{\sigma}^{e}\delta\rho_{\sigma'}^{e}$, $f_{\sigma,\sigma'}^{epc,ee} = \delta^{2}E^{epc}/\delta\rho_{\sigma}^{e}\delta\rho_{\sigma'}^{e}$,

$f^{epc,pp} = \delta^{2}E^{epc}/\delta\rho^{p2}$, and $f_{\sigma}^{epc,ep} = f_{\sigma}^{epc,pe} = \delta^{2}E^{epc}/\delta\rho^{p}\delta\rho_{\sigma}^{e}$.

Additional Details on NEO-HF(V) and FGH Calculations

The NEO-HF(V) calculations entail diagonalization of an extended NEO coordinate Hessian, as described in detail elsewhere.[4-5] This extended Hessian depends on three matrices: the NEO coordinate Hessian, a matrix composed of the fundamental vibrational excitations of the quantum protons computed with NEO-TDHF,

and a geometric response matrix composed of the derivatives of the expectation values of the quantum protons with respect to the coordinates of the classical nuclei. The NEO Hessian was calculated with the implementation of the analytic theory presented in the main text and with the same reported basis sets. For the NEO-TDHF calculations, previous work indicates that larger electronic and nuclear basis sets are needed to compute accurate proton vibrational excitations. For this reason, the NEO-TDHF calculations were performed using the cc-pVDZ electronic basis set for the classical nuclei, the cc-pV6Z electronic basis set for the quantum protons, and the PB5-G protonic basis set. The PB5-G basis set is composed of five s-type, four p-type, three d-type, two f-type, and one g-type primitive Gaussians ($5s4p3d2f1g$). The proton basis function centers were placed at the positions optimized at the NEO-HF level. We have found that the conventional analog of the geometric response matrix is nearly identical to that calculated at the NEO level because the difference in geometries optimized at the conventional HF and NEO-HF levels is negligible and this geometric property is not sensitive to nuclear quantum effects. Thus, the geometric response matrices were calculated at the optimized NEO geometry using the conventional HF level of theory with the same basis sets as reported in the main paper.

The Fourier grid Hamiltonian (FGH) calculations[6] were performed for the reactant and transition states of $C_4H_9^+$. The grid spanned 0.6 Å from the position of the hydrogen nucleus optimized with conventional HF in each principle direction with 32 grid points over 1.2 Å per dimension. Single-point energy calculations were performed at the conventional HF/6-31G** level with the proton at each of these grid points while all other nuclei remained fixed. Subsequently, the three-dimensional Schrödinger equation was

solved for the proton moving on this potential energy surface, and the zero-point energy was determined as the energy of the ground vibrational state relative to the lowest-energy point on the potential energy surface.

Asymmetric Transition State Search

To further test the efficacy of the transition state search algorithm, we investigated an asymmetric version of the hydride transfer reaction from Figure 3.1 with an additional methyl group on one of the two central carbon atoms, $C_5H_{11}^+$. The conventional HF and NEO-HF transition states for this $C_5H_{11}^+$ asymmetric system were found using the same search algorithm as used for the symmetric cases in the main paper but with the minimal STO-3G electronic basis set and sp protonic basis set described above. As in the symmetric case, the conventional HF and NEO-HF transition state geometries were found to be comparable. The frequencies of the conventional HF and NEO-HF imaginary normal modes were calculated to be $768i$ cm^{-1} and $834i$ cm^{-1}, respectively. The dot product between these two imaginary normal modes, excluding the normal mode elements corresponding to the coordinates of the quantum proton for conventional HF, is 0.253. Renormalization of the conventional HF mode after this exclusion produces a dot product of 0.905. The Cartesian coordinates associated with each imaginary normal mode vector are given in Table B7.

Geometries for $C_4H_9^+$ Species

All cartesian coordinates are provided in Angstroms. The NEO-HF geometries used the same basis sets as described in chapter 3 and the above sections. NEO-DFT geometries for these species are also provided and used the same basis sets as the

NEO-HF calculations in conjunction with the B3LYP electronic exchange-correlation functional and the epc17-2 electron-proton correlation functional.

NEO-HF $C_4H_9^+$ Reactant/Product State

C	0.6055634092	0.3550756206	-0.0428896647
C	-0.5573770509	-0.4487512344	-0.3288602284
C	1.9618355593	-0.1536686215	0.1308019147
H	-0.3984015286	-1.4939763575	-0.0899057789
C	-1.9241573703	0.1001812888	0.0936112613
H	2.1389700201	-0.0513568711	1.2100826812
H	2.6956363414	0.4860868805	-0.3473018607
H	2.0769248896	-1.1922514748	-0.1430263595
H	-2.0580923037	1.1266616361	-0.2265678749
H	-2.0386351889	0.0492605371	1.1691832590
H	-2.7046142765	-0.4986412976	-0.3548293258
H	0.4704161434	1.4272472879	0.0153476913
H	-0.4574440234	-0.3923148264	-1.4493081735

NEO-HF $C_4H_9^+$ Transition State

C	0.5869258343	0.3708687154	0.0055918117
C	-0.5506922845	-0.4150505864	-0.0200586359
C	1.9912829590	-0.1469672573	0.1066420805
H	-0.4067911601	-1.4854965962	-0.0276031748
C	-1.9568434728	0.0990952382	0.0762663617
H	2.3392548266	0.0800771171	1.1103338749

H   2.6427969019   0.3648847155   -0.5894506847

H   2.0490410122   -1.2158467807   -0.0487228464

H   -2.0121673457   1.1731381415   -0.0393344661

H   -2.3222659967   -0.1657914788   1.0643383875

H   -2.5959469922   -0.3855431249   -0.6501378605

H   0.4428215452   1.4408800721   0.0361855934

H   0.0274565682   -0.0007414014   -1.1410761969

NEO-DFT $C_4H_9^+$ Reactant/Product State

C   0.6184086974   0.3498316677   -0.0147054019

C   -0.5460733111   -0.4439402143   -0.3119562682

C   1.9673527779   -0.1578617202   0.1718878062

H   -0.3975116855   -1.5112167094   -0.1069019695

C   -1.9291299087   0.0980342620   0.1093772010

H   2.2413139282   0.0545435036   1.2295835073

H   2.7061703929   0.4348451264   -0.3901855543

H   2.0824252053   -1.2267878735   -0.0091322963

H   -2.0538693368   1.1529219883   -0.1532186285

H   -2.0598068314   -0.0142055479   1.1895615762

H   -2.7157793341   -0.4733551399   -0.3871537083

H   0.4813441835   1.4351420518   0.0438566600

H   -0.4885747403   -0.3791311232   -1.4371628973

NEO-DFT $C_4H_9^+$ Transition State

C   0.5973010371   0.3703953665   0.0029619627

C   -0.5599063810   -0.4148034924   -0.0270757706

C   1.9929920634   -0.1480823559   0.1052737047

H   -0.4158874393   -1.4978449061   -0.0416197835

C   -1.9582386931   0.1003030410   0.0742492163

H   2.3475542583   0.1147559191   1.1116073266

H   2.6599694124   0.3525050367   -0.6015088105

H   2.0562170415   -1.2314489627   -0.0129164351

H   -2.0194436174   1.1873293310   -0.0057481102

H   -2.3283929133   -0.1980293232   1.0646980816

H   -2.6139325852   -0.3728641430   -0.6611890891

H   0.4531122403   1.4532863793   0.0268127206

H   0.0235279714   -0.0019951161   -1.1525707690

Table B1: Optimized geometry of HCN at the NEO-HF/STO-3G/*sp* level.[a]

	X	y	z
C	0.0000000000	0.0000000000	0.9684140792
N	0.0000000000	0.0000000000	-1.2085828830
H	0.0000000000	0.0000000000	2.9046475823

[a]All coordinates are given in Bohr.

Table B2: Semi-numerical Hessian for HCN at the NEO-HF/STO-3G/*sp* level.[a]

	C_x	C_y	C_z	N_x	N_y	N_z
C_x	-0.00009	0.00000	0.00000	-0.00008	0.00000	0.00000
C_y	0.00000	-0.00009	0.00000	0.00000	-0.00008	0.00000
C_z	0.00000	0.00000	1.73530	0.00000	0.00000	-1.73529
N_x	-0.00005	0.00000	0.00000	0.00006	0.00000	0.00000
N_y	0.00000	-0.00005	0.00000	0.00000	0.00006	0.00000
N_z	0.00000	0.00000	-1.73529	0.00000	0.00000	1.73529

[a]All elements are in units of Hartree/Bohr^2. A symmetric five-point stencil of step size 0.001 Bohr was used to take numerical first derivatives of analytic gradient elements to yield the semi-numerical Hessian elements.

Table B3: Analytic Hessian for HCN at the NEO-HF/STO-3G/*sp* level.[a]

	C_x	C_y	C_z	N_x	N_y	N_z
C_x	0.00009	0.00000	0.00000	-0.00009	0.00000	0.00000
C_y	0.00000	0.00009	0.00000	0.00000	-0.00009	0.00000
C_z	0.00000	0.00000	1.73530	0.00000	0.00000	-1.73530
N_x	-0.00009	0.00000	0.00000	0.00009	0.00000	0.00000
N_y	0.00000	-0.00009	0.00000	0.00000	0.00009	0.00000
N_z	0.00000	0.00000	-1.73530	0.00000	0.00000	1.73530

[a]All elements are in units of Hartree/Bohr^2.
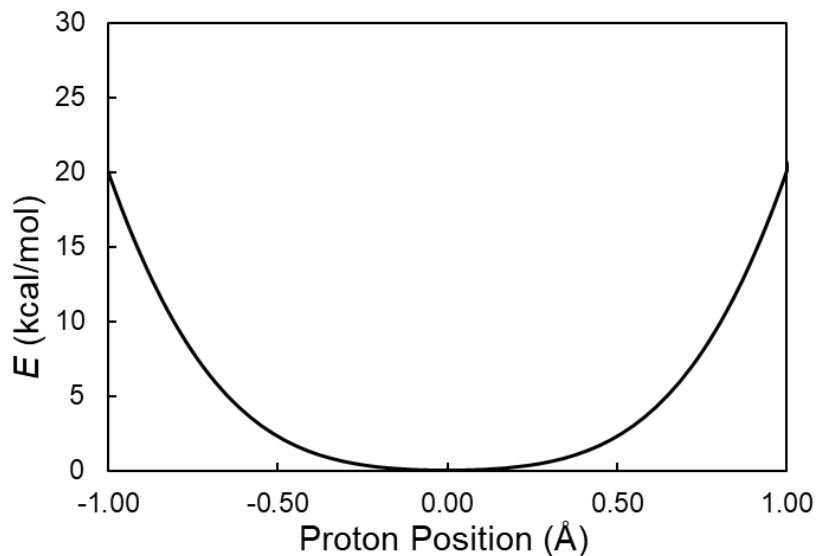
Figure B1: Proton potential energy curve at the transition state for $C_4H_9^+$ determined at the conventional HF/6-31G** level of theory. This curve was generated by moving the proton along the proton transfer axis with all other nuclei remaining fixed. The proton transfer axis was chosen to be the line in the same plane as the transferring proton and the central carbon atoms, parallel to the line connecting the central carbon atoms, and passing through the transferring proton position at the transition state. The proton moves in a single-well potential for this system at the transition state geometry.
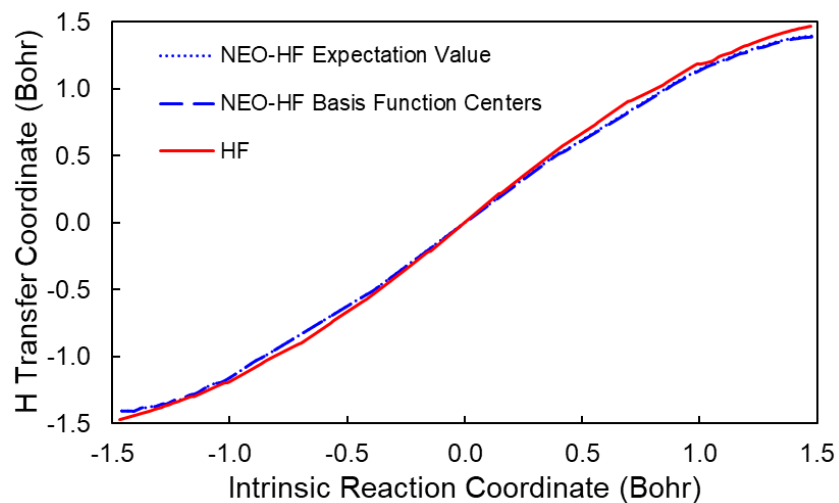
Figure B2: Hydrogen transfer coordinate along the central portion of the conventional HF and NEO-HF MEPs calculated at the level of theory described in the main paper. The hydrogen transfer coordinate is defined as the difference between the donor carbon-hydrogen distance and the acceptor carbon-hydrogen distance. The intrinsic reaction coordinate is calculated in Cartesian coordinates. For NEO-HF, the dotted blue line is the expectation value of this quantity, and the dashed blue line is the basis function center position.

Table B4: Imaginary normal mode vectors from conventional HF, NEO-HF(V), and NEO-HF calculations at the transition states for $ClCH_3Cl^-$ and $C_4H_9^+$. [a]

		HF	NEO-HF(V)	NEO-HF	HF Renormalized
$ClCH_3Cl^-$	C_{1x}	0.000	0.000	0.000	0.000
	C_{1y}	0.000	0.000	0.000	0.000
	C_{1z}	0.939	0.919	0.972	0.970
	Cl_{2x}	0.000	0.000	0.000	0.000
	Cl_{2y}	0.000	0.000	0.000	0.000
	Cl_{2z}	-0.167	-0.166	-0.167	-0.172
	Cl_{3x}	0.000	0.000	0.000	0.000
	Cl_{3y}	0.000	0.000	0.000	0.000
	Cl_{3z}	-0.167	-0.166	-0.167	-0.172
	H_{4x}	0.000	0.000	---	---
	H_{4y}	0.000	0.000	---	---
	H_{4z}	0.144	0.183	---	---
	H_{5x}	0.000	0.000	---	---
	H_{5y}	0.000	0.000	---	---
	H_{5z}	0.144	0.183	---	---
	H_{6x}	0.000	0.000	---	---
	H_{6y}	0.000	0.000	---	---
	H_{6z}	0.144	0.183	---	---
$C_4H_9^+$	C_{1x}	0.030	0.026	0.029	0.059
	C_{1y}	-0.017	-0.017	-0.056	-0.033
	C_{1z}	0.188	0.172	0.271	0.369
	C_{2x}	0.033	0.029	0.033	0.065
	C_{2y}	-0.010	-0.011	-0.045	-0.020
	C_{2z}	-0.188	-0.173	-0.275	-0.369
	C_{3x}	-0.007	-0.003	-0.029	-0.014
	C_{3y}	0.024	0.024	0.030	0.047
	C_{3z}	-0.021	-0.016	-0.045	-0.041
	H_{4x}	0.038	0.034	0.042	0.075
	H_{4y}	-0.010	-0.010	-0.045	-0.020
	H_{4z}	0.131	0.079	0.354	0.257
	C_{5x}	-0.007	-0.003	-0.030	-0.014
	C_{5y}	0.023	0.023	0.028	0.045
	C_{5z}	0.022	0.018	0.047	0.043
	H_{6x}	0.075	0.082	0.107	0.147
	H_{6y}	0.170	0.164	0.336	0.334
	H_{6z}	-0.070	-0.066	-0.138	-0.137
	H_{7x}	-0.086	-0.082	-0.165	-0.169
	H_{7y}	0.007	0.004	-0.034	0.014

	HF	NEO-HF(V)	NEO-HF	HF Renormalized
H_{7z}	-0.112	-0.110	-0.228	-0.220
H_{8x}	0.001	0.005	-0.009	0.002
H_{8y}	0.008	0.009	-0.006	0.016
H_{8z}	0.118	0.116	0.251	0.232
H_{9x}	0.003	0.007	-0.005	0.006
H_{9y}	0.013	0.013	0.003	0.026
H_{9z}	-0.118	-0.115	-0.252	-0.232
H_{10x}	0.074	0.082	0.107	0.145
H_{10y}	0.167	0.163	0.331	0.328
H_{10z}	0.078	0.075	0.155	0.153
H_{11x}	-0.088	-0.085	-0.170	-0.173
H_{11y}	0.002	-0.001	-0.044	0.004
H_{11z}	0.111	0.111	0.227	0.218
H_{12x}	0.040	0.035	0.049	0.078
H_{12y}	-0.005	-0.007	-0.032	-0.010
H_{12z}	-0.131	-0.078	-0.354	-0.257
H_{13x}	-0.636	-0.671	---	---
H_{13y}	-0.580	-0.574	---	---
H_{13z}	-0.017	-0.019	---	---

[a]The NEO-HF calculations were performed with the 6-31G** electronic and PB4-D protonic basis sets, and the conventional HF calculations were performed with the 6-31G** electronic basis set. For the renormalized HF calculations, the elements corresponding to the quantum protons for the corresponding NEO-HF calculations were excluded, and the resulting vector was renormalized. All units are in Angstroms.

Table B5: Conventional HF and NEO-HF(V) vibrational frequencies for the transition state of ClCH$_3$Cl$^-$.[a]

Mode #	Conventional HF	NEO-HF(V)
1	413*i*	410*i*
2	202	200
3	202	200
4	213	211
5	988	1098
6	988	1098
7	1208	1295
8	1537	1579
9	1537	1579
10	3392	3271
11	3606	3476
12	3606	3476

[a]All calculations were performed at the level of theory given in the main text. The frequencies are given in units of cm^{-1}.

Table B6: Conventional HF and NEO-HF(V) vibrational frequencies for the transition state of $C_4H_9^+$.[a]

Mode #	Conventional HF	NEO-HF(V)
1	165*i*	118*i*
2	195	197
3	259	262
4	274	273
5	309	311
6	518	518
7	860	874
8	914	914
9	1070	1077
10	1120	1120
11	1129	1134
12	1219	1215
13	1246	1280
14	1282	1281
15	1380	1702
16	1435	1433
17	1455	1437
18	1548	1545
19	1550	1550
20	1585	1585
21	1589	1581
22	1602	1602
23	1616	1615
24	1734	1734
25	2274	2217
26	3203	3202
27	3203	3205
28	3283	3284
29	3284	3283
30	3314	3313
31	3314	3314
32	3330	3328
33	3341	3339

[a]All calculations were performed at the level of theory given in the main text. The frequencies are given in units of cm^{-1}.

Table B7: Imaginary normal mode vectors from conventional HF and NEO-HF calculations at the transition states for $C_5H_{11}^+$. [a]

	HF	NEO-HF	HF Renormalized
C_{1x}	-0.012	0.115	-0.043
C_{1y}	0.011	-0.056	0.039
C_{1z}	0.180	0.689	0.645
C_{2x}	-0.045	-0.132	-0.161
C_{2y}	0.015	0.029	0.054
C_{2z}	-0.138	-0.293	-0.495
C_{3x}	-0.003	0.002	-0.011
C_{3y}	0.002	-0.010	0.007
C_{3z}	-0.030	-0.165	-0.108
C_{4x}	-0.003	0.010	-0.011
C_{4y}	0.000	0.003	0.000
C_{4z}	-0.028	-0.168	-0.100
H_{5x}	-0.065	-0.234	-0.233
H_{5y}	0.042	0.106	0.151
H_{5z}	0.097	0.181	0.348
H_{6x}	-0.010	-0.009	-0.036
H_{6y}	-0.004	-0.105	-0.014
H_{6z}	-0.025	-0.211	-0.090
H_{7x}	-0.001	-0.042	-0.004
H_{7y}	0.002	-0.006	0.007
H_{7z}	-0.020	-0.145	-0.072
H_{8x}	0.019	0.074	0.068
H_{8y}	-0.025	-0.073	-0.090
H_{8z}	-0.011	-0.085	-0.039
H_{9x}	-0.011	-0.049	-0.039
H_{9y}	0.008	0.074	0.029
H_{9z}	-0.024	-0.167	-0.086
H_{10x}	0.007	0.104	0.025
H_{10y}	0.018	0.096	0.065
H_{10z}	-0.032	-0.245	-0.115
H_{11x}	0.019	0.055	0.068
H_{11y}	0.001	-0.009	0.004
H_{11z}	-0.009	-0.058	-0.032
C_{12x}	-0.004	0.008	-0.014
C_{12y}	0.003	0.009	0.011
C_{12z}	0.008	0.003	0.029
H_{13x}	0.019	0.052	0.068
H_{13y}	-0.001	0.005	-0.004

	HF	NEO-HF	HF Renormalized
H$_{13z}$	-0.012	-0.030	-0.043
H$_{14x}$	-0.015	-0.036	-0.054
H$_{14y}$	0.020	0.078	0.072
H$_{14z}$	0.000	-0.016	0.000
H$_{15x}$	0.002	0.045	0.007
H$_{15y}$	0.026	0.133	0.093
H$_{15z}$	0.003	-0.012	0.011
H$_{16x}$	0.836	---	---
H$_{16y}$	-0.455	---	---
H$_{16z}$	0.128	---	---

[a] For this test on an asymmetric system, the NEO-HF calculations were performed with the minimal STO-3G electronic and *sp* protonic basis sets, and the conventional HF calculations were performed with the STO-3G electronic basis set. For the renormalized HF imaginary normal mode vector, the elements corresponding to the quantum proton were excluded, and the resulting vector was renormalized. All units are in Angstroms.

References

(1)   Pople, J. A.; Krishnan, R.; Schlegel, H. B.; Binkley, J. S., Derivative studies in hartree-fock and møller-plesset theories. *Int. J. Quantum Chem.* **1979,** *16*, 225-241.

(2)   Johnson, B. G.; Fisch, M. J., An implementation of analytic second derivatives of the gradient-corrected density functional energy. *J. Chem. Phys.* **1994,** *100*, 7429-7442.

(3)   Deglmann, P.; Furche, F.; Ahlrichs, R., An efficient implementation of second analytical derivatives for density functional methods. *Chem. Phys. Lett.* **2002,** *362*, 511-518.

(4)   Yang, Y.; Schneider, P. E.; Culpitt, T.; Pavošević, F.; Hammes-Schiffer, S., Molecular Vibrational Frequencies within the Nuclear–Electronic Orbital Framework. *J. Phys. Chem. Lett.* **2019,** *10*, 1167-1172.

(5)   Culpitt, T.; Yang, Y.; Schneider, P. E.; Pavošević, F.; Hammes-Schiffer, S., Molecular Vibrational Frequencies with Multiple Quantum Protons within the Nuclear-Electronic Orbital Framework. *J. Chem. Theory Comput.* **2019,** *15*, 6840-6849.

(6)   Webb, S. P.; Hammes-Schiffer, S., Fourier grid Hamiltonian multiconfigurational self-consistent-field: A method to calculate multidimensional hydrogen vibrational wavefunctions. *J. Chem. Phys.* **2000,** *113*, 5214-5227.

C.   Supplemental Information for Chapter 4

Supporting Information for Molecular Vibrational Frequencies within the Nuclear-Electronic Orbital Framework

Yang Yang[†], Patrick E. Schneider[†], Tanner Culpitt, Fabijan Pavošević, and Sharon Hammes-Schiffer*

Department of Chemistry, Yale University

225 Prospect Street, New Haven, Connecticut 06520 USA

*Corresponding author: sharon.hammes-schiffer@yale.edu

[†]These authors contributed equally to this work.

Proof that Derivative of the NEO Energy with Respect to Expectation Value of Quantum Nucleus Vanishes

In this subsection, we provide a derivation for Eq. (4.11). For simplicity we assume that the system has only a single quantum nucleus, but the extension of this proof to multiple quantum nuclei is straightforward due to the localization of the quantum nuclei in molecular systems. The fully converged NEO solution corresponds to the nuclear density associated with the lowest total energy E_0, and this nuclear density produces an expectation value of the quantum nucleus, $\mathbf{r}_q$, that is completely defined by this density according to Eq. (4.8). Because the NEO solution is variational, any other nuclear density that leads to the same or different expectation value would be associated with an energy greater than or equal to E_0, and any other expectation value of the quantum nucleus would be associated with an energy greater than or equal to E_0. Thus, based on the variational nature of the fully converged NEO solution, $\partial E / \partial \mathbf{r}_q = 0$.

For completeness, we also include a more rigorous mathematical derivation. A NEO solution corresponds to a density $\rho(\mathbf{r})$ for the quantum nucleus, and this nuclear density is associated with the expectation value $\mathbf{r}_q$ defined in chapter 4. For a given expectation value $\mathbf{r}_q$, however, an infinite number of nuclear densities could produce this value:

$$\left\{ \rho^1(\mathbf{r}), \rho^2(\mathbf{r}), \cdots, \rho^\infty(\mathbf{r}) \right\} \to \mathbf{r}_q . \tag{C1}$$

For a given nuclear density $\rho^n(\mathbf{r})$, a NEO calculation in which only the electronic densities are optimized can be performed, and each of these calculations produces an

energy E^n:

$$\left\{\rho^1(\mathbf{r}), \rho^2(\mathbf{r}), \cdots, \rho^\infty(\mathbf{r})\right\} \to \left\{E^1, E^2, \cdots, E^\infty\right\}. \tag{C2}$$

Note that, in general, these energies are not fully converged NEO energies. The nuclear density associated with the lowest energy is defined to correspond to the expectation value $\mathbf{r}_q$, as expressed mathematically by

$$\rho_{\mathbf{r}_q}(\mathbf{r}) = \arg\left(\min_{\rho(\mathbf{r}) \in \{\rho(\mathbf{r}) | \rho(\mathbf{r}) \to \mathbf{r}_q\}} \left(E(\mathbf{r}_c, \rho(\mathbf{r}))\right)\right) \tag{C3}$$

and

$$E(\mathbf{r}_c, \mathbf{r}_q) := E\left(\mathbf{r}_c, \rho_{\mathbf{r}_q}(\mathbf{r})\right). \tag{C4}$$

For a fully converged NEO-DFT solution with nuclear density $\rho^0(\mathbf{r})$ and $\rho^0(\mathbf{r}) \to \mathbf{r}_q$, the nuclear density has been optimized to achieve the lowest energy under the density normalization condition, leading to

$$E\left(\mathbf{r}_c, \rho^0(\mathbf{r})\right) \leq E(\mathbf{r}_c, \rho(\mathbf{r})). \tag{C5}$$

More specifically,

$$E(\mathbf{r}_c, \mathbf{r}_q) = E\left(\mathbf{r}_c, \rho^0(\mathbf{r})\right) \leq E(\mathbf{r}_c, \rho'(\mathbf{r})) \quad \text{for all} \quad \rho'(\mathbf{r}) \in \{\rho(\mathbf{r}) | \rho(\mathbf{r}) \to \mathbf{r}_q\} \tag{C6}$$

and

$$E(\mathbf{r}_c, \mathbf{r}_q) = E\left(\mathbf{r}_c, \rho^0(\mathbf{r})\right) \leq E\left(\mathbf{r}_c, \rho_{\mathbf{r}'_q}(\mathbf{r})\right) = E\left(\mathbf{r}_c, \mathbf{r}'_q\right). \tag{C7}$$

Thus, according to the definition given in Eq. (C3), the energy reaches its minimum at the nuclear density corresponding to the fully converged NEO solution, and

$$\frac{\partial E}{\partial \mathbf{r}_q} = 0. \tag{C8}$$

Derivation of an Analytical Expression for the Response Matrix

In this subsection, an analytical expression for the quantity given in Eq. (4.17) is presented. Based on Eqs. (4.1) and (4.8), elements of this matrix may be defined as

$$\mathbf{R}_{ij} = \frac{\mathrm{d}r_{q_i}}{\mathrm{d}r_{c_j}} = \frac{\partial r_{q_i}}{\partial r_{c_j}} + \sum_k \frac{\partial r_{q_i}}{\partial r_{b_k}} \frac{\mathrm{d}r_{b_k}}{\mathrm{d}r_{c_j}} . \tag{C9}$$

Note that the ith expectation value can be written as

$$r_{q_i} = r_{b_i} + \langle \mathbf{r} \rangle^{\mathrm{p}_i,0} = r_{b_i} + \int \mathbf{r} \rho^{\mathrm{p}_i,0}(\mathbf{r}) \mathrm{d}\mathbf{r} = r_{b_i} + \sum_{\mu'\nu'} P_{\mu'\nu'}^{\mathrm{p}_i} \Delta_{\mu'\nu'}^{i,0} , \tag{C10}$$

where $\rho^{\mathrm{p}_i,0}$ is the ith quantum nuclear density centered at the origin, $P_{\mu'\nu'}^{\mathrm{p}_i}$ is a one-particle density matrix based on the SCF solution for the ith quantum nucleus, and $\Delta_{\mu'\nu'}^{i,0}$ are dipole integrals for the ith protonic basis function center at the origin. Moreover, the last factor of Eq. (C9) can be produced by manipulating Eq. (4.5) to produce

$$\frac{\mathrm{d}r_{b}}{\mathrm{d}r_{c}} = -\left(\frac{\partial^2 E}{\partial r_{b}^2} \right)^{-1} \left(\frac{\partial^2 E}{\partial r_{b}\partial r_{c}} \right) = -\mathbf{H}_{2,\mathrm{bb}}^{-1} \mathbf{H}_{1,\mathrm{bc}} . \tag{C11}$$

Now, the partial derivatives of r_{q_i} of Eq. (C9) are given by

$$\frac{\partial r_{q_i}}{\partial r_{c_j}} = \sum_{\mu'\nu'} \left(\frac{\partial P_{\mu'\nu'}^{\mathrm{p}_i}}{\partial r_{c_j}} \Delta_{\mu'\nu'}^{i,0} + P_{\mu'\nu'}^{\mathrm{p}_i} \frac{\partial \Delta_{\mu'\nu'}^{i,0}}{\partial r_{c_j}} \right) = \sum_{\mu'\nu'} \frac{\partial P_{\mu'\nu'}^{\mathrm{p}_i}}{\partial r_{c_j}} \Delta_{\mu'\nu'}^{i,0} , \tag{C12}$$

and

$$\frac{\partial r_{q_i}}{\partial r_{b_k}} = \delta_{ik} + \sum_{\mu'\nu'} \left(\frac{\partial P_{\mu'\nu'}^{\mathrm{p}_i}}{\partial r_{b_k}} \Delta_{\mu'\nu'}^{i,0} + P_{\mu'\nu'}^{\mathrm{p}_i} \frac{\partial \Delta_{\mu'\nu'}^{i,0}}{\partial r_{b_k}} \right) = \delta_{ik} + \sum_{\mu'\nu'} \frac{\partial P_{\mu'\nu'}^{\mathrm{p}_i}}{\partial r_{b_k}} \Delta_{\mu'\nu'}^{i,0} . \tag{C13}$$

The derivatives of these dipole integrals with respect to basis function centers are zero due to these dipole integrals being defined for a single basis function center at the origin. As alluded to in chapter 4, the derivatives of density matrix elements can be obtained through a coupled-perturbed NEO-SCF calculation. Combining Eqs. (C9), (C12), and (C13) yields the final expression for elements of the response matrix:

$$\frac{dr_{q_i}}{dr_{c_j}} = \frac{dr_{b_i}}{dr_{c_j}} + \sum_{\mu'\nu'}\left[\left(\frac{\partial P_{\mu'\nu'}^{p_i}}{\partial r_{c_j}} + \sum_k \frac{\partial P_{\mu'\nu'}^{p_i}}{\partial r_{b_k}}\frac{dr_{b_k}}{dr_{c_j}}\right)\Delta_{\mu'\nu'}^{i,0}\right]. \tag{C14}$$

Table C1: Vibrational Frequencies (in cm^{-1}) Calculated with Conventional DFT with Harmonic Treatment and with NEO-DFT(V) with Different Basis Function Center Positions for TDDFT

	Vibrational Mode	Experiment	NEO-DFT(V)[a,b]	NEO-DFT(V)[a,c]	Conv. Harmonic[d]
HCN [e]	CH stretch	3311	3317	3292	3439
	CN stretch	2097	2191	2190	2201
	CH bend	712	789	796	773
HNC [f]	NH stretch	3653	3645	3641	3814
	NC stretch	2024	2100	2100	2105
	NH bend	462	568	607	480
HCFO[g]	CH stretch	2976	2947	2899	3081
	CO stretch	1834	1885	1884	1891
	CH in-plane bend	1344	1329	1311	1370
	CF stretch	1070	1075	1061	1069
	CH out-of-plane bend	1000–1050	1061	1053	1039
	OCF scissor	661	665	665	665
HCF$_3$ [h]	CH stretch	3035	2988	2935	3119
	CH bend	1376	1353	1341	1388
	CF asymmetric stretch	1152	1134	1133	1139
	CF symmetric stretch	1137	1128	1128	1133
	CF simultaneous bend	700	693	693	694
	FCF scissor	508	501	501	501
FHF^{-} [i]	FH stretch	1331	1695	1695	1451
	FH bend	1286	1302	1302	1360
	FF stretch	583	617	617	625

[a]NEO-DFT/B3LYP/epc17-2 with electronic and nuclear basis sets given in the text. [b]Quantum proton basis function centers for NEO-TDDFT placed at conventional covalent hydrogen bonding distance. [c]Quantum proton basis function centers for NEO-TDDFT placed at the expectation value of the proton determined by NEO-DFT. [d]DFT/B3LYP; cc-pVTZ and cc-pV6Z* electronic basis sets for the heavy atoms and hydrogen, respectively. [e]Experimental data from Ref. 20. [f]Experimental data from Ref. 21. [g]Experimental data from Ref. 22. [h]Experimental data from Ref. 23. [i]Experimental data from Ref. 24.

Table C2: Vibrational Frequencies (in cm^{-1}) Calculated with Conventional DFT with Harmonic and VSCF Treatments and with NEO-DFT(V)

	Vibrational Mode	Experiment	NEO-DFT(V)[a]	DFT/VSCF[b]	Conv. Harmonic[b]
HCN [c]	CH stretch	3311	3317	3365	3439
	CN stretch	2097	2191	2183	2201
	CH bend	712	789	868	773
HNC [d]	NH stretch	3653	3645	3690	3814
	NC stretch	2024	2100	2084	2105
	NH bend	462	568	721	480
HCFO[e]	CH stretch	2976	2947	2965	3081
	CO stretch	1834	1885	1871	1891
	CH in-plane bend	1344	1329	1379	1370
	CF stretch	1070	1075	1058	1069
	CH out-of-plane bend	1000–1050	1061	1069	1039
	OCF scissor	661	665	665	665
HCF$_3$ [f]	CH stretch	3035	2988	3004	3119
	CH bend	1376	1353	1405	1388
	CF asymmetric stretch	1152	1134	1148	1139
	CF symmetric stretch	1137	1128	1130	1133
	CF simultaneous bend	700	693	694	694
	FCF scissor	508	501	502	501
FHF^{-} [g]	FH stretch	1331	1695	1940	1451
	FH bend	1286	1302	1372	1360
	FF stretch	583	617	621	625

[a]NEO-DFT/B3LYP/epc17-2 with electronic and nuclear basis sets given in the text. [b]DFT/B3LYP; cc-pVTZ and cc-pV6Z* electronic basis sets for the heavy atoms and hydrogen, respectively; vibrational self-consistent-field (VSCF) calculations performed with the GAMESS program. [c]Experimental data from Ref. 23 of chapter 4. [d]Experimental data from Ref. 24 of chapter 4. [e]Experimental data from Ref. 25 of chapter 4. [f]Experimental data from Ref. 26 of chapter 4. [g]Experimental data from Ref. 27 of chapter 4.

Table C3: Vibrational Frequencies (in cm^{-1}) Calculated with NEO Hessian with Born-Oppenheimer Separation of Quantum Proton, NEO-TDDFT with Fixed Classical Nuclei, and NEO-DFT(V)

	Vibrational Mode	Experiment	NEO-DFT(V)[a]	NEO Hessian[a]	NEO-TDDFT[b]
HCN [c]	CH stretch	3311	3317	---	3112
	CN stretch	2097	2191	2294	---
	CH bend	712	789	---	671
HNC [d]	NH stretch	3653	3645	---	3481
	NC stretch	2024	2100	2160	---
	NH bend	462	568	---	493
HCFO[e]	CH stretch	2976	2947	---	2838
	CO stretch	1834	1885	1905	---
	CH in-plane bend	1344	1329	---	1284
	CF stretch	1070	1075	1077	---
	CH out-of-plane bend	1000–1050	1061	---	806
	OCF scissor	661	665	670	---
HCF$_3$ [f]	CH stretch	3035	2988	---	2875
	CH bend	1376	1353	---	1277
	CF asymmetric stretch	1152	1134	1156	---
	CF symmetric stretch	1137	1128	1154	---
	CF simultaneous bend	700	693	699	---
	FCF scissor	508	501	505	---
FHF^{-} [g]	FH stretch	1331	1695	---	1674
	FH bend	1286	1302	---	1286
	FF stretch	583	617	617	---

[a]NEO-DFT/B3LYP/epc17-2 with electronic and nuclear basis sets given in the text. [b]NEO-TDDFT/B3LYP/epc17-2 with electronic and nuclear basis sets given in the text and quantum proton basis function centers placed at conventional covalent hydrogen bonding distance. [c]Experimental data from Ref. 23 of chapter 4. [d]Experimental data from Ref. 24 of chapter 4. [e]Experimental data from Ref. 25 of chapter 4. [f]Experimental data from Ref. 26 of chapter 4. [g]Experimental data from Ref. 27 of chapter 4.

D.   Supplemental Information for Chapter 5

Supporting Information for Molecular Vibrational Frequencies with Multiple Quantum Protons within the Nuclear-Electronic Orbital Framework

Tanner Culpitt[†], Yang Yang[†], Patrick E. Schneider, Fabijan Pavošević, and Sharon Hammes-Schiffer[*]

Department of Chemistry, Yale University

225 Prospect Street, New Haven, Connecticut 06520 USA

[*]Corresponding author: sharon.hammes-schiffer@yale.edu

[†]These authors contributed equally to this work

Table D1: NEO-TDDFT Excitation Energies (cm^{-1}) in Ascending Order[a]

	NEO-TDDFT
H_2O_2	346
	500
	1251
	1358
	3491
	3491
H_2CO	322
	1003
	1045
	1449
	2625
	2687
H_2NF	292
	1123
	1246
	1518
	3179
	3193

[a]The lowest excitation energy for each species corresponds to a rotational mode.